

Washington University in St. Louis

## Washington University Open Scholarship

---

All Theses and Dissertations (ETDs)

---

January 2011

### Advances in real-time thoracic guidance systems

Ryan Smith

*Washington University in St. Louis*

Follow this and additional works at: <https://openscholarship.wustl.edu/etd>

---

#### Recommended Citation

Smith, Ryan, "Advances in real-time thoracic guidance systems" (2011). *All Theses and Dissertations (ETDs)*. 327.

<https://openscholarship.wustl.edu/etd/327>

This Dissertation is brought to you for free and open access by Washington University Open Scholarship. It has been accepted for inclusion in All Theses and Dissertations (ETDs) by an authorized administrator of Washington University Open Scholarship. For more information, please contact [digital@wumail.wustl.edu](mailto:digital@wumail.wustl.edu).

WASHINGTON UNIVERSITY IN ST. LOUIS

School of Engineering and Applied Science

Department of Biomedical Engineering

Thesis Examination Committee:

Parag J. Parikh, Chair

Dennis Barbour

Shelton Caruthers

Dennis Hallahan

Daniel A. Low

Daniel Moran

ADVANCES IN REAL-TIME THORACIC GUIDANCE SYSTEMS

by

Ryan L. Smith

A dissertation presented to the Graduate School of Arts and Sciences  
of Washington University in partial fulfillment of the  
requirements for the degree of

DOCTOR OF PHILOSOPHY

May 2011  
Saint Louis, Missouri

copyright by  
Ryan L. Smith  
2011

## ABSTRACT OF THE DISSERTATION

Advances in real-time thoracic guidance systems

by

Ryan L. Smith

Doctor of Philosophy in Biomedical Engineering

Washington University in St. Louis, 2011

Research Advisor: Professor Parag J. Parikh

Substantial tissue motion ( $>1\text{cm}$ ) arises in the thoracic/abdominal cavity due to respiration. There are many clinical applications in which localizing tissue with high accuracy ( $<1\text{mm}$ ) is important. Potential applications include radiation therapy, radio frequency ablation, lung/liver biopsies, and brachytherapy seed placement. Recent efforts have made highly accurate sub-mm 3D localization of discrete points available via electromagnetic (EM) position monitoring. Technology from Calypso Medical® allows for simultaneous tracking of up to three implanted wireless transponders. Additionally, Medtronic Navigation uses wired electromagnetic tracking to guide surgical tools for image guided surgery (IGS).

Utilizing real-time EM position monitoring, a prototype system was developed to guide a therapeutic linear accelerator to follow a moving target (tumor) within the lung/abdomen. In a clinical setting, electromagnetic transponders would be bronchoscopically implanted into the lung of the patient in or near the tumor. These transponders would affix to the lung tissue in a stable manner and allow real-time



position knowledge throughout a course of radiation therapy. During each dose of radiation, the beam is either halted when the target is outside of a given threshold, or in a later study the beam follows the target in real-time based on the EM position monitoring. We present quantitative analysis of the accuracy and efficiency of the radiation therapy tumor tracking system.

EM tracking shows promise for IGS applications. Tracking the position of the instrument tip allows for minimally invasive intervention and alleviates the trauma associated with conventional surgery. Current clinical IGS implementations are limited to static targets: *e.g.* craniospinal, neurological, and orthopedic intervention. We present work on the development of a respiratory correlated image guided surgery (RCIGS) system. In the RCIGS system, target positions are modeled via respiratory correlated imaging (4DCT) coupled with a breathing surrogate representative of the patient's respiratory phase/amplitude. Once the target position is known with respect to the surrogate, intervention can be performed when the target is in the correct location. The RCIGS system consists of imaging techniques and custom developed software to give visual and auditory feedback to the surgeon indicating both the proper location and time for intervention. Presented here are the details of the IGS lung system along with quantitative results of the system accuracy in motion phantom, ex-vivo porcine lung, and human cadaver environments.

# Acknowledgments

*You're going to get yourself overeducated and no one will hire you.* —  
Grandpa Patterson

I owe my gratitude to many people for the completion of this dissertation. I would first like to thank my principal investigator, Dr. Parag Parikh. He has helped sculpt me from an unrefined student with some technical skills to someone who can view an experiment with a top-down perspective and plan accordingly. My original ‘charge in an figure it out when I get there’ mindset can be useful, however when other people (more important than myself) are involved, it is good practice to have an experiment as well thought out as possible prior to execution. These abilities will serve me well in my future scientific endeavors. I would also like to thank the members of my committee for their guidance throughout my tenure. Dr. Dennis Barbour has acted as a surrogate mentor and informed me on graduate school policy since my adviser was new to the department when I started. Your thoroughness is appreciated. I found Dr. Shelton Caruthers’ and Dr. Dan Moran’s classes to be particularly interesting and well designed. Dr. Dan Low has been integral during my time at Washington University. His proximity to our lab and willingness to let me sit in on his lab meetings has provided me with numerous pieces of insight. Dr. Dennis Hallahan also deserves special mention for his eagerness to serve on my committee without much notice. Dr. Lakshmi Santanam, Trilogy Expert, was also very instrumental in my first couple projects as a graduate student. I’d like to thank my undergraduate research adviser, Dr. Gabe Spalding, for helping increase my interest in science as a whole. Finally, I would like to acknowledge Dr. Martin Mayse for his continued guidance throughout my PhD. During my first few months, we worked on a project for Calypso Medical together, and since then he has provided me with countless pieces of wisdom over numerous Belgium libations. I wish you and your new company the best.

I owe special gratitude to all the current and former members of the Parikh and Low labs. Kate Malinowski kept me sane and organized while working late developing films in the dark room. Jie Wen is one of the most gifted electronics designers I have ever had the pleasure of working with. Camille Noel’s knowledge of clinical workflow

and procedures proved very useful. JiaJia Ge, Deshan Yang, and Shyam Bharat both offered fruitful discussions and feedback on my work.

I have had the support of many friends during my years as a graduate student. There are far too many to list, but some of those that I spent the most time with are: Chris Butts, Paul Watkins, Pat ‘Sallywag’ Kavanagh, Justin Brooks, Ben Filas, Sydney Schaefer, Dan Peterson, Jen Kentos, Casey Arcese, Ikenna ‘Big Ike’ Odinaka, and Dylan McCreedy. For those friends reading this that aren’t on the list, you know who you are and this was not an attempt to slight you, so stop whining.

Finally I would like to thank all my family, and especially my parents. Their love and support has been limitless since I was a child and without them I would be nowhere near the person that I am today. Their understanding when I make mistakes has grown over the years, and I hope to do half as well as they did parenting if I eventually dupe someone into procreating with me. I love you all.

Ryan L. Smith

*Washington University in Saint Louis*  
*May 2011*

# Contents

<b>Abstract</b> . . . . .	<b>ii</b>
<b>Acknowledgments</b> . . . . .	<b>iv</b>
<b>List of Tables</b> . . . . .	<b>ix</b>
<b>List of Figures</b> . . . . .	<b>x</b>
<b>1 Introduction</b> . . . . .	<b>1</b>
1.1 Specific Aim 1: Incorporate real-time electromagnetic position monitoring into a spatial gating solution for motion management in the delivery of radiation therapy. . . . .	4
1.2 Specific Aim 2: Incorporate real-time electromagnetic position monitoring into a Dynamic Multileaf Collimator (DMLC) tracking system for highly accurate continuous radiation delivery to mobile targets . .	4
1.3 Specific Aim 3: Determine the accuracy of an internal fiducial marker with known position at predicting adjacent target motion. . . . .	4
1.4 Specific Aim 4: Develop a robust system for image guided surgery (IGS) applications in the presence of respiratory motion. . . . .	4
<b>2 Linear Accelerator EM Gating</b> . . . . .	<b>5</b>
2.1 Introduction . . . . .	5
2.2 Gating: Latency Estimates . . . . .	8
2.3 Gating: Clinical Dosimetry . . . . .	10
2.4 Gating: Discussion . . . . .	15
<b>3 DMLC Tracking</b> . . . . .	<b>17</b>
3.1 Introduction . . . . .	17
3.2 DMLC Tracking: Latency Estimates . . . . .	18
3.3 DMLC Tracking: Geometric Accuracy . . . . .	18
3.4 DMLC Tracking: Dosimetric Accuracy . . . . .	21
3.5 DMLC: Tracking: Efficiencies . . . . .	22
3.6 DMLC: Tracking: Discussion . . . . .	25
<b>4 Internal Fiducial Motion Correlation</b> . . . . .	<b>28</b>
4.1 Fiducial Correlation: Motivation . . . . .	28
4.2 Fiducial Correlation: Methods . . . . .	30

4.2.1	Dataset and Techniques . . . . .	30
4.2.2	Correlation Radius . . . . .	31
4.2.3	Tumor Correlation . . . . .	32
4.3	Fiducial Correlation: Results . . . . .	33
4.3.1	Motion Correlation: General Lung Results . . . . .	33
4.3.2	Motion Correlation: Tumor Centric Results . . . . .	35
4.4	Fiducial Correlation: Discussion . . . . .	35
<b>5</b>	<b>Lung Image Guided Surgery . . . . .</b>	<b>39</b>
5.1	Introduction . . . . .	39
5.2	Methods and Materials . . . . .	42
5.2.1	RCIGS System Overview . . . . .	43
5.2.2	System Accuracy: Overview . . . . .	50
5.2.3	System Accuracy: Phantom Assessment . . . . .	52
5.2.4	System Accuracy: Ex-Vivo Porcine Assessment . . . . .	53
5.2.5	System Accuracy: Human Cadaver Assessment . . . . .	58
5.3	Results . . . . .	60
5.3.1	Phantom Assessment . . . . .	60
5.3.2	Porcine Assessment . . . . .	63
5.3.3	Cadaver Assessment . . . . .	63
5.4	Discussion . . . . .	64
<b>6</b>	<b>Discussion . . . . .</b>	<b>66</b>
<b>Appendix A Abbreviations and Acronyms . . . . .</b>		<b>69</b>
<b>Appendix B Definition of terms . . . . .</b>		<b>70</b>
B.1	Linear Accelerators . . . . .	70
B.2	4DCT . . . . .	71
B.3	IMRT . . . . .	72
B.3.1	S-IMRT . . . . .	72
B.3.2	D-IMRT . . . . .	72
B.4	Dosimetric Analysis . . . . .	73
B.4.1	Difference Maps . . . . .	73
B.4.2	Distance to Agreement (DTA) . . . . .	74
B.4.3	Gamma ( $\gamma$ ) Tool . . . . .	74
B.5	Intra/Inter -fraction motion . . . . .	75
B.6	Washington University 4D Phantom . . . . .	76
B.7	Respiratory Motion Model . . . . .	77
B.8	Target Localization Techniques . . . . .	78
B.9	Calypto Electromagnetic Position Monitoring . . . . .	80
B.10	Medtronic StealthStation . . . . .	81

References . . . . .	82
Curriculum Vitae . . . . .	95

# List of Tables

3.1	Dosimetry Failure Rates. Gamma failure rates were reported for all cases. Note that failure rates for D-IMRT plans were comparable for gating and DMLC tracking. S-IMRT gating outperformed DMLC tracking. Gating and DMLC tracking outperformed no intervention in both plans. . . . .	22
3.2	Efficiency Values. Delivery efficiencies were recorded in the form of Beam on Time and Total Time for each of the delivery conditions. Values along with associated duty cycles are reported. The duty cycle values are normalized to the static delivery case (100% indicates no efficiency drop due to intervention). . . . .	25
4.1	Correlation Radius Values. Correlation radii values to represent 3mm motion. Means and standard deviations are reported for each lobe in units of cm. Tumor correlation radii were significantly higher ( $p < 0.005$ ) than the healthy lung tissue radii values. . . . .	33
5.1	Porcine Intervention Accuracies. The target to needle tip errors are reported. Additionally, the target motion and depth are reported. . .	63
5.2	Cadaver Intervention Accuracies. The target to needle tip errors are reported. Additionally, the target motion and depth are reported. . .	64

# List of Figures

2.1	Gating setup. The 4D phantom moves the attached film phantom in realistic breathing trajectories. Real-time position information of the transponders implanted in the film phantom are acquired via the array and sent to a decision making computer. Each position measurement is analyzed to determine whether it is inside a predefined 3D volume. If so, the beam is turned on and delivery proceeds. If the position is outside the volume, a Beam Hold is enacted and delivery halts until the target returns. . . . .	9
2.2	Latency histograms for the gating system. . . . .	10
2.3	Lung trajectories reconstructed from a 4DCT and spirometry from a lung cancer patient.[45] . . . . .	11
2.4	Dose difference maps. Films irradiated in the presence of clinically relevant motion were subtracted from the static ‘gold standard’ case. A) The entire dose profile with the ROI indicated via a box.. B) The high gradient region of interest as denoted by the box in A). C/D) Normalized difference maps were calculated to show over- and under-dosing as a percentage of maximum dose. Red and blue regions indicate over and under dosing respectively. Gating reduces the spread and magnitude of dose mismatch that occurs in the presence of motion. . . . .	12
2.5	Gamma Maps. Gamma maps for the gated and non-gated cases are displayed. As described previously, the gamma tool allows for simultaneous analysis of both distance to agreement and dose difference. Lower values indicate higher dosimetric agreement. . . . .	13
2.6	Gating reduces dose blurring and improves dose gradients when compared to no intervention. Here, dose gradients of line profiles are analyzed for lines at y=3mm, 8mm, and 13mm (b-d). Raw data is plotted with a polynomial fit overlaid. It is evident that gating improves dose gradients to match the delivery in the absence of motion. . . . .	14
3.1	Target (BB) and MLC aperture trajectories in the run recorded with no prediction. These values were used to calculate the total temporal latency of the system ( 220 ms). Figure credit Sawant <i>et al.</i> [81]. . . . .	19
3.2	Distributions of geometric accuracy for three different motion trajectories. Figure credit Sawant <i>et al.</i> [81] . . . . .	20



3.3	Difference maps were produced after registering the dose profiles in the presence of motion with the film obtained via static delivery (the ‘gold standard’). The control from runs in the absence of motion are given as a reference in each case. . . . .	23
3.4	Gamma values were calculated for each of the moving images. The values for the distance to agreement criterion $\Delta d = 3\text{mm}$ and the dose agreement criterion $\Delta D = 3\%$ of the maximum dose. The control runs in the absence of motion is given as a reference for each case. . . . .	24
4.1	Correlation Radius Technique: Lung lobes and tumor were contoured at expiration (1). Deformable registration was performed between inhalation and exhalation CT scans to obtain motion vectors (2). Seed points were selected at random, ten per lung lobe (3). A spherical region growing algorithm was employed to determine the maximum radius at which 95% of the surrounding voxels correlated with the seed voxel motion (4). . . . .	32
4.2	Histograms of correlation radii values for each lobe. Notice increased correlation radii values for the upper lobes when compared to the lower lobes. Correlation radii values were capped at 7cm, which resulted in the 7cm peak in the low motion Right Upper lobe. . . . .	34
4.3	Correlation Radii Maps. Regularly spaced voxel within the lung were analyzed using the process described in Figure 4.1. Correlation maps were produced to display how well the anatomy correlates with adjacent anatomy within the thoracic cavity. Red indicates low correlation with surrounding anatomy motion, blue indicates high correlation. . . . .	36
4.4	Correlation Tumor Maps: Motion correlation values were observed with respect to the tumor centroid (indicated by white point). It is evident that correlation is variable based on the divergence of local motion vectors. . . . .	38
5.1	Medtronic StealthStation. The field generator (black, foreground) and the Medtronic StealthStation (background) are shown. A position sensitive magnetic field is generated with respect to the field generator, which allows for precise location monitoring of EM tools in the tracking volume. . . . .	42

5.2	Lung IGS Workflow. 4DCT images are acquired based on a respiratory waveform from a pneumotachograph connected to the patient’s mouth piece. The 4DCT images are sent to the RCIGS planning software, as well as a contouring workstation for target definition with respect to respiratory phase. The StealthStation receives entry and target points from the RCIGS planning software, the exhalation CT, and the real-time tool position via EM position monitoring. The StealthStation offers real-time visual guidance to the physician on the location of the needle tip inside the patient. Four target points with respect to respiratory phase are sent from the Pinnacle workstation to the 5D model computer. The model parameters ( $\alpha/\beta$ ) are input to the RCIGS guidance software, along with the real-time respiratory waveform. From here, the RCIGS guidance software determines the position of the target in real-time, and indicates the proper time for intervention to the physician via auditory and visual feedback. . . . .	44
5.3	RCIGS Software Architecture. The RCIGS package is built on open source software libraries. The libraries provide a means for segmentation, visualization and fast data manipulation in C++. The Visualization Toolkit (VTK) and Insight Toolkit (ITK) packages rely on commonly used lower level techniques and libraries such as the GDCM (DICOM image reading/writing), OpenGL (computer visualization), and VNL (numerics) . . . . .	47
5.4	Lung IGS Planning Software. Target, entry and approach trajectories are visually displayed along with respiratory correlated imaging. This allows the physician to determine whether critical structures enter the approach path as a result of respiration prior to surgical intervention. . . . .	47
5.5	Pneumotachograph. A pneumotach head (A, side profile: F) is attached to a custom fabricated circuit board. The board offers voltage output corresponding to raw air flow (B) after analogue low pass filtering (C). Additionally, there is on-board analogue to digital conversion and encoding (D) in order to interface via a serial port (E) with a Philips Brilliance CT scanner. . . . .	48
5.6	Lung IGS Intervention Software. The respiratory waveform is displayed to the physician. Binary auditory and visual feedback is given to the physician when the target is within a predetermined range. The static intervention target is shown as a yellow dot with multi-plane views. The position of the red dot changes in real-time based on the previously calibrated 5D model indicating the target position as a function of the respiratory surrogate. . . . .	49

5.7	Pneumotach Calibration. A pneumotachograph was constructed to obtain highly accurate tidal volume recordings. The calibration waveform was obtained using a 600ml syringe. Standard deviations were obtained at inhalation (1.6%) and exhalation (0.2%) using peak detection. . . . .	50
5.8	System Accuracy Models. The RCIQS system was tested in robotic phantom, porcine, and human cadaver environments. The table outlines the problem each model attempted to address, as well as a quantitative success metric. . . . .	51
5.9	Lung IGS Phantom Study Schematic. A 4D motion phantom recreates realistic motion trajectories. A bellows device receives the respiratory signal via a surrogate axis and a computer calculates the target position using a pre-calibrated 5D model. This information is used to guide the physician on when to intervene. When an intervention is performed, the position of an AxiEM marker on the motion phantom arm is recorded along with the position of the surgeon's tool tip. This allows for quantitative analysis of the accuracy of the temporal guidance system. . . . .	54
5.10	Porcine Lungs. The lungs were affixed in a housing which maximized the amount of anterior/posterior and superior/inferior motion by restricting the lateral edges. The lungs were attached to ventilator and inflated via positive pressure. . . . .	55
5.11	Surgical tools. An AxiEM stylette with PEEK guide sheath/needle as well as a bare AxiEM stylette are shown. . . . .	57
5.12	Target/Intervention accuracy assessment. The needle tip and target are defined inside of clinical treatment planning software. The 3D offset is recorded for each run. Yellow grid marks = 1cm increments. . . . .	58
5.13	Cadaver Registration. Several small radiopaque CT contrast markers were affixed to the chest wall for registration. The markers have a circular hole in the middle, which is the same size as the head of an EM tool. The tool is touched in each of the markers during exhalation, and the StealthStation matches these points in CT room coordinates (with respect to the black magnetic field generator) with the associated points defined on the CT image. . . . .	59
5.14	Lung Motion: Modeling Errors. The output from the 5D model used to determine the tumor position during treatment was compared with the actual tumor trajectory. Errors are reported for the entire waveform (blue) as well as only at exhalation (yellow). . . . .	61
5.15	Lung Motion: Phantom Intervention Errors. Intervention was performed on a moving target. A histogram of the errors from 25 interventions is shown. . . . .	62

5.16	Pleural Effusion. Substantial fluid buildup (A) was present in one lung prior to draining via a chest tube affixed to a vacuum source. The lung was collapsed (B) prior to draining and this might have reduced the amount of respiratory related target motion for the two targets implanted into this lung. The right is a CT of the same lung after draining the fluid. . . . .	64
B.1	The Washington University 4D Phantom. . . . .	75
B.2	Lung motion model. The motion of the object at baseline (circle) is shown at a given phase point (square). Component vectors related to the tidal volume ( $\vec{r}_v$ ) and airflow ( $\vec{r}_f$ ) predict the position of the object ( $\vec{r}_p$ ) with respect to baseline ( $r_{p0}$ ) at any phase of the breathing cycle.	76

# Chapter 1

## Introduction

The accuracy of intervention on targets within the body has increased in conjunction with advances in technology. In areas ranging from surgery to radiation therapy, treatments and diagnostic procedures are becoming more precise and less invasive.

For targets within the lung and abdomen, respiration causes substantial motion and tissue deformation. Targets near the diaphragm can move at amplitudes up to several centimeters. With recent advances in interventional techniques, the accuracy of many systems are currently limited by respiratory motion. Failure to account for this motion can lead to inaccuracies, complications and decrease the effectiveness of procedures within the lung and abdomen.

For biopsies of targets within the lung, the diagnostic yield decreases as the spatial error associated with the biopsy increases. It is more complicated to obtain accurate samples of mobile targets due to the fact that the physician is now intervening in both space and time. Conventionally these procedures have been guided using real-time imaging, such as fluoroscopy or ultrasound. In clinical use, both of these modalities are limited to two dimensions. Fluoroscopic imaging delivers ionizing radiation to both the surgeon and patient, and ultrasound suffers from low soft tissue contrast. Many pulmonologists will only attempt biopsies on tumors of larger size ( $>1\text{cm}$ ) due to accuracy limitations. A more accurate means of intervening on mobile tumors within the lung would allow physicians to biopsy smaller lesions; providing early detection and improvement in patient outcomes.

Radio frequency ablation (RFA) also could benefit from respiratory correlated guidance. In this technique, lesions are heated using a radio frequency probe. Currently

RFA is commonly used for liver lesions, however clinically stereotactic radiosurgery is preferred over RFA for lesions within the lung. Liver applications are currently limited to regions far from the diaphragm and large blood vessels due to respiratory motion and heat dissipation concerns respectively. Failure to account for respiratory motion could lead to the probe being positioned incorrectly, resulting in ablation of healthy tissue. A respiratory correlated intervention system for RFA has the potential to increase accuracy and allow for minimally invasive procedures in the lung and liver on targets proximal to the diaphragm.

In radiation oncology, linear accelerators are capable of delivering radiation to the patient with high accuracy (1 mm). Inaccuracies can result from daily routine patient alignment, or respiratory motion within a treatment. Although most modern linear accelerators are equipped with on-board imaging (OBI) systems, the computational power needed to segment and determine a tumor location in real-time is not available. Additionally, many linear accelerators offer cone beam CT imaging, however acquisition takes approximately 60 seconds and as a result motion blur artifacts are substantial. In order to account for inaccuracies associated with the target position and ensure the target receives the prescribed radiation dose, margins, or buffer areas surrounding a target, are added and irradiated during the treatment. Current clinical margins at Washington University Medical School for standard lung tumors are 1cm additions on each side. Increasing the accuracy at which the target location is known could result in decreased treatment margins and spare healthy tissue from irradiation. Healthy tissue dose is the limiting factor in escalating the dose to tumors. It has been shown for non-small cell lung cancer (NSCLC) that escalating the dose to the tumor volume ( $>70$  Gy) can provide better local control than lower doses ( $<70$  Gy) [10, 77]. Increased accuracy in the presence of motion shows promise for escalating dose to the tumor site while sparing surrounding healthy tissue.

A system from Calypso Medical provides small implantable wireless transponders which are sequentially queried to report the position of up to three points within the patient's body. An array is placed above the patient, and the transponder positions are monitored with respect to the array via electromagnetics. The specifics regarding how the system works are described in Appendix B.9. Balter et al have reported submillimeter accuracy when tracking the transponders moving at 3 cm/s in a volume that is 14x14 cm in width, and up to 27 cm away from the source array [2]. In a

study from Santanam et al the system was again found to be sub-mm accurate as confirmed by onboard kilovoltage imaging [78]. The system is currently FDA cleared for use in the prostate, and potential applications in the lung and abdomen (where motion is substantial) are promising.

Additionally, Medtronic Navigation has developed a system of tracking surgical instrument tips in real-time. The StealthStation system is currently used for craniospinal applications in which the patient's head is stationary. The system displays the tool tip overlaid on an *a priori* acquired CT or MRI image. Guidance is provided in real-time to ensure the physician is taking the intended path to the target. The system currently is not used for targeting within the lung or abdomen due to respiratory motion and soft tissue deformation concerns. Surgical navigation within these areas would be useful for tumor biopsies, radio frequency ablation (RFA), or brachytherapy seed placement.

Imaging systems provide high spatial accuracy, however the temporal accuracy of target localization is not suitable for real-time lung target interventions. Due to their high temporal accuracy, the aforementioned electromagnetic systems have potential to increase treatment capabilities in both radiation therapy as well as image guided surgery procedures. This dissertation covers work associated with creating new interventional systems for lung applications by integrating electromagnetic tracking. In the following chapters, these specific aims are addressed in more detail:

- 1.1 Specific Aim 1: Incorporate real-time electromagnetic position monitoring into a spatial gating solution for motion management in the delivery of radiation therapy.
- 1.2 Specific Aim 2: Incorporate real-time electromagnetic position monitoring into a Dynamic Multileaf Collimator (DMLC) tracking system for highly accurate continuous radiation delivery to mobile targets
- 1.3 Specific Aim 3: Determine the accuracy of an internal fiducial marker with known position at predicting adjacent target motion.
- 1.4 Specific Aim 4: Develop a robust system for image guided surgery (IGS) applications in the presence of respiratory motion.



# Chapter 2

## Linear Accelerator EM Gating

### 2.1 Introduction

The goal of radiation therapy is to maximize the absorbed dose to the target volume while minimizing the dose to surrounding healthy tissue. Intrafraction motion due to respiration can cause the tumor to move considerably throughout treatment. The displacements associated with respiration can be up to 3 cm within the thorax. [41] To account for this motion, radiation oncologists must incorporate substantial margins (typically 1 cm superior/inferior and 0.5 cm for both anterior/posterior and lateral) in the design of each planning target volume (PTV). This leads to large volumes of irradiated normal tissue that can limit the total dose that the patient can safely receive. This has led researchers to explore beam gating techniques with the goal of more accurate radiation delivery to tumors impacted by respiratory motion.

Respiratory correlation has been used extensively in CT and MR imaging in an effort to reduce breathing related image artifacts.[74, 69] More recently, similar techniques have been employed to localize the tumor and gate the linear accelerator.[91, 49, 35, 37, 8] Conventional gating setups use a variety of techniques to measure breathing motion including: optically tracked external marker blocks, thermocouples, thermistors, strain gauges, and pneumotachographs.[38] Current techniques rely on the use of external markers or sensors to determine the internal position of the target. Although a correlation exists between external markers and internal tumor position, for some patients external marker trajectories do not serve as an adequate surrogate for internal tumor position.[16]

Respiration induces considerable deformation within the thoracic cavity. As the diaphragm contracts, internal anatomy compresses and distends. Often the external anatomy exhibits good correlation with the motion of the internal structures such as the diaphragm and/or lung tumors.[49, 16] The external anatomy moves due to respiration, however studies have shown considerable differences between external anatomy and internal motion. These differences can come in the form correlated motion with a phase lag between the external and internal motion, or less frequently the motion might not exhibit correlation. Margeras and Yorke have reported up to a 0.5 second lag between Varian RPM marker block position and diaphragm position measured fluoroscopically.[51] Koch et al found that correlation was poor and unstable unless the external surrogate measuring skin surface position was near the tumor.[36] In a study from Berbeco et al, lung tumor motion was measured via continuous fluoroscopy concurrently with measurement of external abdominal surface positions.[7] The amount of residual tumor motion, defined as the amount of tumor motion during a respiratory gate based upon the movement of the external surrogate, showed large fluctuations (>300%) for both intra- and inter-fraction motion. The residual motion was found to be up to 8 mm in magnitude, which strongly suggests that external position monitoring cannot accurately reflect the internal position of a tumor for all cases. The periods in which external and internal motion exhibit poor correlation are often transient; however these transient periods may have dosimetric implications.[68]

The lack of correlation between internal/external positions has led investigators to examine alternative techniques for accurately tracking the position of targets inside the thoracic cavity. Shirato et al developed a real-time target tracking system that uses four integrated kilovoltage imaging systems.[89] The fluoroscopic imaging system used in this technique provides accurate information on the location of discrete points inside the abdomen. However, accurate tracking of the target comes at the expense of an increased imaging dose. For a single fluoroscope, the estimated skin surface dose rate can be up to 118 cGy/h.[93] In addition, for 3D target tracking, stereoscopic fluoroscopes are necessary which means further accumulated dose due to imaging.

The Synchrony<sup>TM</sup>Respiratory Tracking System (RTS) treatment option of the CyberKnife robotic radiotherapy system provides another image based system for tracking internal fiducial markers.[85] With this technique, gold fiducials are placed inside the thoracic cavity near the tumor while the patient wears a vest with LEDs that

indicate the position of the chest or abdomen. Before the treatment begins, a series of orthogonal x-ray images are acquired that are used to correlate the position of the external markers to the internal fiducials. A correspondence model is developed and periodic images are obtained during the course of delivery to ensure the continued validity of the correspondence model. While the Synchrony™ RTS delivers a lower radiation dose to the patient as compared to continuous fluoroscopic imaging, this is achieved at the expense of intermittent absolute knowledge of internal positions. TG75 states that the entrance dose per image can be as high as 0.2 cGy.[64] For a 2 hour session with imaging performed every 30 seconds, the patient receives 48 cGy over the course of the treatment. Alternative image based solutions have been investigated which utilize the on board imaging (OBI) functionality of many modern linear accelerators.[6] Similarly to the fluoroscopy based solutions previously mentioned, OBI solutions deliver dose to the patient in order to image and track internal markers/tumors. Another factor limiting this technique is the fact that high energy MV scatter from the treatment beam can degrade the image quality of the kV images typically used for tracking.[47] Imaging based methods do have the advantage of providing information about the surrounding tissue, which a pure electromagnetic position monitoring solution cannot provide.

Continuous electromagnetic position monitoring is now available without additional dose to the patient (Calypso Medical, Seattle WA). The system uses one or more wireless transponders which are subject to performance testing as part of the manufacturing operation to ensure they can stand up to high levels of radiation throughout the treatment process. The transponders are currently implanted into the prostate via a 14-gauge needle in a procedure similar to existing gold fiducial implants currently in use clinically. During treatment planning, the location of the transponders is recorded with respect to isocenter and a plan is developed. During delivery, an array is placed above the patient. Four source coils in the array excite the transponders via magnetic induction. After excitation, 32 receiver coils in the array detect the resulting response signal. Each transponder has a unique resonant frequency, and they are sequentially excited in order to independently query position information. The array is registered to the room via stereoscopic infrared cameras, and hence the transponder position is known with respect to isocenter. Balter et al have reported submillimeter accuracy when tracking the transponders moving at 3 cm/s in a volume that is 14x14 cm in width, and up to 27 cm away from the array.[2] In a study

from Santanam et al the system was again found to be sub-mm accurate as confirmed by concurrent onboard kilovoltage imaging.[78] In a clinical prostate cancer treatment study, Willoughby et al have shown the system to be functional in a linac environment, even when the linac is treating directly through the array.[108] To date there have been no published failures of the transponders due to radiation dose. The system is currently FDA cleared for use in the prostate and prostatic bed. Potential applications in the lung and abdomen (where motion is substantial) are promising. In this study, we have investigated the feasibility of using real-time electromagnetic tracking for linac gating. The system uses a spatial gating technique which gates the beam via absolute 3D position of the internal fiducials (Figure 2.1) as opposed to using phase or amplitude like conventional external surrogate systems currently use. This approach has two primary advantages: (1) the beam is gated off of the internal position of the tumor as opposed to an external surrogate and (2) it does not require any additional imaging dose.

## 2.2 Gating: Latency Estimates

In order to characterize the system initial latency estimates were performed. If the latency between the time the target leaves the volume to the gating of the linear accelerator is large when compared with the velocity of the target, this can lead to substantial dosimetric error. In an initial study to determine the latency of the system, the signal directly from the dynamic phantom was compared with the “target current” test-point signal from the linear accelerator using a logic analyzer. Target current is the current measured at the metal target of the linear accelerator’s electron beam and hence this signal is analogous to the presence or absence of the treatment beam. Using the target current as opposed to radiographic methods permits a more precise measurement of latency using standard test equipment. It also facilitates acquisition of large numbers of beam transitions for accumulating a histogram of latencies. The Calypso system was set to monitor positions at 30hz with an update period of approximately 26ms. Based on this method, a histogram of latencies was generated over the motion from 200 circular motion cycles (Figure 2.2).

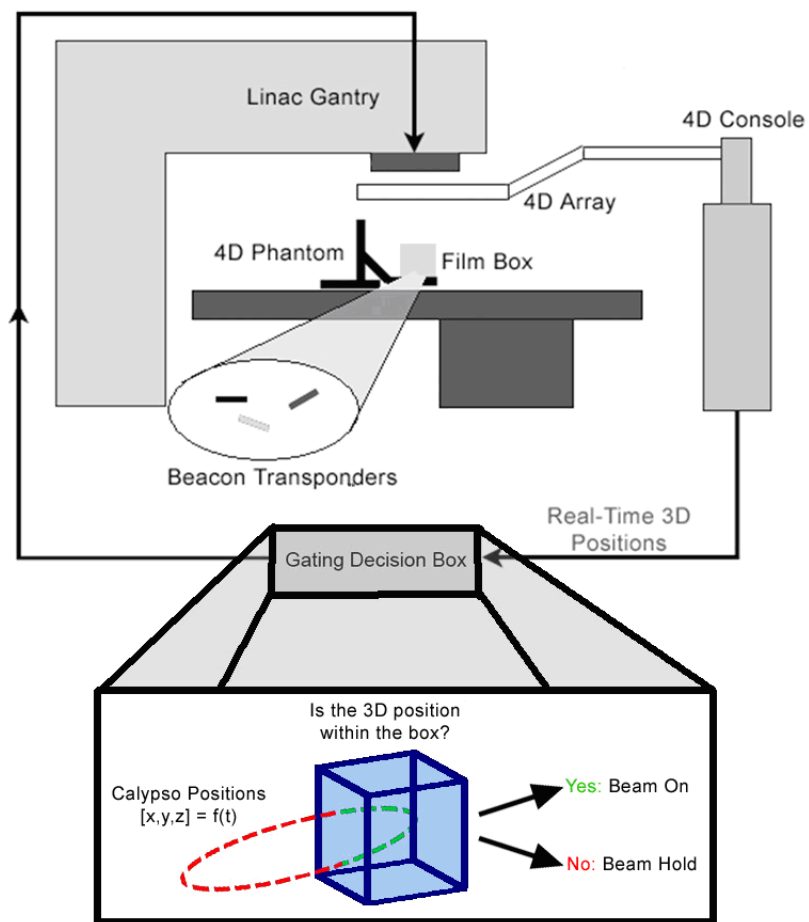


Figure 2.1: Gating setup. The 4D phantom moves the attached film phantom in realistic breathing trajectories. Real-time position information of the transponders implanted in the film phantom are acquired via the array and sent to a decision making computer. Each position measurement is analyzed to determine whether it is inside a predefined 3D volume. If so, the beam is turned on and delivery proceeds. If the position is outside the volume, a Beam Hold is enacted and delivery halts until the target returns.

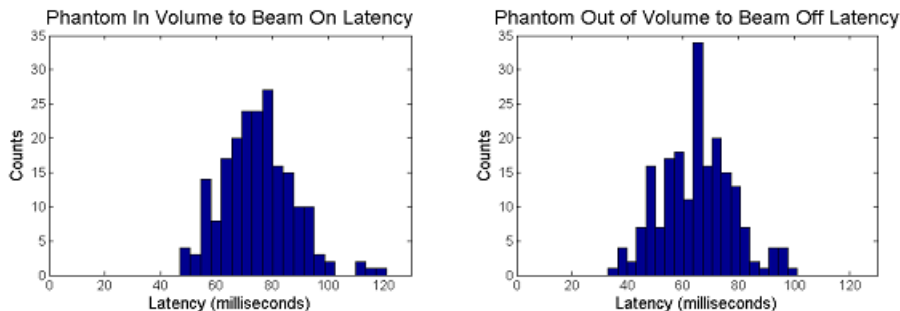


Figure 2.2: Latency histograms for the gating system.

The latencies were broken down into two categories: beam-on latency and beam-off latency. Beam-on latency is defined as the time duration from target entering gating volume (as indicated by signal from motion phantom) to first observed target current pulse on the LINAC. Beam-off latency is defined as the time duration from target leaving gating volume (as indicated by signal from motion phantom) to last observed target current pulse on the linac. The mean latencies between transponder position and linear accelerator modulation were found to be  $75.0 \pm 12.7$  msec for beam-on and  $65.1 \pm 12.9$  msec for beam-off given as mean  $\pm 1$  standard deviation (Figure 2.2). The difference between the beam-on and beam-off times could be attributed to asymmetry in the LINAC turn-on and turn-off times, or partially due to imperfect alignment of the phantom with respect to the Calypso gating volume. The range in the latencies can be attributed to the software implementation of the gating decision unit, as well as the finite integration times of the transponders (26ms). The latency associated with enacting a Beam Hold or reestablishing treatment via the linear accelerator is relatively small, approximately 17 msec [22]. Given the experimental setup, this value is incorporated into the total latency values reported for the spatial gating system. Update rates and latencies of the system are comparable to optical [28] and fluoroscopy [91] based gating systems reported previously.

## 2.3 Gating: Clinical Dosimetry

In addition, clinically relevant dosimetric analyses were performed. A four field, 6MV, 200 cGy, 3DCRT treatment plan for a random lung cancer patient was selected for

this study. The treatment plan was developed using Pinnacle version 7.1 (Philips, Madison, WI) and delivered via a Varian Trilogy linear accelerator. The phantom in this study was comprised of a standard solid water phantom with one sheet of the solid water replaced with an equivalently sized acrylic slab containing three electromagnetic transponders as well as a piece of radiographic film. For each exposure, the film was placed in the coronal plane. The platform was programmed using respiratory motion data measured for a lung cancer patient using 4DCT and spirometry (Figure 2.3) [45].

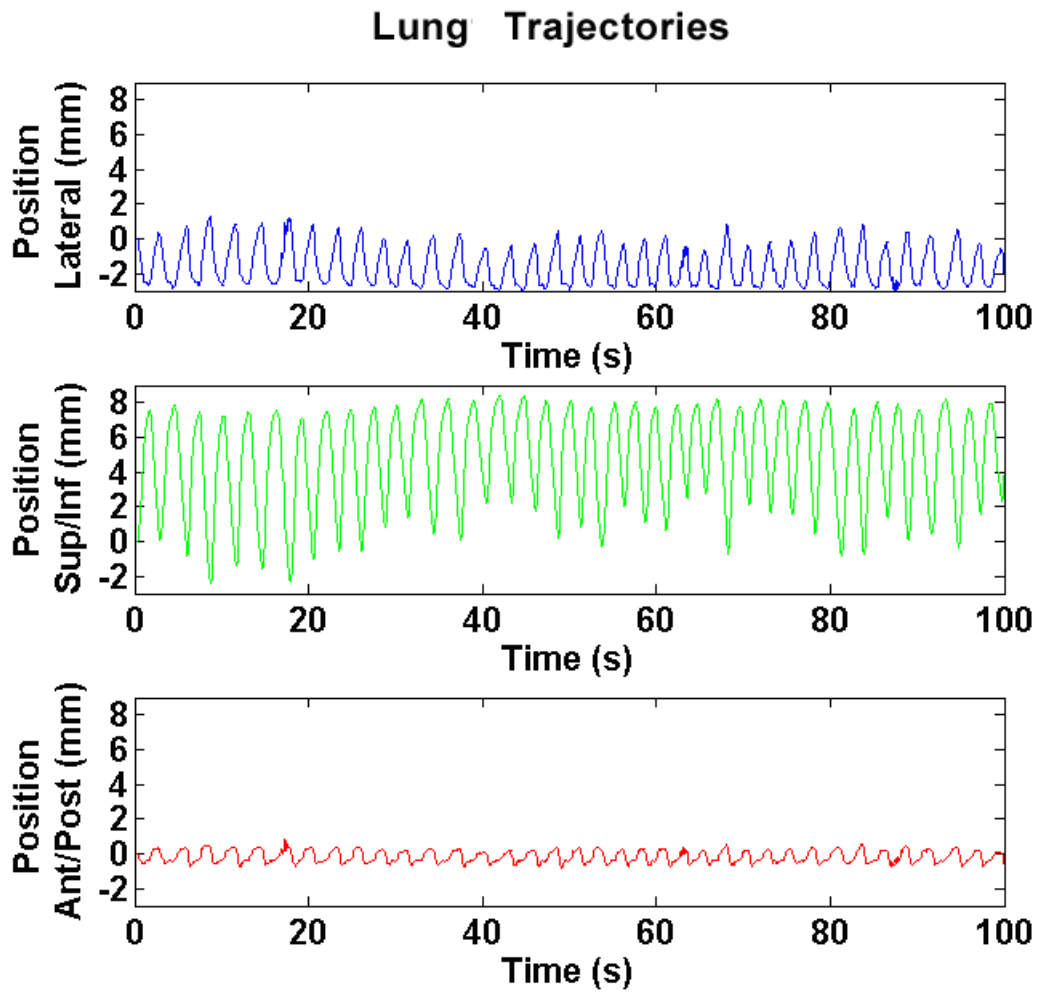


Figure 2.3: Lung trajectories reconstructed from a 4DCT and spirometry from a lung cancer patient.[45]

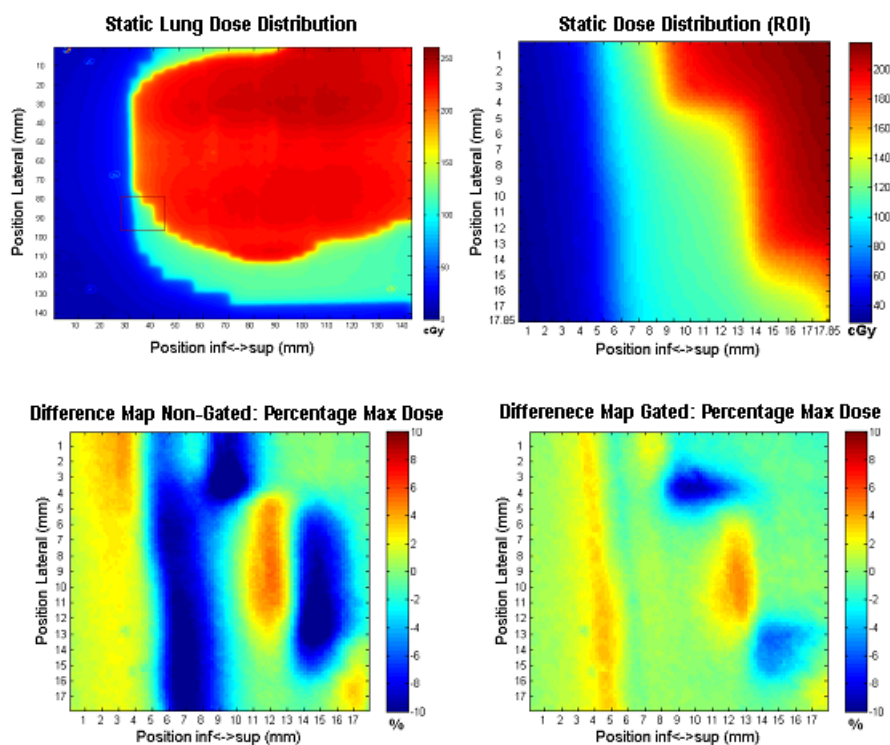


Figure 2.4: Dose difference maps. Films irradiated in the presence of clinically relevant motion were subtracted from the static ‘gold standard’ case. A) The entire dose profile with the ROI indicated via a box.. B) The high gradient region of interest as denoted by the box in A). C/D) Normalized difference maps were calculated to show over- and under-dosing as a percentage of maximum dose. Red and blue regions indicate over and under dosing respectively. Gating reduces the spread and magnitude of dose mismatch that occurs in the presence of motion.



Dosimetric films were utilized to determine the dose profile from one fraction of treatment. One baseline run with no motion was used to generate a static film. This film was used as the ideal dose distribution in the absence of patient motion. The static film was compared with films irradiated using the same treatment plan delivered both with and without gating in the presence of motion. Using beam gating, better dose localization was observed and the film results show better correlation with the static dose distribution (Figure 2.4). The effects of gating were most evident in the regions of high dose gradient, as the non-gated case effectively ‘blurs’ the dose over the region that passes through the isocenter during respiratory motion. Difference maps show that dose blurring found in the non-gated dynamic case is significantly reduced when the gating solution is implemented (Figure 2.4). Dosimetric analysis was performed to quantify the level of over/under dosing. For the no intervention case, 32.1% of points failed to be within  $\pm 10$  cGy from the ideal dose and 8.6% failed for  $\pm 20$  cGy. For gating, 3.4% failed for  $\pm 10$  cGy and 0.0% failed to be within  $\pm 20$  cGy.

Gamma analysis was performed on both the non-gated and gated films. Although no points failed a 3mm/3% test, 8.3% of the points in the non-gated film failed at 1.5mm/1.5% compared to 0% of the points in the gated film (Figure 2.5).

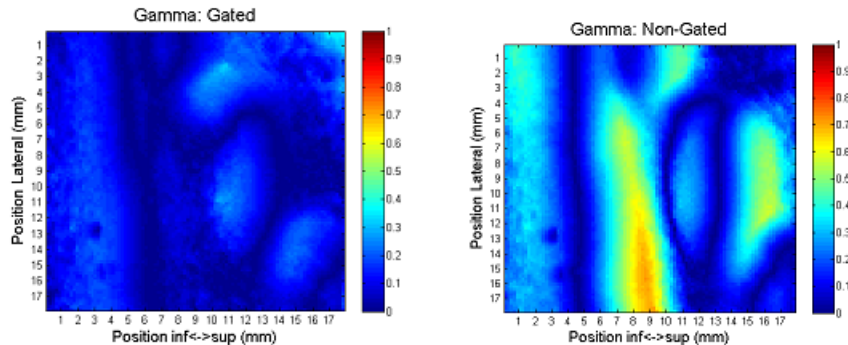


Figure 2.5: Gamma Maps. Gamma maps for the gated and non-gated cases are displayed. As described previously, the gamma tool allows for simultaneous analysis of both distance to agreement and dose difference. Lower values indicate higher dosimetric agreement.

It is evident in multiple line profiles that gating produces an increase in achievable dose gradients (Figure 2.6). This increase in dose gradients has clinical implications. For targets that are close to critical structures, it is ideal to have high dose to the

target with rapid falloff of the dose to spare the adjacent tissue. Increasing the achievable dose gradients in the presence of motion ensures better dose conformity to the target and increases tissue sparing to adjacent tissue. Patient throughput is a clinical concern. Even when considering the small gating window used for these preliminary studies, the duty cycle was 47% and 49% respectively for each of the two lung trajectories. This shows that for most cases the increase in treatment time is small when compared to the time spent initially aligning the patient and moving the gantry to the various beam angles. This will not be the case for instances of drastic motion or when the target leaves the gating volume for an extended period of time.

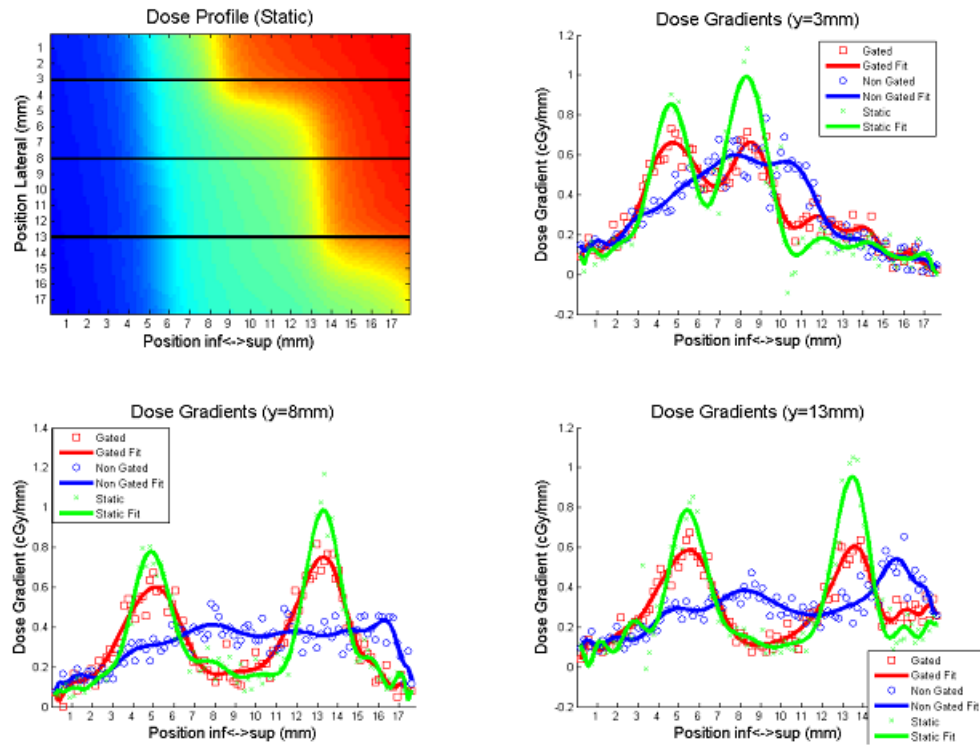


Figure 2.6: Gating reduces dose blurring and improves dose gradients when compared to no intervention. Here, dose gradients of line profiles are analyzed for lines at  $y=3\text{mm}$ ,  $8\text{mm}$ , and  $13\text{mm}$  (b-d). Raw data is plotted with a polynomial fit overlaid. It is evident that gating improves dose gradients to match the delivery in the absence of motion.

## 2.4 Gating: Discussion

Gating is a widely used technique for dose localization. One of the limiting factors in the effectiveness of gating is that most implementations use external markers to predict internal movement of tumors. Although studies have shown correlation between external and internal motion, variations on the order of 1 cm have been found between internal fiducial motion and external markers.[16, 7] Thus it is important to implement a solution for determining the precise location of internal anatomy without exposing the patient to additional imaging dose throughout the course of treatment.

It has been shown that large latencies can produce a phase mismatch between beam gating and tumor position.[86] For the initial studies shown here, a software based decision making setup was implemented. For a clinical implementation, a hardware based solution would offer lower latencies. The latencies associated with our system are as good as or better than alternative options. For instance, fluoroscopic and optical gating systems claim latencies of 90 ms[89] and 170 ms[28] respectively. Note that the low latencies associated with our setup demonstrated a measurable dosimetric difference without the use of predictive algorithms.[86] This internal tracking implementation can be incorporated with any linear accelerator in a standard size vault.

In a clinical implementation the exact dimensions of the 3D gating volume will likely vary from patient to patient. The 3D volume would be chosen based on a number of factors: the relationship and level of correlation between the transponder and the tumor as evidenced via respiratory correlated imaging, the proximity to normal structures, the amount of target motion, and the desired efficiency of the treatment. The number of implanted transponders does have an adverse affect on the update rate of the system. The use of a single transponder increases the acquisition frequency for the spatial position information, but at the expense of rotational information obtained via multiple transponders. Studies are needed to determine the cost/benefit from acquiring spatial information from multiple transponders when compared to the additional latency associated with multiple transponder readings. For instance, in a potential clinical implementation multiple transponders could be used during the patient setup process, but a single transponder localized for gating throughout the treatment.

Work is needed to ensure that implantation in the lung is safe. Pneumothorax is a typical complication with percutaneous implantation of a fiducial in the lung. Although bronchoscopic implants have lower pneumothorax rates (1.8%)[26] than implants done percutaneously (33%)[105], additional work is needed to ensure the system is safe for patient use. Work in developing a bronchoscopic implantation technique for electromagnetic transponders is promising.[56]

Additionally, the implanted EM transponders have been shown to be stable in the prostate case. Targeting of a lung tumor may be more challenging since the transponders will not likely have a fixed relationship to the lung tumor. Incorporation of the uncertainty will affect the size of a gating window. Work on a modified transponder design with stability features shows good fixation to the lung tissue.[56]

If left unchecked, breathing motion prevents high dose gradient regions in which the delivered dose to the surrounding healthy tissue decays rapidly. High dose gradients are necessary for dose escalation to tumor sites while ensuring that surrounding critical structures do not receive substantial dose. As noted in Figure 2.6, the dose gradients achieved via the gating solution are larger when compared to no intervention in the presence of motion.

In conclusion, an electromagnetic tracking system has been successfully interfaced with a linac gating system. The latencies measured were comparable to other real-time radiation therapy systems, and film experiments using realistic lung trajectories showed that gating provides significant dosimetric improvements. The aforementioned gating study has been published in a peer reviewed journal.[95]

# Chapter 3

## DMLC Tracking

### 3.1 Introduction

Due to the widespread adoption of MLCs for use with conformal and IMRT treatments, it is intuitive and cost effective to implement a motion management solution relying on already implemented hardware. Dynamic MLC (DMLC) tracking is a technique that attempts to mitigate the dosimetric error associated with target motion by updating the positions of the beam-attenuating leaves based on real-time target position. This technique effectively moves the aperture such that the beam is continuously centered on the target. This technique alleviates some of the problems associated with gating. For instance, if a prostate target moves outside of the gating volume indefinitely due to rectal filling, a gating solution requires the therapist to enter the treatment room and reposition the patient. At the time of this manuscript, there has been much published on DMLC tracking [33, 71, 72], however there are currently no clinical implementations. Additionally, to date all published work on MLC tracking has relied on external position monitoring, which has associated limitations as noted previously in the Background and Significance section. We intend to implement an MLC tracking solution in which the beam aperture is moved corresponding to real-time output from the Calypso electromagnetic position monitoring system. In order to characterize the system latency estimates, geometric accuracy and dosimetric measurements must be performed.

## 3.2 DMLC Tracking: Latency Estimates

There are a variety of factors contributing the latency between target position measurement and MLC response. There is an integration time associated with electromagnetic position monitoring. Once positions are acquired, new leaf positions must be determined based on the new location of the target. Additionally, the leaves have finite velocities and hence the time required to move into position must also be accounted for. Here we define latency as the time between when the target is at a given location and the time at which MLC aperture is centered at that location. If the latency of the system is substantial when compared to the velocity of the target, it is necessary to implement prediction algorithms in order to maximize geometric accuracy. In an experiment designed to characterize the latency of the DMLC tracking system, a motion phantom was programmed to move in a sinusoidal trajectory ( $\pm 1.5$  cm, 15 cycles/min) parallel to the direction of leaf motion. The phantom carried Calypso Beacon transponders, as well as a steel BB that shows up clearly on Electronic Portal Imaging Device (EPID) images. EPID images were continuously recorded as the static prediction window of the DMLC tracking system was systematically varied for each run from 0 to 250 ms. The EPID images were segmented offline in order to determine both the location of the steel BB as well as the center of the MLC defined aperture. The BB location is analogous to the instantaneous position of the target, and based on the spatial offset between this position and the center of the aperture the latency of the system was calculated to be 220ms. Target and aperture trajectories recorded in the absence of motion are shown in Figure 3.1.

## 3.3 DMLC Tracking: Geometric Accuracy

The geometric accuracy of the system was characterized in a similar manner to the method used for calculating the latency of the system. EPID images were acquired and segmented to determine the geometric offset between the target as indicated by the steel BB and the MLC defined aperture center. For the geometric analysis, the motion phantom was programmed with the following three trajectories: a respiratory trace showing high variability, recorded using a dual-fluoroscopic real-time radiotherapy (RTRT) system [91], a respiratory trace showing moderate variability, recorded

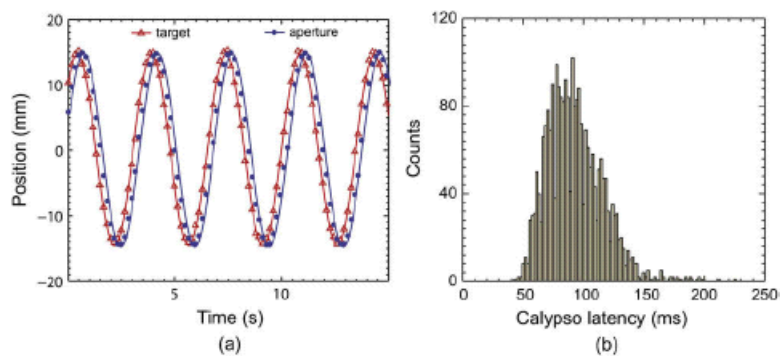


Figure 3.1: Target (BB) and MLC aperture trajectories in the run recorded with no prediction. These values were used to calculate the total temporal latency of the system ( 220 ms). Figure credit Sawant *et al.* [81].

using the Synchrony system [100] and a prostate motion trace showing relatively high variability, recorded using the Calypso system [39]. For all geometric accuracy measurements, the DMLC tracking system was set to update using 220ms prediction. Figure 3.2 shows the geometric accuracy of the system for the aforementioned trajectories. Accuracy parallel and orthogonal to leaf orientation is characterized independently due to independent physical limitations of the MLC leaves. The geometric results were evaluated favorably and have been published in a peer reviewed journal.[81]

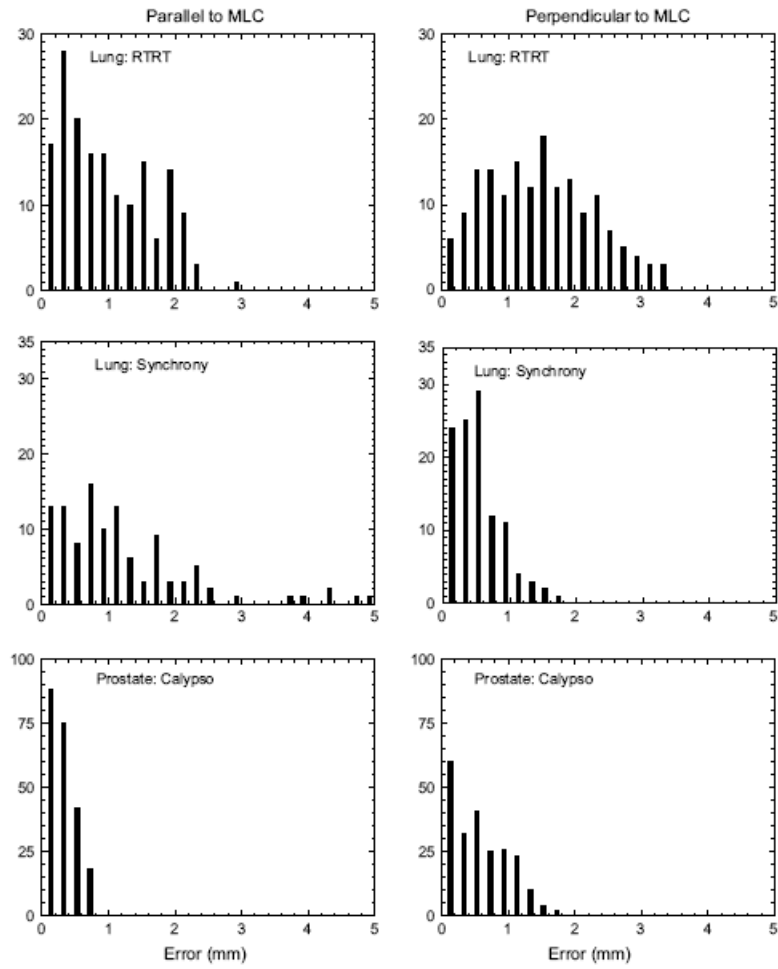


Figure 3.2: Distributions of geometric accuracy for three different motion trajectories. Figure credit Sawant *et al.* [81]



### 3.4 DMLC Tracking: Dosimetric Accuracy

Even with known geometric accuracy of the system, there remain some clinical questions regarding implementation. Interplay between the IMRT delivery technique and tumor motion can lead to dosimetric error [27, 102, 5]. Moreover, the addition of a motion tracking system to MLC movement during delivery adds complexity to the therapy quality assurance. Here we intend to investigate the dosimetric effects of coupling the electromagnetic position measurement guided DMLC tracking system with IMRT delivery for targets with substantial intrafraction motion and compare the dosimetric accuracy of this technique with gating via internal position monitoring. Our hypothesis was that an integrated electromagnetic position measurement - DMLC tracking system should show similar dosimetric results to electromagnetic position measurement - gating system, but with improved efficiency.

Similar to the previous experiments, the Calypso system was configured to output 3D positions in real-time. The following settings were used for all cases: gantry  $90^\circ$ , collimator  $90^\circ$ , 200 MU delivered via a 6 MV photon beam. The MLC leaves for both the S-IMRT and D-IMRT plans are aligned in the superior/inferior (primary) direction of motion. The delivered dose for each plan was approximately 100 cGy at isocenter. The moving phantom was loaded with a single film aligned in the sagittal plane at isocenter and irradiated as it moved with two different plans: (1) an S-IMRT field, and (2) a D-IMRT field. The phantom was programmed with no motion, or with motion obtained from a lung cancer patient using the CyberKnife Synchrony (Accuray, Sunnyvale, CA) tracking system [100]. The trajectory had a frequency of 23 breaths/min and had the following peak to peak amplitudes: 7mm lateral, 23 mm sup/inf, and 6 mm ant/post. The breathing trajectory was relatively periodic, however not totally uniform throughout the treatment. Dosimetric results in the presence of motion were recorded for each plan using three different effector systems: no intervention, DMLC tracking, and a 4mm x 4mm x 4mm spatial gating system. The comparators for the dosimetric results in the presence of motion were the dose results obtained with a static target.

Plan	Intervention	3%, 3mm	6%,6mm	$\pm 3\text{cGy}$	$\pm 5\text{cGy}$
Step+Shoot	Gating	0.18%	0.00%	10.91%	3.26%
Step+Shoot	DMLC	1.21%	0.00%	7.53%	2.73%
Step+Shoot	None	2.45%	0.16%	10.86%	5.02%
D-IMRT	Gating	0.22%	0.00%	3.30%	0.64%
D-IMRT	DMLC	0.24%	0.20%	7.20%	2.02%
D-IMRT	None	1.55%	1.09%	13.06%	4.99%

Table 3.1: Dosimetry Failure Rates. Gamma failure rates were reported for all cases. Note that failure rates for D-IMRT plans were comparable for gating and DMLC tracking. S-IMRT gating outperformed DMLC tracking. Gating and DMLC tracking outperformed no intervention in both plans.

Figure 3.3 shows the dose difference maps between the effector systems and the static ‘gold standard’ film. For the S-IMRT case (Figure 3.3a), the DMLC tracking difference map and gating difference map show similar amounts of mismatch, though the locations of the mismatch differ. For the single field D-IMRT difference maps (Figure 3.3b), the gating and DMLC tracking films are comparable. The dose in the interior of the region is relatively homogeneous, and as a result a difference map is not the best metric for observing dose artifacts due to motion. In the S-IMRT delivery, the percentage of points with a difference of  $\pm 3$  cGy from the static case were 10.91% and 7.53% for gating and DMLC tracking respectively; for the D-IMRT 3.30% failed for gating while 7.20% failed for DMLC tracking (Table 3.1). Analysis of the gamma output for 3mm and 3% shows that gating outperforms DMLC tracking for the S-IMRT case with failure rates of 0.18% and 1.21% respectively (Figure 3.4). For the D-IMRT case the two intervention methods were comparable, with failure rates of 0.22% for gating and 0.24% for DMLC tracking (Table 3.1). Both methods of intervention outperform no intervention with failure rates of 2.45% and 1.45% in the presence of motion for the S-IMRT and the D-IMRT plan.

### 3.5 DMLC: Tracking: Efficiencies

In addition to dosimetric accuracy, the delivery efficiencies were recorded for each case. The ‘Beam-On Time’ and ‘Total Time’ displayed on the console of the linac were recorded for each delivery. These metrics are used to determine the efficiency of

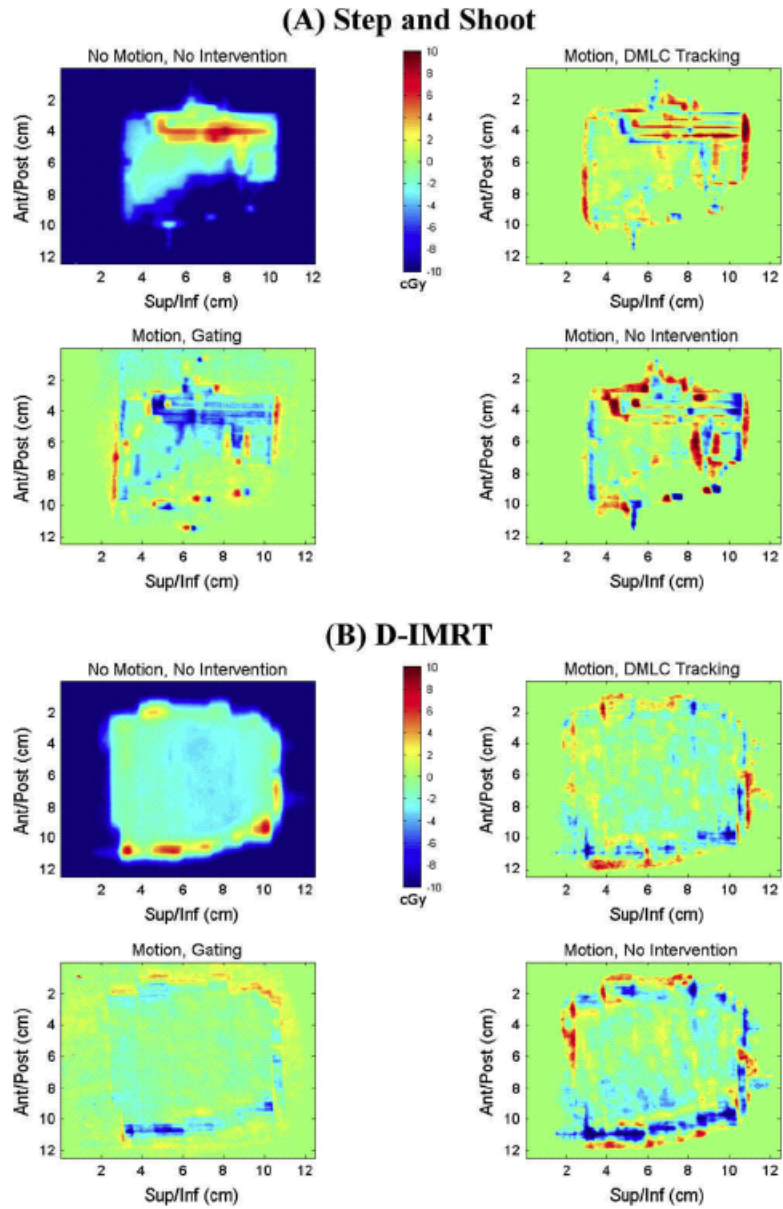


Figure 3.3: Difference maps were produced after registering the dose profiles in the presence of motion with the film obtained via static delivery (the ‘gold standard’). The control from runs in the absence of motion are given as a reference in each case.

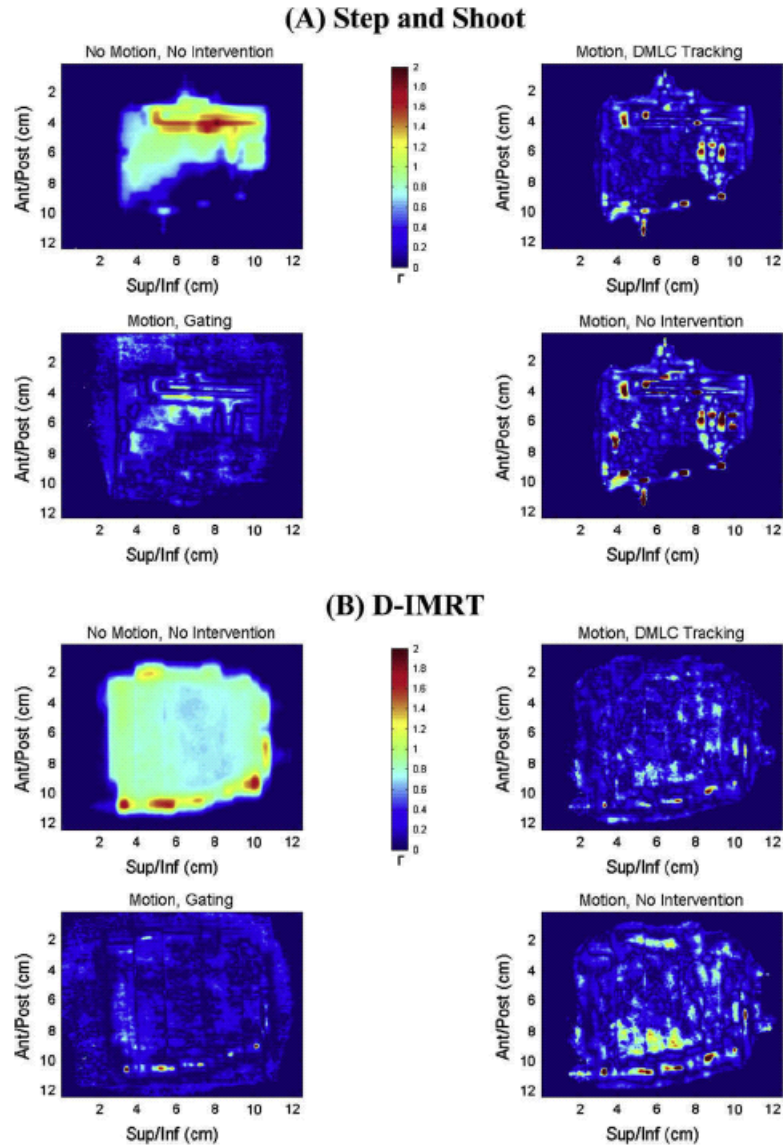


Figure 3.4: Gamma values were calculated for each of the moving images. The values for the distance to agreement criterion  $\Delta d = 3\text{mm}$  and the dose agreement criterion  $\Delta D = 3\%$  of the maximum dose. The control runs in the absence of motion is given as a reference for each case.

<b>Plan</b>	<b>Intervention</b>	<b>Beam On Time (min)</b>	<b>Total Time (min)</b>	<b>Duty Cycle (Normalized)</b>
Step+Shoot	Gating	0.30	1.68	38%
Step+Shoot	DMLC	0.32	0.60	100%
Step+Shoot	None	0.32	0.64	100%
D-IMRT	Gating	0.30	0.53	22%
D-IMRT	DMLC	0.32	0.36	100%
D-IMRT	None	0.33	0.35	100%

Table 3.2: Efficiency Values. Delivery efficiencies were recorded in the form of Beam on Time and Total Time for each of the delivery conditions. Values along with associated duty cycles are reported. The duty cycle values are normalized to the static delivery case (100% indicates no efficiency drop due to intervention).

delivery for each effector system. Delivery without intervention requires Beam Holds as the leaves in the MLC move from position to position. Our metric for efficiency uses a normalized duty cycle in which 100% matches the efficiency of delivery without intervention. Results show that DMLC tracking provides for drastic improvements in delivery efficiency when compared to beam gating (Table 3.2). DMLC tracking and beam gating showed duty cycles of 100% and 38% when delivering the S-IMRT plan. In addition DMLC tracking outperformed gating in the D-IMRT plan (100% and 22% respectively). The dosimetric and efficiency results have been published in a peer reviewed journal.[96]

### 3.6 DMLC: Tracking: Discussion

We have successfully implemented a tracking system that does not rely on ionizing radiation or an external tumor surrogate for the detection of internal targets. The DMLC tracking solution shows promise for the reduction of motion-related dosimetric errors. However there are several details that still need to be addressed. For the case of the D-IMRT plan, the gating solution produced comparable dosimetric output when compared with the DMLC tracking. The D-IMRT plan shows relatively few high dose gradient regions in the center of the dose distribution. As a result, in the interior of the target the dosimetric errors associated with superior inferior motion are not as evident from a difference map.

The S-IMRT delivery to the moving phantom with no intervention corresponds to a convolution of the beam profile for each step-and-shoot segment with the motion of the phantom during delivery of that segment. With gating, the delivery corresponds to a convolution with the residual motion within the gating window. Therefore, one would expect small blurring of the dose profiles with dosimetric errors related to the size of the gating volume. The errors associated with DMLC tracking are not as lucid. Here, the discrepancy with the static case is caused by failure to align instantaneously to the target position and the coarse (one leaf width) aperture resolution orthogonal to the leaf direction. It is possible that the target motion oscillated in a fashion that dictated a shift back and forth of one leaf position in the anterior/posterior direction, this could lead to substantial dosimetric error on the order of the size of the 1 leaf (5 mm). It should be noted that our algorithm did not use subleaves to estimate motion orthogonal to the leaf direction.[82] As a result, a shift in the anterior/posterior direction is ‘all or nothing’ which could have potentially led to the dosimetric error seen in the S-IMRT DMLC tracking films.

It is notable that increased efficiency has potential for dosimetric implications, not just patient throughput. If the patient is on the table considerably longer (*e.g.* when using a very small gating window), it is possible the patient will move due to discomfort. Though not in the scope of this experiment, this motion has potential dosimetric consequences.

There is further work to be done on the system. Currently there is variable latency in the position monitoring which is not taken into account by the prediction algorithm. Setting a fixed latency for the position monitoring, or accounting for the variable latency in the MLC tracking algorithm would provide for better geometric (and hence dosimetric) results. In addition, reducing the overall latency of the system as a whole would provide for better dosimetric results. Incorporating target deformation and rotation into the beam shaping is another potential improvement for the system. Work needs to be done to evaluate a variety of treatment plans to ensure the MLC tracking algorithm is robust and accurate when applied to any conventionally generated treatment plan.

There are plans for commercialization of this system. It may be safer to implement the system for prostate cancer management, since there are currently approved uses

for Calypso Beacon implantation for that location. Further uses, such as lung tumor tracking, will need a new transponder design that can be safely inserted in the thorax. It is not clear whether changes in treatment planning software will be necessary, though they may be desirable to fully take advantage of the DMLC tracking capability. The tools for quality assurance of the system will have to be developed, and may include motion phantoms such as the one used in this work. Safety and reliability of a commercial implementation will have to be investigated in a more thorough manner than this preliminary work.

In summary, we have integrated a system that senses real-time internal anatomy positions without the use of ionizing radiation with a DMLC tracking system to deliver continuous dose to a moving target. The dose profiles are comparable with an internal gating solution, eliminate the uncertainties inherent in the use of chest wall surrogates for tumor position, and show much higher delivery efficiencies with the promise of increased clinical confidence in the delivered dose. More work is left to be done in further improving the dosimetric results in an effort to create a system that delivers accurate radiation with sub millimeter intrafraction motion management, as well as designing a solution for routine quality assurance of the system.

# Chapter 4

## Internal Fiducial Motion Correlation

### 4.1 Fiducial Correlation: Motivation

Radiation therapy often relies on fractionated treatment, which requires repeated patient positioning. Motion associated with respiration can be on the order of centimeters. For targets in the lung and abdomen, respiratory motion complicates accurate radiation delivery.

In order to mitigate the effects of motion, external surrogates have been employed to monitor the breathing cycle and ‘gate’ the beam such that it only irradiates during exhalation. While these surrogates offer a noninvasive option for motion management, the degree to which external respiratory surrogates reflect internal tumor motion varies.[13, 7, 16]

Recent work has shown that implanted fiducial tumor surrogates are safe and stable throughout the course of treatment. In a study from Kupelian et al, CT imaging was used to assess the proximity between an implanted metal fiducial and the GTV centroid throughout the course of treatment.[40] The average 3D variation in the GTV center relative to the marker was 2.6mm, with all cases <5mm. Although tumor shrinkage was apparent as a result of radiation, fiducials in or near tumors were relatively stable throughout treatment. Additionally, there was no incidence of pneumothorax in the 6 patients that underwent transbronchial implantation.



Real-time applications using internal fiducials as analogues for tumor motion have been developed, and the use of implanted fiducials in or near a target of interest has seen widespread adoption for daily patient alignment.[91, 39, 108] We have previously published use of wireless electromagnetic transponders (Calypso Medical, Seattle WA) for radiation therapy to increase dosimetric accuracy in the presence of respiratory motion.[95, 96, 81] The transponder positions with respect to isocenter are continuously monitored in real-time using electromagnetics. In an initial study, the real-time internal fiducial position was used to gate the beam.[95] In later studies, the beam aperture was effectively ‘moved’ using dynamic multileaf collimator (DMLC) tracking in order to follow the real-time position of a transponder.[96, 81]

The Cyberknife Synchrony system and the ExacTrac X-Ray 6D IGRT system (BrainLAB) rely on stereoscopic X-ray imaging in order to determine the position of an internal fiducial in real-time.[83, 63] A correlation model developed at the start of treatment relates the internal fiducial motion with respect to infrared markers attached to the patient’s surface. Intermittent imaging is employed to confirm and continually update the correlation model. Using this position, the beam is moved using a robotic arm or gated in order to mitigate the effects of respiratory motion.

The degree to which the motion of an implanted lung fiducial marker correlates with the motion of a tumor typically deteriorates with increased implantation distance between the fiducial and the tumor. It has been shown that increasing the proximity between an external respiratory sensor and internal target increases the correlation.[36] Similarly, increasing the distance between an implanted fiducial and the target has the potential to increase the error resulting from deformation between the fiducial/target. For fiducials in the lung, bronchoscopic implantation is typically favored over percutaneous implantation due to the reduced risk of pneumothorax.[40] Distal airways are smaller in diameter and limit access to peripheral lesions, which typically exhibit large amplitudes of motion ( 1-4 cm). As a result, the proximity of the internal transponder and the target of interest is limited by the bronchial tree structure.

While the previous studies have investigated the overall fixation of an internal marker for lung tumor tracking, there has not been a quantitative assessment of how close a fiducial marker must be placed with respect to a tumor in order to ensure accurate motion representation. We intend to investigate the level at which an implanted

internal fiducial can predict the intrafraction motion of surrounding anatomy within the lung. This knowledge will increase the confidence of the fiducial-based intervention systems and potentially allow for decreased PTV margins, sparing healthy tissue.

## 4.2 Fiducial Correlation: Methods

### 4.2.1 Dataset and Techniques

Ten randomly chosen primary lung cancer patients underwent 4DCT scans in the supine position. The scans were performed using a Philips Brilliance 16 slice CT scanner (Philips Medical Systems) that was operated in cinè mode with a stationary couch during the scan. The axial slice thickness was set at 1.5mm, which yielded a total thickness of 24mm for each couch position (16 slices x 1.5mm/slice). For each axial slice, 25 images were acquired over the course of two to three breathing cycles. Respiration was monitored using spirometry and a pneumatic bellows pressure sensor attached to the patient’s abdomen.[46] Each acquired image was synchronized with a corresponding tidal volume as measured by respiratory monitoring devices. The 4DCT scans were reconstructed at maximum inspiration and maximum expiration using amplitude-based reconstruction techniques described previously.[44] The decision to use only maximum inspiration and maximum expiration phases was based on the fact that previously published results have shown that hysteresis derived motion is typically less of a factor than tidal volume related motion.[113]

Each 4DCT dataset was imported into clinical treatment planning software (Pinnacle v. 8.0u, Philips Medical). The tumor and four main lobes of the lung (right/left upper/lower) were contoured at exhalation. The right middle lobe was not contoured due to its lack of size. Both inhalation and exhalation scans, along with the contours, were exported and loaded into custom software developed in MATLAB (2007a, The MathWorks) in order to perform deformable registration.[110]

Deformable registration was performed using the Horn-Schunck optical flow algorithm[24] in order to obtain motion vectors between exhalation and inhalation for each voxel within the thoracic cavity. After the vectors were obtained for each patient, they were

manually inspected to ensure the vector magnitude increased near the diaphragm and the motion vectors matched with the motion of internal high contrast landmarks, such as bronchial branch points. Each scan was reviewed in detail by one of the authors [RS].

Once the vectors were manually verified, two studies were performed. In the first study, a series of regularly spaced ‘seed points’ (every 4th voxel. 4mm spacing lateral and anterior/posterior with 6mm spacing superior inferior) throughout each lobe were selected to determine the degree of correlation with surrounding tissue motion. In the second study, ‘tumor-centric’ analysis was performed to evaluate the effects of increased rigidity associated with cancerous tissue on motion vector correlation in areas surrounding a tumor.

### 4.2.2 Correlation Radius

A region growing algorithm was employed to determine the maximum radius at which the magnitude of the vector motion of 95% of the voxels surrounding a seed point correlated to within 3mm of the motion of the seed voxel. The technique for the correlation radius analysis is outlined in Figure 4.1. A seed point array with 4mm spacing in the lateral and anterior/posterior directions and 6mm spacing in the superior/inferior directions was analyzed. For each seed point, the region-growing algorithm expanded radially with an increment ( $\Delta r$ ) of 1mm. After each iteration, the exhalation to inhalation motion vectors within the spherical region surrounding the seed point were compared to the motion of the seed voxel. If the motion vector for a given voxel correlated to within the spatial threshold (3mm) when compared with the motion of the seed voxel, the voxel was considered accepted via our criteria. The spherical region expanded to the maximum radius value at which 95% of the voxels within the region correlated to within 3mm. Voxels not within the same lung lobe as the seed voxel were disregarded.

### 4.2.3 Tumor Correlation

In order to quantitatively analyze whether the increased rigidity associated with cancerous tissue affects the surrounding tissue correlation, the volumetric centroid of the tumor was selected as the representative tumor motion vector. This vector represents the offset of the tumor between maximum exhalation and maximum inhalation. The motion vector from the tumor centroid was compared with the motion vectors of all surrounding tissue within the lungs. If it is assumed that a given voxel moves in a rigid manner with respect to the tumor centroid, this difference effectively represents the intrafraction motion error if a fiducial was placed at that voxel. Differences in the tumor motion vector and the surrounding tissue were plotted using color overlays indicating the motion correlation of surrounding tissue motion with that of the tumor.

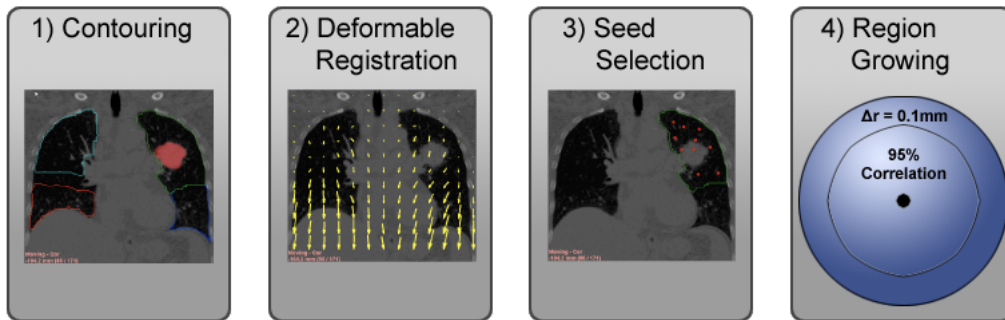


Figure 4.1: Correlation Radius Technique: Lung lobes and tumor were contoured at expiration (1). Deformable registration was performed between inhalation and exhalation CT scans to obtain motion vectors (2). Seed points were selected at random, ten per lung lobe (3). A spherical region growing algorithm was employed to determine the maximum radius at which 95% of the surrounding voxels correlated with the seed voxel motion (4).

## 4.3 Fiducial Correlation: Results

### 4.3.1 Motion Correlation: General Lung Results

Correlation radius values were obtained for each patient. In one patient (35), the motion within the right upper lobe was minimal and hence the vectors correlated to within 3mm regardless of seed point position. The radius values for this patient were set at the maximum radius value (7cm). The mean correlation radii for each lobe are shown in the Table 4.1. Additionally, histograms of the radii values for each lobe can be found in Figure 4.2. Tumor correlation radii values were found to be higher than those of healthy lung tissue ( $p < 0.005$ ) indicating that the increased rigidity associated with cancerous tissue makes surrounding lung tissue motion highly correlated. Additionally, the upper lobes were found to have radii values significantly higher than the lower lobes ( $p < 0.005$ ).

<b>Lobe</b>	<b>Mean (std)</b>
Left Lower	1.7 (1.1)
Right Lower	1.6 (1.1)
Left Upper	2.1 (1.0)
Right Upper	2.9 (1.8)
Tumor	3.1 (1.8)

Table 4.1: Correlation Radius Values. Correlation radii values to represent 3mm motion. Means and standard deviations are reported for each lobe in units of cm. Tumor correlation radii were significantly higher ( $p < 0.005$ ) than the healthy lung tissue radii values.

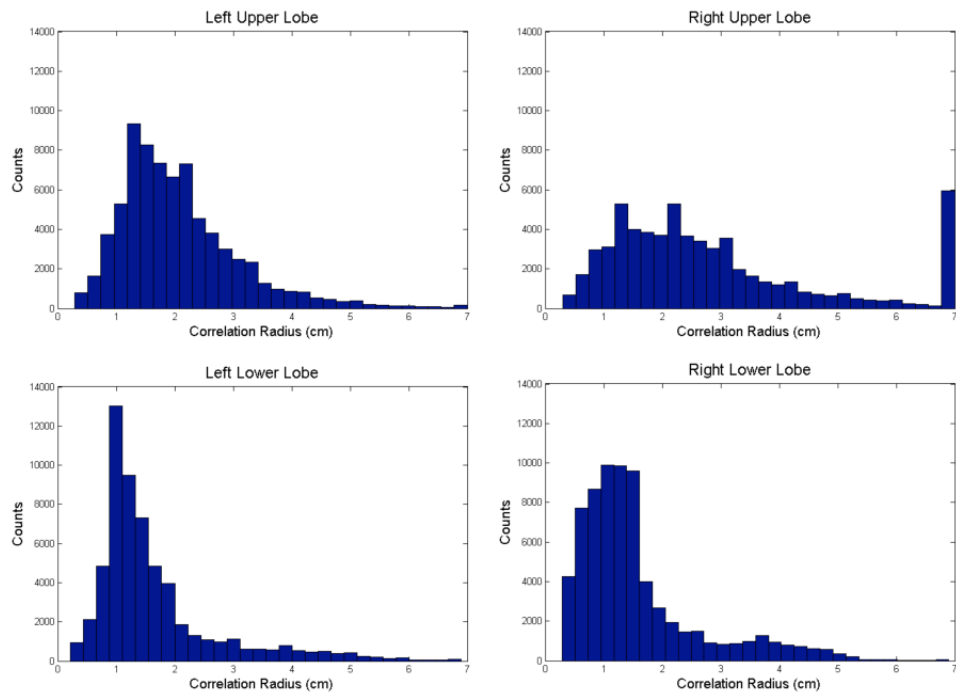


Figure 4.2: Histograms of correlation radii values for each lobe. Notice increased correlation radii values for the upper lobes when compared to the lower lobes. Correlation radii values were capped at 7cm, which resulted in the 7cm peak in the low motion Right Upper lobe.

Correlation maps were made for each patient (Figure 4.3). The maps show a coronal and sagittal view take at the carina and middle of the left lung respectively. For each map, the interpolated correlation radii for each voxel are overlaid. The correlation with surrounding tissue varies substantially with position and is inversely related to the divergence of the motion vector field (Equation 4.1).

$$\vec{T} \propto (\nabla \cdot \vec{M})^{-1} \quad (4.1)$$

where

$$\begin{aligned} \vec{T} &= \text{Surrounding Tissue Correlation} \\ \vec{M} &= \text{Motion Vector Field} \end{aligned}$$

Correlation radius maps were made for each patient. The background of each map is a coronal slice containing the carina as a reference landmark. The centroid of each circle overlay is the location of the seed voxel. The radius of each circle overlay is the maximum correlation radius for each given seed voxel (Figure 4.3). It is evident that there is considerable patient to patient as well as lobe to lobe variation in correlation radius.

### 4.3.2 Motion Correlation: Tumor Centric Results

Correlation values between the volumetric centroid of the tumor and the surrounding tissue were calculated. The correlation with surrounding tissue is plotted in Figure 4.4. Variations in tumor motion correlation with surrounding tissue are evident due to local variations in the divergence of the motion vector field. Tumor motions ranged from 1.6mm to 12.0mm with a mean motion of 6.0mm across all patients.

## 4.4 Fiducial Correlation: Discussion

It is evident that the radius at which surrounding tissue motion correlates with an internal point within the lung is highly variable both from patient to patient as well

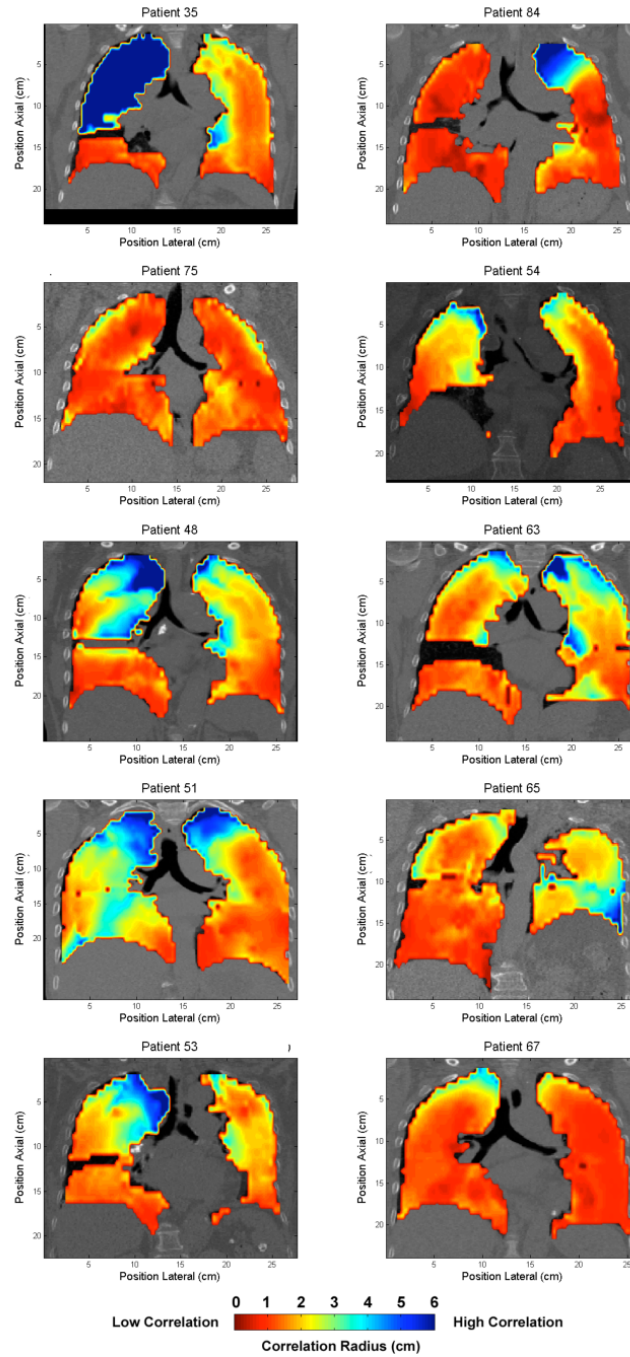


Figure 4.3: Correlation Radii Maps. Regularly spaced voxel within the lung were analyzed using the process described in Figure 4.1. Correlation maps were produced to display how well the anatomy correlates with adjacent anatomy within the thoracic cavity. Red indicates low correlation with surrounding anatomy motion, blue indicates high correlation.



as from point to point within a single patient. As a result, clinical decisions such as reducing PTV margins due to an internal fiducial based motion management solution should account for both the error associated with the tracking system, as well as the error associated with tumor/fiducial correlation.

As deformable modeling techniques and computing power improve, a potential implementation could incorporate real-time deformation between the tumor and respiratory surrogate at time of treatment. However, given other uncertainties which contribute to increased margins such as lack of robust knowledge of what surrounding tissue is potentially harmful as well as daily alignment and changes in internal morphology, it is likely that considerable time will pass before real-time deformable intervention is clinically implemented. As a result, focused efforts on obtaining a patient by patient routine for determining rigid correlation between internal targets and implanted fiducials will provide confidence in fiducial-based treatment delivery for mobile targets.

Deformable registration techniques are computationally intensive, however in practice they can be automated to a large extent. Additionally, although computation time is a concern, on order the registration and region growing algorithm presented here take less than the amount of time associated with conventional D-IMRT planning. A system in which the data from a 4DCT scan is loaded into a software package, deformable registration is automatically performed (possibly overnight using traditionally idle computational resources), and correlation maps such as those in Figure 4.4 are presented to the physician could provide useful feedback in treatment decisions.

A general rule on where to implant with respect to the tumor was not established. Typically tissue motion correlation deteriorates when moving in the superior/inferior direction. This is usually the largest component vector of respiratory motion and generally has the largest divergence of the vector field. This relationship was not the case for many of the patients found in Figure 4.4. In summary, internal motion correlation is highly patient specific as well as specific to the lobe within the lung based on the breathing patterns for a given patient.

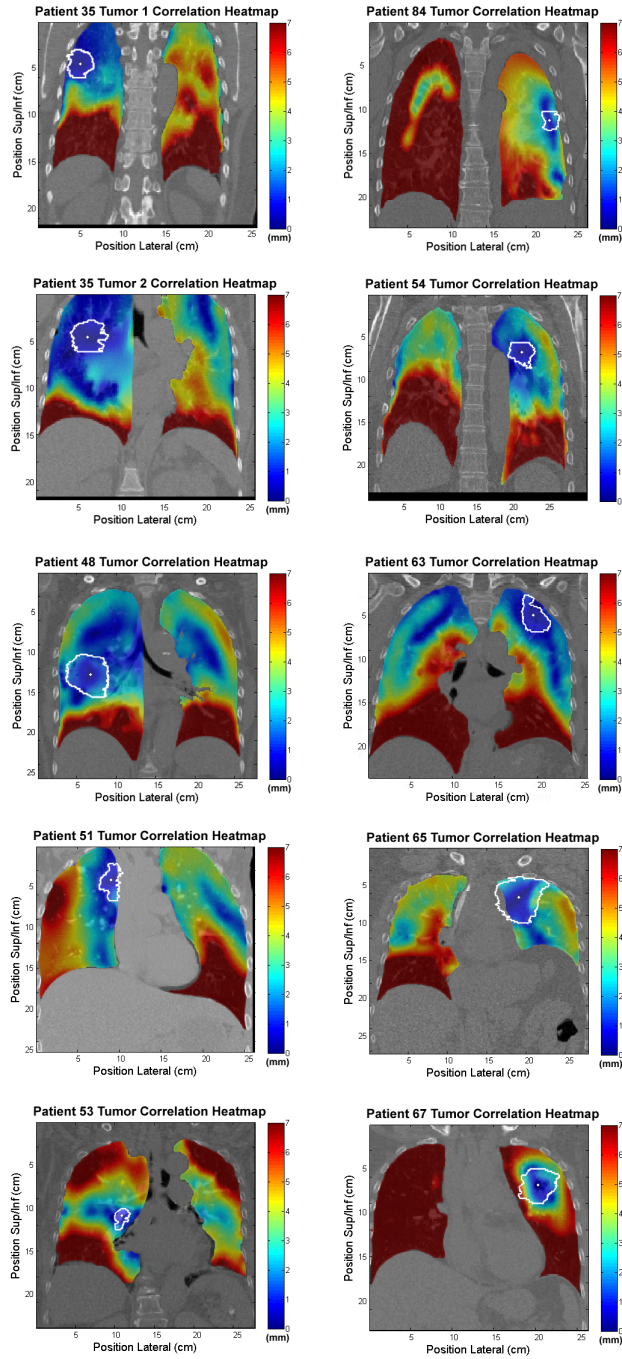


Figure 4.4: Correlation Tumor Maps: Motion correlation values were observed with respect to the tumor centroid (indicated by white point). It is evident that correlation is variable based on the divergence of local motion vectors.

# Chapter 5

## Lung Image Guided Surgery

### 5.1 Introduction

Advancements in surgical intervention have drastically improved outcomes as well as minimized the complications associated with invasive procedures. Effort has been made to minimize the trauma associated with surgical procedures by incorporating technology. Decreasing the invasiveness of surgery has the potential to result in increased survival rates, fewer complications as well as a reduced recovery time prior to returning to normal healthy life.

The advent of minimally invasive technologies has impacted medical practice from diagnostic to interventional procedures. Image guided surgery (IGS) offers the physician alternative imaging approaches during surgical intervention. Currently, commercial IGS products focus on neurosurgery[18], orthopedic[61] and otolaryngologic[19] applications. A surgical system that could reduce trauma for procedures within the thorax and abdomen is appealing.

Procedures in the lung/abdomen that would benefit from IGS include radio frequency ablation (RFA), lung biopsies, as well as brachytherapy seed placement. In RFA, radio frequency energy is imparted through a catheter to ablate a tumor. RFA offers local heating from inside a tumor, assuming the guidance system to get the catheter in the proper location is sufficiently accurate. As a result, this modality has the potential to reduce trauma to adjacent healthy tissue when compared with conventional external beam stereotactic radiotherapy. Currently, RFA is not routinely clinically implemented in the lung, however procedures in the heart and liver are routine.

The use of needle biopsy techniques is widespread in efforts to determine malignancy of lesions within the lung. In order to guide the physician, imaging techniques such as computed tomography (CT) and fluoroscopy are routinely employed. Even when using advanced imaging techniques, the diagnostic accuracies of needle biopsies are poor when the lesions are small.[101, 42] Li et al report a drop in diagnostic accuracy from 96% to 74% when comparing nodules of diameter  $>1.5\text{cm}$  and  $\leq 1.5\text{cm}$  respectively.[42] Tumors have been shown to move at amplitudes  $>1\text{cm}$  due to respiration;[50, 99] failure to account for this motion will lower biopsy accuracy rates, especially for smaller lesions. As a result, many institutions currently will not attempt to biopsy lesions less than a centimeter in diameter. Creating a system capable of sufficient accuracy to biopsy small lesions could provide the potential for early detection. Early detection has shown to be a key factor in survival rates. Henschke *et al* report early diagnosis of Stage I lesions resulted in a five year survival rate of 90%, compared with patients diagnosed with Stage III or IV lesions which have 5 year survival rates of 15%.[23]

Finally, brachytherapy seed placement could benefit from an accurate respiratory correlated guidance system. In brachytherapy, a radioactive source is placed inside of the body in order to irradiate a tumor. This allows for more localized radiation and sparing of healthy tissue, however it is reliant on accurate placement of the seed source. As a result, the procedure has conventionally been limited to percutaneous use in the prostate, cervix, and breast. Brachytherapy has been used in the lung, however it has been limited to intraoperative use due to the imprecision of percutaneous or bronchoscopic seed placement in the presence of motion.

There are some current commercial minimally invasive lung guidance systems. The superDimension InReach system provides a minimally invasive means for bronchoscopic lung biopsies. The system relies on electromagnetic position monitoring of a catheter inserted through the working channel of a bronchoscope. Registration between *a priori* acquired CT or MRI images and the room coordinate system is performed by advancing the bronchoscope down several pathways. The EM coordinates in doing so are then compared with the pathways on the autosegmented volumetric imageset. During a procedure, the bronchoscope is advanced until it cannot continue due to the width of the surrounding bronchiole. From here, the EM catheter and surrounding guide sheath are advanced without the use of real-time bronchoscopic

imaging. The position of the catheter tip is shown on the previously acquired volumetric images. The catheter is mechanically steerable, and the position of the distal tip is updated in real-time on the computer console. Once in the correct location, the guide sheath surrounding the catheter is left in place, the catheter is removed and bronchoscopic tools are employed to gather tissue samples. The superDimension is novel in that it provides minimally invasive access to distal sites conventionally unreachable by a bronchoscope, however there are some limitations. The system does not attempt to account for tissue motion due to respiration. Additionally, the published accuracy results for the system are limited to the spatial accuracy of the EM tracking system. This fails to address the spatial accuracy of intervention in a human, which has inaccuracies related to registration and respiratory motion.

The Philips PercuNav system uses EM tracked instruments along with real-time ultrasound registered to *a priori* acquired volumetric images. It offers automated registration of the real-time ultrasound images to the volumetric imagesets via tracking the ultrasound probe in 3D. The PercuNav system does have some rudimentary respiratory gating capabilities, however there is no real-time modeling of the tumor trajectory for intervention in the lungs.

The StealthStation Treon system from Medtronic Navigation is routinely used in craniospinal minimally invasive procedures. Similar to the previously mentioned systems, this system uses electromagnetic navigation over *a priori* acquired volumetric images. The system is widely used in cranial applications, however it is currently not for clinical use in the lungs or abdomen. The StealthStation offers two methods for registration. In point based registration a series of CT contrast markers are defined both on the CT image and in the room coordinate system by systematically touching the EM tools to each point. Alternatively, tracer based registration relies on tracing a known structure such as the bridge of the nose and forehead using an EM tool, and the acquired points are automatically matched to the autosegmented skull surface in the CT image. Once registration is performed, the system shows the position of the catheter in real-time, however there is currently no motion model for respiratory correlated IGS. More information on the StealthStation is included in Appendix B.10

We incorporated previously published tissue modeling[45] based on respiratory correlated imaging (4DCT) in an effort to develop an IGS system that accounts for target

motion and improves the accuracy of minimally invasive needle biopsy techniques in the lung. A temporal guidance and planning system was developed and the accuracy of the system is characterized in phantom, ex-vivo porcine and human cadaver settings. The system works in conjunction with a Medtronic StealthStation, provided to [RS] as part of a computer aided surgery grant from Medtronic Navigation.



Figure 5.1: Medtronic StealthStation. The field generator (black, foreground) and the Medtronic StealthStation (background) are shown. A position sensitive magnetic field is generated with respect to the field generator, which allows for precise location monitoring of EM tools in the tracking volume.

## 5.2 Methods and Materials

A commercially available IGS solution (StealthStation) was employed in order to track the tips of interventional tools via electromagnetics. A field generator connected to the StealthStation creates a position dependent magnetic field inside of the patient. The system uses tools with two copper wire coils near the tip that act as inductors. Based on the amount of current induced in the coils of the tool from the surrounding magnetic field, the positions of the AxiEM tools are known to sub-mm

accuracy in three dimensions (Figure 5.1). The respiratory correlated image guided surgery (RCIGS) system consists of additional software that communicates with the StealthStation via application programming interfaces (APIs). The RCIGS system works in conjunction with the StealthStation to offer temporal guidance to the physician for intervention on moving targets. The RCIGS surgical guidance planning and intervention is described in Figure 5.2.

## 5.2.1 RCIGS System Overview

### 4DCT acquisition

A respiratory correlated imaging technique (4DCT) using a commercial CT scanner (Philips Brilliance 64 or Philips Brilliance Big Bore 16 depending on availability) was employed to obtain a series ( $n=4$ ) of volumetric images, each of which correlate with a specific phase/amplitude of the breathing cycle as indicated by a respiratory surrogate. The respiratory surrogate used was a pneumotachograph (Figure 5.5) which provides an accurate, calibrated representation of tidal volume and airflow throughout the image acquisition. The imaging mode was retrospective helical reconstruction, with a voltage of 120kVp and current of 133mAs.[65] For more information on the details of 4DCT acquisition, please refer to Appendix B.2

### Target Position

After 4DCT imaging, the reconstructed DICOM images are network transferred to a research system containing Philips Pinnacle (version 8.1y). Pinnacle is a clinical radiation therapy treatment planning software package which offers a robust environment for manual image segmentation and contouring. Targets were defined using a lung viewing window (W:1600, L:-600) and their position centroids recorded on each of the volumetric images from the 4DCT. This provides a location of the target based on the signal from an external respiratory surrogate. At the completion of this stage, 4 target locations are available with corresponding tidal volume and airflow measurements from the respiratory surrogate.

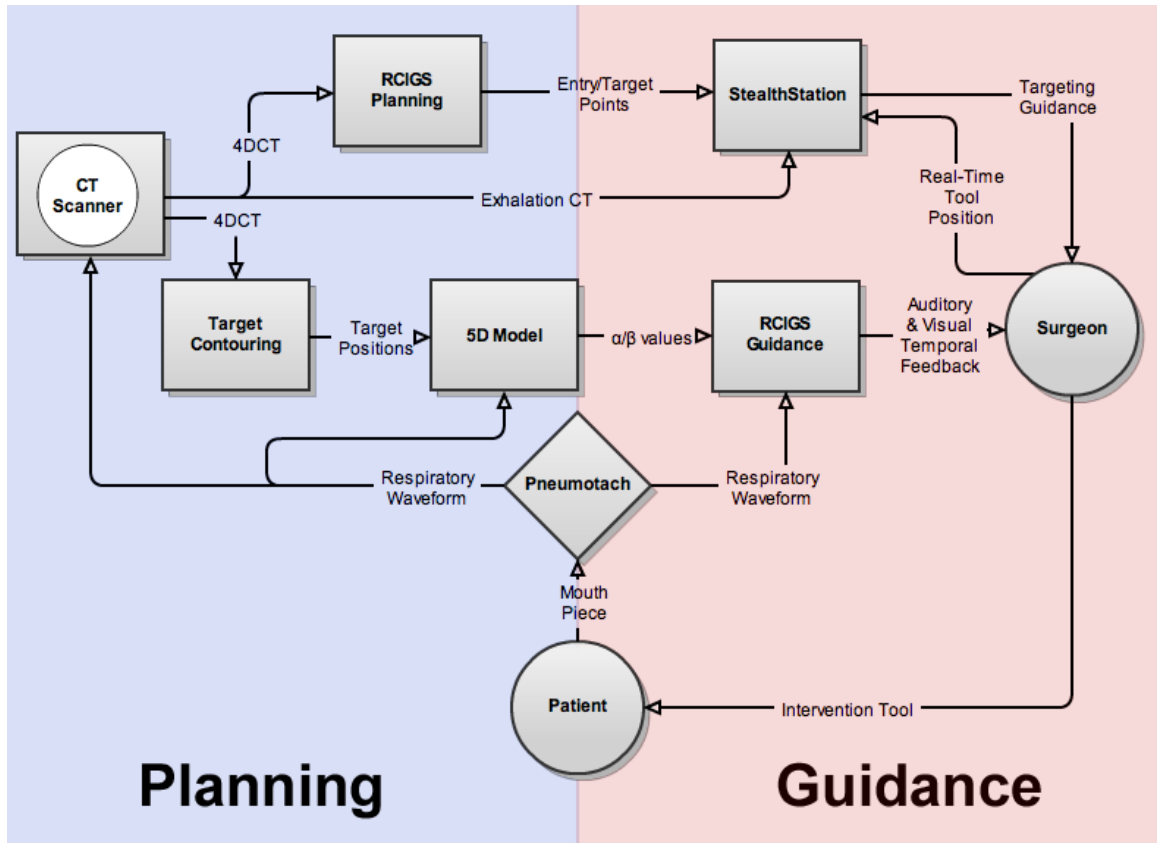


Figure 5.2: Lung IGS Workflow. 4DCT images are acquired based on a respiratory waveform from a pneumotachograph connected to the patient’s mouth piece. The 4DCT images are sent to the RCIGS planning software, as well as a contouring workstation for target definition with respect to respiratory phase. The StealthStation receives entry and target points from the RCIGS planning software, the exhalation CT, and the real-time tool position via EM position monitoring. The StealthStation offers real-time visual guidance to the physician on the location of the needle tip inside the patient. Four target points with respect to respiratory phase are sent from the Pinnacle workstation to the 5D model computer. The model parameters ( $\alpha/\beta$ ) are input to the RCIGS guidance software, along with the real-time respiratory waveform. From here, the RCIGS guidance software determines the position of the target in real-time, and indicates the proper time for intervention to the physician via auditory and visual feedback.



## Model Calibration

The 4 target positions along with tidal volume and airflow measurements are used to calibrate a previously described model for respiratory motion. In short, the model is parameterized via the 4 known target positions and at completion the model can accurately predict with the position of the target at any tidal volume and airflow rate in real-time. The details of the model are not included here for the sake of brevity, but can be found in previously published work[45] as well as Appendix B.2.

## Surgical Plan

Once the target position is known for any tidal volume and airflow, a location and time of intervention is selected. The location should attempt to maximize the time at which the target is relatively stationary and respiration is reproducible. This typically occurs at exhalation. Once the entry and target points for the plan are selected, custom software displays the motion of tissue within the lung to ensure critical structures do not move into the surgical path as a result of respiration (Figure 5.4).

The planning software was written in C++ using the following open source libraries: the visualization toolkit (VTK) for image processing and visualization, the insight toolkit (ITK) for image segmentation and registration and the Fast Light Toolkit (FLTK) for graphical user interface (GUI) generation. The aforementioned toolkits provide a framework for reading and manipulating 3D medical image datasets without programming the low level functions for image interaction in C++. This allowed for rapid deployment of software without solving tedious computer science problems that have previously been investigated. The relation in which the frameworks are employed is displayed in Figure 5.3

The RCIGS planning software displays the trajectory of the needle tip with respect to the motion of the tissue due to respiration. In order to achieve this goal, a 4DCT dataset consisting of a series (4-10) of 3D volumetric images is loaded from the hard drive into RAM. The memory required for this task is approximately 1.5GB, which is available on currently affordable consumer computers. The CT images are displayed

using three orthogonal views. Once the 4DCT datasets are loaded, the trajectory of the tooltip is overlaid. The approach trajectory can be modified if it interferes with critical structures. The motion of the tissue due to respiration can be simulated, and the software loops through the various phases of the 4DCT while updating the displays in real-time. This allows for evaluation of critical structure motion due to respiration, and the path to the target can be modified accordingly. The software also has basic window/level functionality available in most image display software in order to increase contrast depending on the region of interest within the body.

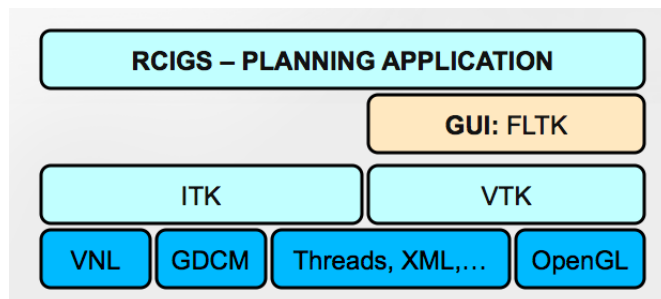


Figure 5.3: RCIGS Software Architecture. The RCIGS package is built on open source software libraries. The libraries provide a means for segmentation, visualization and fast data manipulation in C++. The Visualization Toolkit (VTK) and Insight Toolkit (ITK) packages rely on commonly used lower level techniques and libraries such as the GDCM (DICOM image reading/writing), OpenGL (computer visualization), and VNL (numerics)

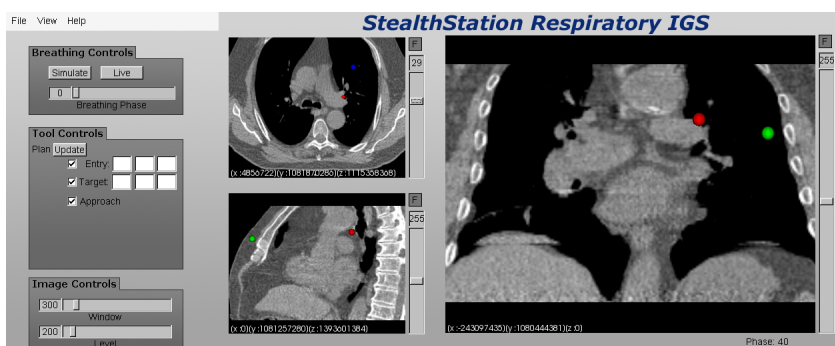


Figure 5.4: Lung IGS Planning Software. Target, entry and approach trajectories are visually displayed along with respiratory correlated imaging. This allows the physician to determine whether critical structures enter the approach path as a result of respiration prior to surgical intervention.

## Surgical Guidance

Once the surgical plan is established; part of the RCIGS software package (Figure 5.6) guides the physician on when to perform the intervention. The position of the target is known in real-time based on the signal from the respiratory surrogate, and the target position is displayed to the physician. Additionally, visual and auditory feedback are given when the target is within a predefined volume. This allows the physician to advance the needle and/or perform the tissue resection when the target is in the appropriate location. Due to the limits imposed by human motor skills, intervening on a point static in space at a time in which the target is at that location is more accurate attempting to follow the target with the needle as it moves through the entire range of motion.

The real-time guidance software was developed in C# using National Instruments Measurement Studio for data acquisition and display. Measurement studio provides a series of .NET libraries and classes for building measurement and automated display applications using Microsoft Visual Studio. A pneumotachograph was employed to obtain accurate tidal volume and airflow measurements. The device consists of a chamber

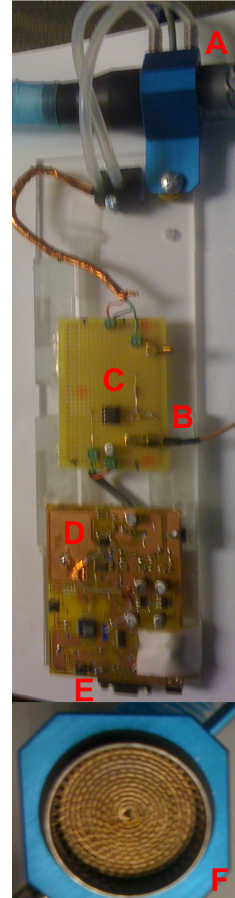


Figure 5.5: Pneumotachograph. A pneumotach head (A, side profile: F) is attached to a custom fabricated circuit board. The board offers voltage output corresponding to raw air flow (B) after analogue low pass filtering (C). Additionally, there is on-board analogue to digital conversion and encoding (D) in order to interface via a serial port (E) with a Philips Brilliance CT scanner.

exit is laminar (Figure 5.5). The pressure at the entrance and exit is fed to a differential pressure transducer. This pressure differential is proportional to the flow through the device. Low pass filtering is done to get rid of high frequency noise, and efforts were made to minimize the drift in the circuit over time. The board offers on-board analogue to digital conversion and encodes the respiratory signal in a manner to directly communicate with a Philips Brilliance CT scanner. The electrical circuit used for the board was based on a schematic from an industry partner, and as a result the circuit is not included here. The board offers raw voltage output to a data acquisition board (DAQ) connected to a PC with the real-time guidance software. The software acquires and displays the respiratory tidal volume signal in real-time. Additionally, the software shows the position of the moving target with respect to the static location of intervention in real-time based on the previously calibrated 5D model.

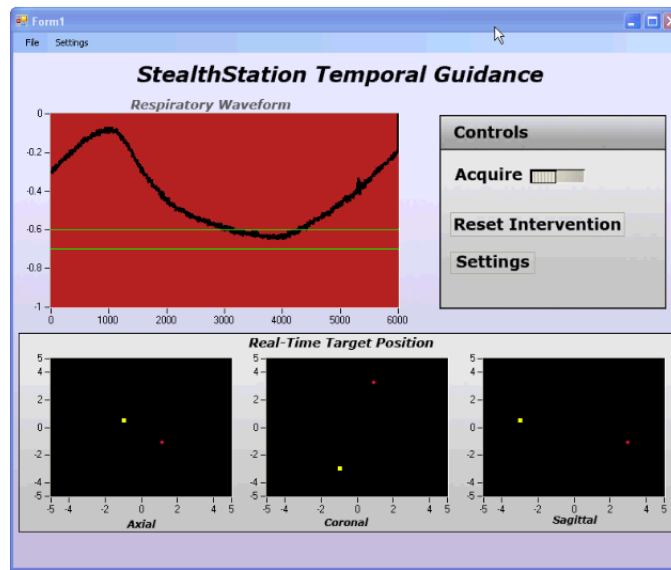


Figure 5.6: Lung IGS Intervention Software. The respiratory waveform is displayed to the physician. Binary auditory and visual feedback is given to the physician when the target is within a predetermined range. The static intervention target is shown as a yellow dot with multi-plane views. The position of the red dot changes in real-time based on the previously calibrated 5D model indicating the target position as a function of the respiratory surrogate.

The pneumotach was calibrated using a precision machined 600 ml syringe to inject a known volume of air through the device. A series of 10 inhalation/exhalations

were performed to determine the reproducibility of the pneumotach for a known tidal volume. The calibration waveform is displayed in Figure 5.7. Peak detection was employed to obtain standard deviations at inhalation (1.6%) and exhalation (0.2%). These variations are suitable for highly accurate respiratory motion modeling, and are likely a result of nonlinearities present at the beginning and end of manually pushing the syringe.

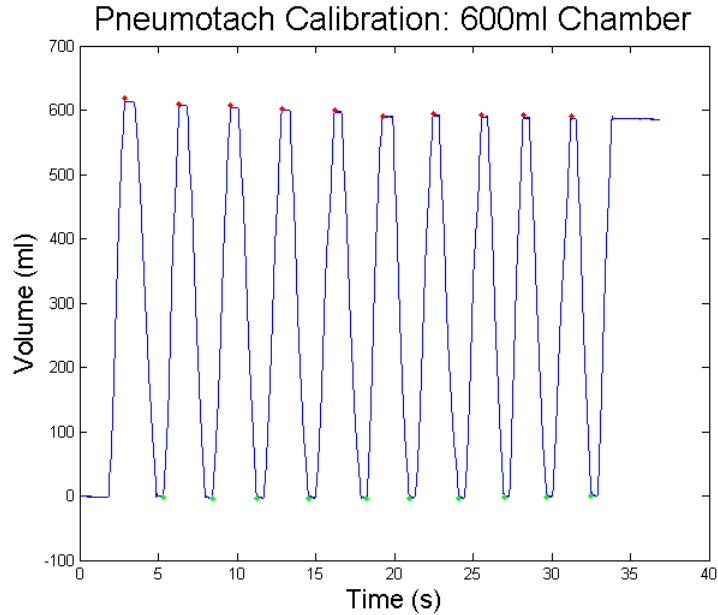


Figure 5.7: Pneumotach Calibration. A pneumotachograph was constructed to obtain highly accurate tidal volume recordings. The calibration waveform was obtained using a 600ml syringe. Standard deviations were obtained at inhalation (1.6%) and exhalation (0.2%) using peak detection.

## 5.2.2 System Accuracy: Overview

In order to develop the RCIGS system and obtain quantitative measurements of the overall accuracy, a series of experiments were designed with increasing difficulty. Motion phantom, *ex-vivo* porcine, and human cadaver models were successively employed and each stage had an associated criteria for success. An overview of the success criteria and problems that each model attempted to address is included in Figure 5.8, with details on each model found in Sections 5.2.3, 5.2.4, 5.2.5 respectively.

<b>Model</b>	<b>Purpose</b>	<b>Success Criteria</b>
Robotic Phantom	-Software Calibration -Motion Intervention Baseline	Mean Errors Modeling: <1mm Intervention: <3mm
Ex-Vivo Porcine Lung	-Soft Tissue Effects Deformation Needle motion	Mean Error Intervention: <4mm
Human Cadaver	-Critical Structures Ribs/Vasculature -Registration on Soft Tissue -Increased Depth	Mean Error Intervention: <5mm Stretch Goal: All Intervention <5mm

Figure 5.8: System Accuracy Models. The RCIGS system was tested in robotic phantom, porcine, and human cadaver environments. The table outlines the problem each model attempted to address, as well as a quantitative success metric.

### 5.2.3 System Accuracy: Phantom Assessment

A robotic motion phantom (Washington University 4D Phantom)[52] was used to initially characterize the accuracy of the system. The goal of the motion phantom study was to characterize both the target motion modeling portion of the RCIGS package, as well as the intervention on a moving target by a surgeon. The phantom was programmed to reproduce the motion from a lung trajectory recorded via an implanted position-monitoring device (Beacon, Calypso Medical) in the lung of a human patient.[56] The arm had several radiopaque markers (IZI Medical MM3005) affixed that are readily apparent on CT imaging. A 4DCT image was acquired of the motion phantom as it moved, which was subsequently used for model calibration and intervention planning according to the RCIGS system. (5.2) Since the original trajectory is known, it is possible to compare the output from our model to the actual trajectory. This was performed both for the entire trajectory as well as for the portion of the trajectory at exhalation, which is when the surgical intervention occurs. Criteria for model calibration success was a mean error of  $<1\text{mm}$  at exhalation, which allows for additional errors associated with positioning the probe, registration, and motion while still allowing for our goal of  $1\text{cm}$  lesion intervention.

Point based registration between the CT image and surgical room coordinate system was performed by using an EM tool to touch several radiopaque markers affixed to the phantom arm, and defining the same positions inside of the StealthStation software on the CT image. An EM ‘patient tracker’ sensor was affixed to the non-moving base of the phantom. This sensor offers a coordinate transformation and ensures the registration is accurate even if the ‘patient’ moves with respect to the field generator. Since the target exhibits motion, it was necessary to know both the location of the surgeon’s tool as well as the location of the phantom arm at the time of simulated intervention. Two electromagnetic tools (AxiEM) were used. One probe was handled by the surgeon performing the intervention [RS], while the other was affixed to the phantom arm to provide the position in real-time as the phantom moved. The phantom arm was hidden from view leaving the surgeon reliant on the guidance software provided from the StealthStation along with the RCIGS package to perform the intervention. Additionally, a static offset was used when selecting a target point such that there was no physical contact between the motion arm and the intervention tool. The motion phantom was programmed to run the same trajectory used during



imaging. When the target/tool were in the correct location as indicated by the RCIGS software, the surgeon simulated intervention by depressing a footswitch. At this time the RCIGS software communicated via TCP/IP over an ethernet link with the StealthStation to obtain the position of both EM tools. The positions (n=25) of the arm and intervention tool were simultaneously recorded for error analysis. Criteria for success were 3D errors between the tool tip and the phantom arm of <3mm, indicating an accuracy of intervention sufficient for a 1cm diameter spherical lesion while allowing for additional errors due to soft tissue registration and deformation in further studies.

#### **5.2.4 System Accuracy: Ex-Vivo Porcine Assessment**

Phantom characterization is useful due to the fact that the target position is known at all times, however it ignores some of the problems associated with intervention in actual tissue. Most notably, the needle tip will move as a result of the motion imparted by surrounding tissue. Additionally, tissue will deform due to the forces imposed by an implantation needle. An ex-vivo porcine model was employed to further analyze the system accuracy in the presence of the aforementioned difficulties.

The RCIGS system was used to guide intervention on simulated targets in porcine lungs (BioQuest, eNasco). The lungs were preserved in propylene glycol, which prevents bacteria growth as well as acts as a desiccant to prevent the lungs from drying out and becoming rigid. The lungs were placed inside of a plastic container supported with foam (Figure 5.10). The trachea was held rigidly, the lateral and posterior sides were supported, with the superior and anterior sides of the lung free to move. The lungs could slide with respect to the container. These efforts were made in order to maximize the amount of superior/inferior and anterior/posterior motion similar to that found in-vivo. Twelve highly attenuating small pieces of 23 gauge copper wire were percutaneously implanted through a Teflon guide sheath into three sets of lungs to serve as targets.

The lungs were attached to a ventilator (Aequitron Medical, LP10) and inflated via positive pressure. The ventilation parameters were 30 bpm, 1.8 liter volume, with 1.2 seconds inspiration time. The pressure exterior of the lung inside the housing was

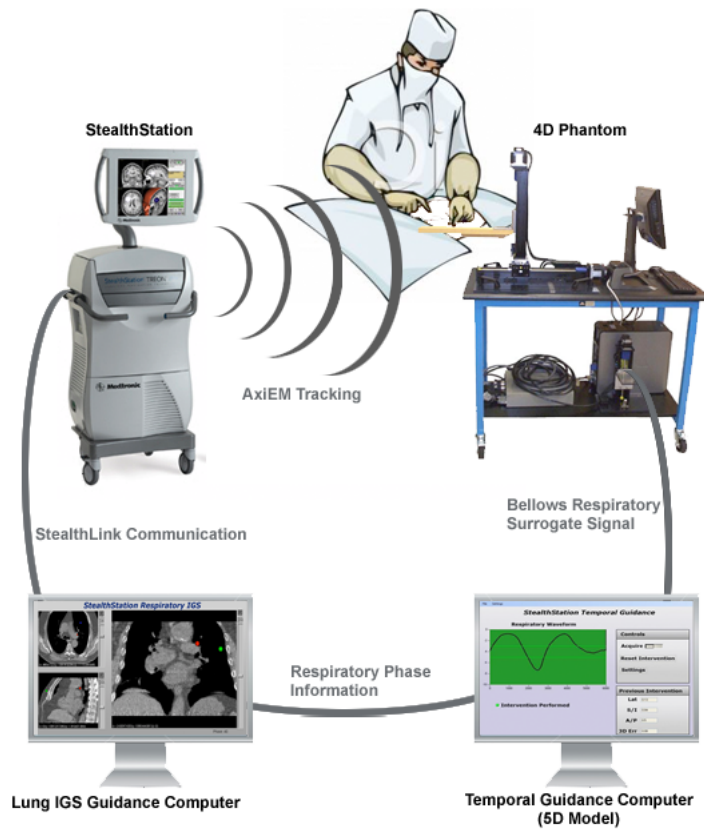


Figure 5.9: Lung IGS Phantom Study Schematic. A 4D motion phantom recreates realistic motion trajectories. A bellows device receives the respiratory signal via a surrogate axis and a computer calculates the target position using a pre-calibrated 5D model. This information is used to guide the physician on when to intervene. When an intervention is performed, the position of an AxiEM marker on the motion phantom arm is recorded along with the position of the surgeon's tool tip. This allows for quantitative analysis of the accuracy of the temporal guidance system.



Figure 5.10: Porcine Lungs. The lungs were affixed in a housing which maximized the amount of anterior/posterior and superior/inferior motion by restricting the lateral edges. The lungs were attached to ventilator and inflated via positive pressure.

unregulated at atmospheric pressure. The expiratory pressure remained constant from breath to breath at 20mm H<sub>2</sub>O via a positive end expiratory pressure (PEEP) valve.

The RCIGS system was used to image, plan, and intervene on each of the targets within the lungs. Point based registration was performed on circular CT contrast markers affixed to the container holding the lungs.



Figure 5.11: Surgical tools. An AxiEM stylette with PEEK guide sheath/needle as well as a bare AxiEM stylette are shown.

During intervention, the EM tool (Figure 5.11) was affixed inside of a piece of 16 gauge Teflon tubing (Small Parts inc.) in which the leading end was cut at an acute angle. The wall thickness of the tubing was high (0.4mm) in order to provide rigidity and effectively make the Teflon guide sheath a needle capable of piercing lung tissue. The EM tool and guide sheath combination was advanced during expiration when the target was in the static approach path defined during planning. Once in place, the EM tool was removed and a piece of copper wire was inserted into the guide sheath. The entire assembly was fixed in place with cyanoacrylate and after all interventions were performed the lungs were imaged again via 4DCT for interventional accuracy assessment. After imaging, the exhalation 4DCT was loaded into clinical radiation therapy treatment planning software (Philips Pinnacle version 8.1y) in order to define the needle tip and target points in 3D (Figure 5.12). Error analysis was performed

in order to define the three dimensional distance between the needle tips and target points.

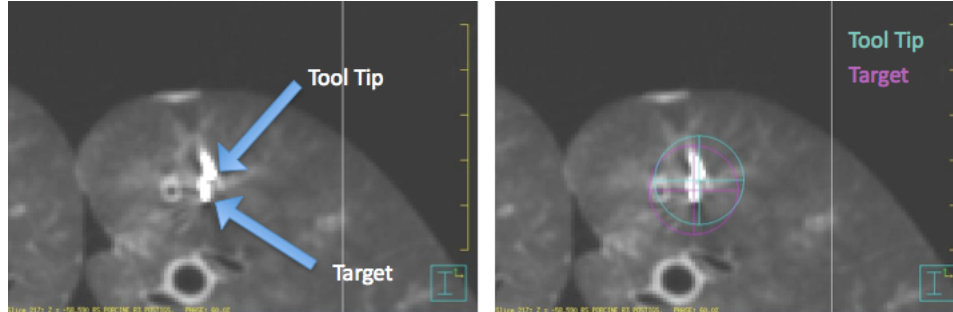


Figure 5.12: Target/Intervention accuracy assessment. The needle tip and target are defined inside of clinical treatment planning software. The 3D offset is recorded for each run. Yellow grid marks = 1cm increments.

### 5.2.5 System Accuracy: Human Cadaver Assessment

Additional concerns arise when using the RCIGS system for intervention in the human lung. For instance, the approach plan must account for both rib and critical structure motion such as vasculature to ensure the needle doesn't interfere. Additionally, the registration technique used for the porcine trial is not applicable in a human cadaver. In order to determine the system accuracy in a clinically relevant scenerio, a human cadaver was utilized.

The thorax of a human cadaver was prepared for respiratory correlated intervention. The carbon fiber couch on a Philips Brilliance CT Scanner was replaced with a wood plan in order to minimize interference with the magnetic fields required for 3D tool location. The torso was placed on the couch and bilateral chest tubes were implanted and affixed to a vacuum unit with a reservoir chamber to collect effusion fluid (Pleur-Evac). Once the pleural space was evacuated, a cuffed endotracheal tube was inserted and connected to a ventilator to inflate the lungs via positive pressure. The settings on the ventilator were as follows: volume = 1 liter, breath per minute = 14, inspiratory time = 1 second, assist/control mode. The torso was imaged via CT to determine optimal locations for target implantation. Four small radiopaque markers constructed of single stranded copper wire were implanted percutaneously into the lungs to serve



as targets. The targets were implanted laterally through a needle with a plunger to evacuate the targets. The targets were implanted with distances of approximately 10cm from the anterior surface to ensure the system is accurate for intervention on deep lesions.

Once the targets were implanted, several circular radiopaque CT markers were affixed to the chest wall and the cadaver was imaged via 4DCT (Figure 5.13). Similarly to the previous porcine and phantom models, point based registration was performed using the CT markers. Unlike the previous models, the registration points are moving due to respiratory induced chest wall expansion and hence the registration must be gated at exhalation. Additionally, a patient tracker EM sensor is affixed to the torso. This sensor also moves/rotates due to chest wall motion. The position of the EM tool is constantly updated based on a coordinate system transformation obtained from the patient tracker. As a result, the position of any EM tracked tool is only accurate during the phase at which registration was performed (exhalation). This is acceptable due to the fact that intervention and needle advancement will be gated at the same phase that registration was performed.

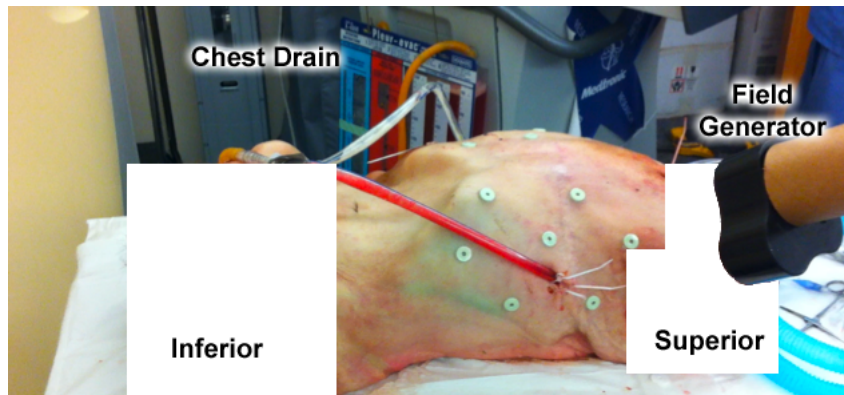


Figure 5.13: Cadaver Registration. Several small radiopaque CT contrast markers were affixed to the chest wall for registration. The markers have a circular hole in the middle, which is the same size as the head of an EM tool. The tool is touched in each of the markers during exhalation, and the StealthStation matches these points in CT room coordinates (with respect to the black magnetic field generator) with the associated points defined on the CT image.

A guide sheath constructed of polyetheretherketone (PEEK) was placed around the EM tool to be used for intervention. PEEK was employed as opposed to the PTFE

(Teflon) tubing used in the porcine model due to the need for a stronger polymer in order to penetrate the chest wall and tissue surrounding the lungs. A metal guide sheath would act as a Faraday cage, shielding the inner tool from the magnetic field and preventing 3D localization. PEEK offers rigidity comparable to steel in a non-ferromagnetic material. The tool/sheath was advanced through a small incision on the anterior surface of the torso. This approach path is different than the lateral path used to implant the targets to ensure the intervention needle was not simply following the hole in the tissue made during target implantation. Once the EM tool was guided to the appropriate position, it was removed from the guide sheath and a piece of copper wire was inserted and affixed with cyanoacrylate. The copper wire is readily visible via CT imaging and was used to determine the efficacy of intervention.

## 5.3 Results

### 5.3.1 Phantom Assessment

Since the trajectory delivered from the phantom is known, this makes it possible to characterize the accuracy of each step of the RCIGS process. The first stage of the process is model calibration via the target locations on a segmented 4DCT image. The calibrated 5D model positions were compared with the actual positions delivered by the motion phantom during imaging to determine the 3D error at the end of this stage. A histogram of the errors is shown in Figure 5.14. Additionally, a histogram of the errors within the exhalation gating window is shown. Note that the errors from modeling decrease when observing exhalation vs. the entire breathing waveform (mean: 0.8 vs. 0.9mm; max: 2.0 vs. 2.9mm respectively).



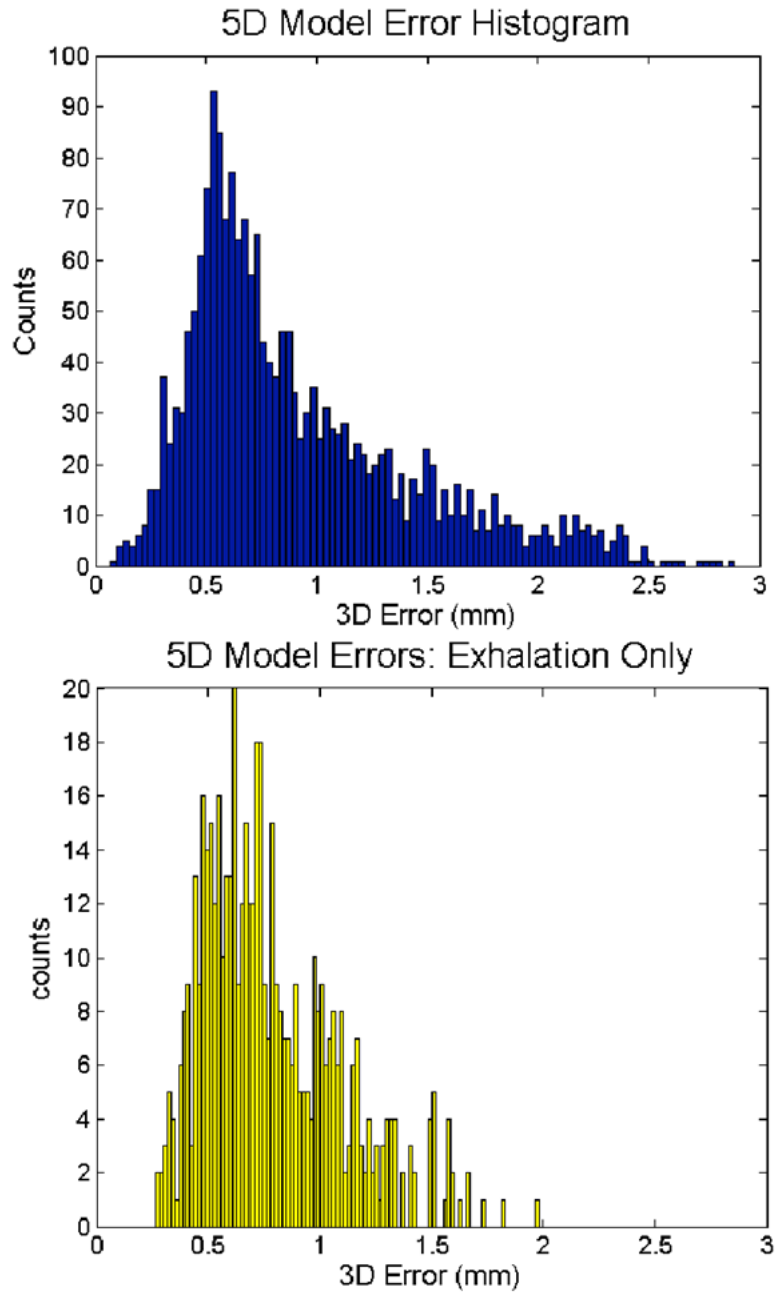


Figure 5.14: Lung Motion: Modeling Errors. The output from the 5D model used to determine the tumor position during treatment was compared with the actual tumor trajectory. Errors are reported for the entire waveform (blue) as well as only at exhalation (yellow).

Once the model was shown to be accurate, intervention was performed as described in the methods section. A total of 25 interventions on a moving target were performed. Errors from the interventions are reported in Figure 5.15. The intervention showed good agreement with a mean error of 2.0mm and a maximum error of 3.3mm.

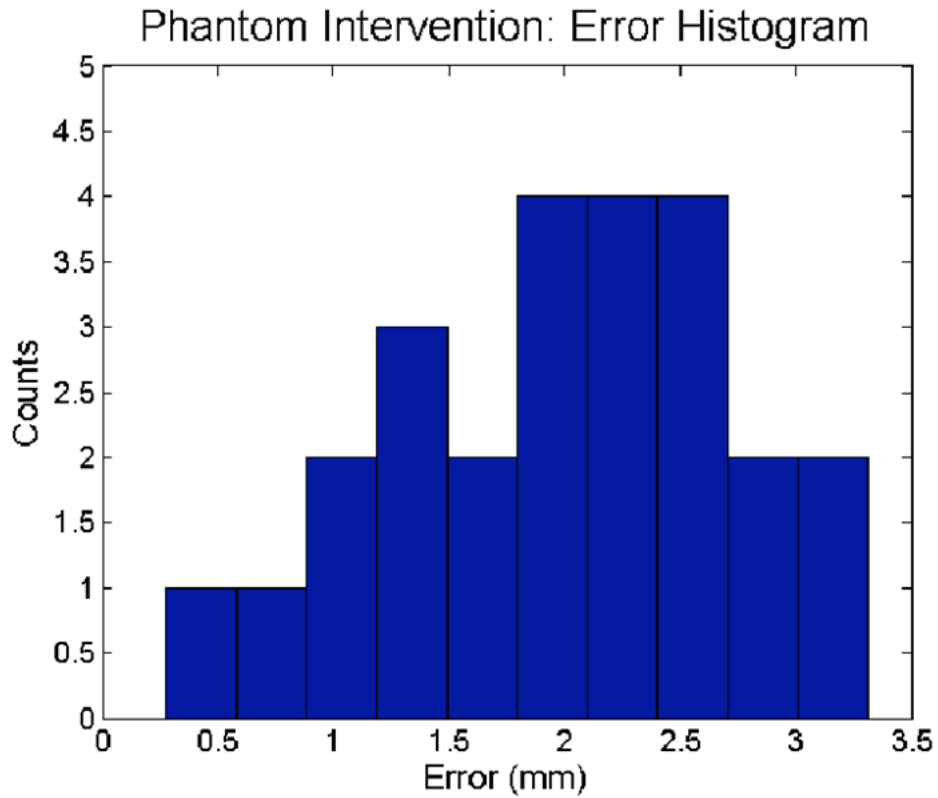


Figure 5.15: Lung Motion: Phantom Intervention Errors. Intervention was performed on a moving target. A histogram of the errors from 25 interventions is shown.

3D Error (mm)	Target Motion (mm)	Target Depth (cm)
2.9	8	2.3
2.6	7	2.4
1.0	10	1.8
4.0	8	3.7
6.9	15	1.2
1.7	12	2.3
2.1	9	1.5
5.6	7	1.2
6.8	15	2.1
4.0	15	2.1
4.4	11	2.2
3.9	11	2.2

Table 5.1: Porcine Intervention Accuracies. The target to needle tip errors are reported. Additionally, the target motion and depth are reported.

### 5.3.2 Porcine Assessment

In Figure 5.12, CT images of the target and tooltip are displayed. Additionally, table 5.1 contains the 3D error between the target and tooltip for each run. 9/12 intervention attempts provided accuracy suitable for intervention on a 1cm tumor. All attempts provided accuracies capable of intervening on a 1.5 cm diameter tumor. The mean error associated with intervention was 3.8mm (SD=0.8mm).

### 5.3.3 Cadaver Assessment

The RCIGS system displayed excellent accuracy in the human cadaver interventions. The table of geometric errors, equivalent tumor biopsy diameter, target depth and target motion is displayed in Table 5.2. The mean accuracy of intervention was found to be 4.0mm, with a mean target depth of 9cm. All target/tooltip errors were less than 5mm, which indicates intervention is suitable for 1cm tumors in 4/4 cases. Additionally, the target depths were large (7-10 cm). As a result, if a target was implanted at a depth larger than this, it is likely the intervention would have been performed from the posterior chest wall as opposed to anterior.

3D Error (mm)	Target Motion (mm)	Target Depth (cm)
4.5	2	7.8
4.8	2	10.1
3.2	4	8.9
3.4	5	9.3

Table 5.2: Cadaver Intervention Accuracies. The target to needle tip errors are reported. Additionally, the target motion and depth are reported.

The motion for the first two targets was minimal (2mm). These targets were both implanted in the right lung of the patient, which had substantial fluid to be drained prior to implantation/intervention (Figure 5.16). The fluid in the pleural space collapsed the lung substantially prior to draining via chest tubes, and as a result the lung possibly exhibited less motion.

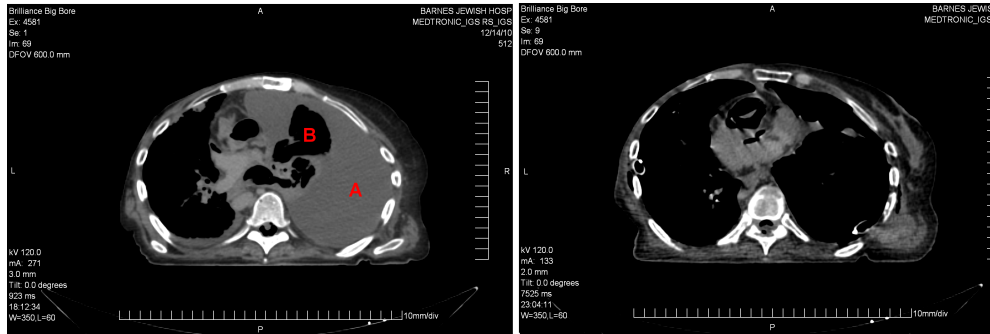


Figure 5.16: Pleural Effusion. Substantial fluid buildup (A) was present in one lung prior to draining via a chest tube affixed to a vacuum source. The lung was collapsed (B) prior to draining and this might have reduced the amount of respiratory related target motion for the two targets implanted into this lung. The right is a CT of the same lung after draining the fluid.

## 5.4 Discussion

The RIGS system shows promise for minimally invasive intervention in the lung/abdomen. There are several commercial systems on the market to currently address the problem, but to date none have published results encompassing the accuracy of the system from start to finish for interventions in the lung.

One group from Georgetown University has showcased their IGS software based on the open source Image Guided Surgery Toolkit (IGSTK).[3] In this study, three live swine were implanted with tumor analogues. The swine were sedated and intervention was performed to determine the accuracy of the guidance system in the presence of respiratory motion. The errors reported were substantially higher than our system ( $9.4\pm 3.0\text{mm}$  vs  $4.0\pm 0.8\text{mm}$ ).

There are improvements to the RCIGS package that would need to be made prior to a clinical implementation. In practice, it is unlikely a pulmonologist would refer a patient to an imaging center at a remote location in order to obtain the 4DCT for respiratory correlated intervention planning. Aside from workflow efficiency concerns, having the patient move between imaging and intervention has the potential to increase registration error. A mobile, compact system for performing CT acquisition has been developed (O-arm Surgical Imaging, Medtronic Navigation). A CT system capable of imaging within a pulmonary intervention suite would allow for increased patient throughput. Additionally, the acquired images would be automatically registered to room coordinates, which alleviates the need for point based registration. This would allow for workflow improvements as well as decrease the errors associated with doing registration on moving soft tissue body surfaces. Bronchoscopic intervention[26] is typically favored over percutaneous intervention[105] due to the reduced rate of pneumothorax. Development of flexible tools would allow for intervention through the working channel of a bronchoscope.

# Chapter 6

## Discussion

In 2006, respiratory correlated imaging was recently seeing clinical acceptance for modeling lung tumor motion and guiding treatment decisions. Volumetric imaging was used for daily alignment, however there was no respiratory correlated imaging used at time of treatment. An external marker block system (RPM, Varian Medical Systems) for gating the treatment beam based on respiration was starting to see adoption in clinical practice, however internal fiducial based systems, such as that offered by Calypso Medical, were not FDA cleared for use in any anatomical location. Since 2006 there have been many significant milestones in clinical radiation therapy technology development. After obtaining FDA clearance for use in the prostate, the Calypso system has been routinely used for daily clinical alignment. Additionally, our group worked in conjunction with Calypso Medical to develop a modified transponder with stabilizing legs that allow for fixation when deployed in the lung. This transponder has recently been implanted in 9/2010 into the first human lung cancer patient. Gating via internal electromagnetic transponders has been through FDA 510k approval and will be implemented clinically in the near future. DMLC guidance has been thoroughly quantified and tested, and once proper safety checks and quality assurance measures are in place, it will see clinical implementation in the next two years.

The use of electromagnetic position monitoring in radiation oncology has been explored, however there are many potential improvements. Implanted transponder position knowledge throughout treatment can be used for more than just guiding the radiation dose in real-time. As shown in the previous chapters, even an accurate guidance system using the effectors we have developed still has geometric and dosimetric

errors over the course of treatment. A system that could model the dose actually delivered to internal structures would allow for adaptive planning. One could propose a system in which the gating/DMLC tracking systems were implemented. After daily treatment, the positions of the transponders and correlated beam-on information are loaded into a deformable modeling application to determine the location of internal structures based on the locations of internal transponders throughout the treatment. The dose is then calculated on a voxel-by-voxel basis using the deformed organ position maps and correlated treatment beam information. The dose for subsequent treatments could then be modified to account for hot/cold spots from motion/alignment errors in previous fractions. If this adaptive system was sufficiently accurate, it has the potential to provide a drastic reduction in treatment margins; which would allow for dose escalation due to reduction in irradiated healthy tissue.

Internal markers have been shown to be safe for implantation and have displayed promise for guiding external beam radiation therapy, however there are room for improvements. They provide high temporal resolution but low spatial resolution (only 1-3 markers conventionally). This is complementary to the high spatial resolution but low temporal resolution offered by current volumetric imaging modalities. Markers have the potential to be implanted into more anatomical locations. Lung implantation has been explored, but is not currently FDA approved. Additional locations include the abdomen or breast tissue. For breast radiation therapy, an alternative solution to the Calypso transponder might be of interest. The transponder is effectively a wire coil, which are not for use in an MRI environment. Since external beam breast therapy is conventionally coupled with a follow up MRI, this means the transponder would have to be removed prior to imaging. An alternative solution from Navotek uses minute radioactive sources implanted in the body. The source can be localized with respect to the linear accelerator head, and the 3D position calculated. The dose from the sources is negligible when compared to that of a conventional radiation therapy treatment, and the source can remain in place following the treatment. Additionally, the sources can be made considerably smaller than the Calypso Beacon transponders, however the system is limited to a single source due to the fact that multiple sources would give a continuous signal which correlates to the superposition of the sources. This means the applications are limited to solely spatial position knowledge, where rotation is not of interest.

A combined cobalt gamma ray source and MRI machine is currently under development (Renaissance System, Viewray Inc.). Non-ionizing imaging available during treatment would provide target volumes and locations in real-time. Techniques reliant on real-time imaging to determine the position of internal anatomy throughout the treatment session could provide more information than a small number of internal fiducial positions. Currently, the computational power is not available for decision making based on real-time image segmentation. However, there are efforts being focused on this technology and it is likely to be implemented in the near future. Volumetric imaging throughout the treatment could potentially allow for the adaptive therapy described previously without the need for deformation modeling based on internal fiducials.

The RCIGS package has further development prior to being ready for a clinical implementation. As mentioned in the discussion, integration with an in-room movable CT scanner (Medtronic O-arm) would be ideal. There is work to be done in order to use the current O-arm for respiratory correlated surgical applications. First, the reconstructed field of view needs to be expanded in order to allow for large planning volumes such as the thorax. Additionally, respiratory correlated imaging is not currently available. A prospective 4DCT acquisition protocol could be developed in which images were only acquired when the patient is at the tidal volume of interest. This method would not only limit the imaging dose to the patient, but provide for less computationally expensive reconstruction times when compared with those of retrospective 4DCT. Additional porcine and cadaver trials will be necessary to ensure the system is robust, but will likely come after integration with the additional hardware.

Radiation therapy tumor tracking has seen substantial improvements in the past several years. Additional advancements in tracking technologies and adaptive radiation therapy planning will further our work. Image guided surgery is still a relatively new field. Surgeons conventionally have less time than radiation oncologists to learn new technologies related to respiratory motion management. Taking the radiation therapy concepts routinely used in the clinic and applying them to further a respiratory correlated image guided surgery package has the potential to improve diagnostic and interventional procedures within the lung and abdomen.



# Appendix A

## Abbreviations and Acronyms

<b>4DCT</b>	four dimensional (respiratory correlated) computed tomography
<b>BEV</b>	beams eye view
<b>CT</b>	computed tomography
<b>CTV</b>	clinical target volume
<b>DMLC</b>	dynamic multileaf collimator
<b>DTA</b>	distance to agreement
<b>EPID</b>	electronic portal imaging device
<b>IGS</b>	image guided surgery
<b>IMRT</b>	intensity modulated radiation therapy
<b>LINAC</b>	linear accelerator
<b>MLC</b>	multileaf collimator ...
<b>NSCLC</b>	non small cell lung cancer
<b>OBI</b>	on board imaging
<b>PTV</b>	planning target volume
<b>RF</b>	radio frequency
<b>RTRT</b>	real-time radiotherapy
<b>RTS</b>	respiratory tracking system

# Appendix B

## Definition of terms

### B.1 Linear Accelerators

In external beam radiation therapy, the source of ionizing radiation must pass through healthy tissue between the radiation source and the target site. Typically several different beam angles are used to irradiate the target and spread the dose to surrounding healthy tissue. In conventional linear accelerator (linac) setups, the entire gantry rotates around the patient to spread the dose to surrounding structures while continuously irradiating the target. This rotating gantry provides multiple beam angles to irradiate a single target site. Coupled with a couch that translates and rotates, non-coplaner beams can be utilized for special cases when avoiding critical structures surrounding the target (*e.g.* spinal cord, rectum).

Tumors are not uniform in size or shape, and as a result efforts are made to produce custom treatments on a per-patient basis. This has led to the use of multileaf collimators (MLCs) attached to the heads of traditional linear accelerator gantries. MLCs are composed of a series of heavy metal (typically tungsten) leaves that highly attenuate the x-rays emitting from the linear accelerator. The leaves are arranged in parallel and can be moved independently with one degree of freedom. The addition of MLCs allows for conformal radiation therapy, in which an aperture is defined for every beam angle that constricts the beam to the target's shape from the particular beam's eye view (BEV). It has been shown that the addition of conformal therapy allows for dose escalation, which has a positive effect on clinical outcomes [112].

## B.2 4DCT

Computed tomography (CT) has become a widely used method for volumetric imaging in both clinical and basic science applications. Conventional CT provides high-resolution tomographic images with high contrast. Although traditional CT images are static in time, a technique known as 4DCT has been developed to image anatomy as it moves due to the respiratory cycle [69, 11, 67]. The final output from a 4DCT is a series of 3D volumetric images in which each 3D image contains the location of the anatomy from a given phase/amplitude of the respiratory cycle.

At Washington University in St. Louis, a 4DCT imageset is acquired using the following method [44]. The patient is placed on the CT couch, and a respiratory surrogate such as a bellows and/or spirometer is affixed. This surrogate will simultaneously record the respiratory waveform throughout image acquisition. A computer receives this respiration signal along with the x-ray ON signal from the CT scanner, and as a result each acquired 2D tomographic image slice can be correlated with respect to the respiration waveform. Each 2D axial slice is oversampled in order to ensure that the given slice is acquired at each phase of the breathing cycle. For instance, if the intended 4DCT will be reconstructed at 10 phases, the output will be 10 volumetric 3D CT images each with all the anatomy corresponding to a given phase/amplitude. For this hypothetical acquisition, 25 images for each slice might be acquired to ensure that the phase of at least one of the images for that slice matches each of the 10 reconstructed phases.

At completion, 4DCT provides CT resolution images with temporal changes in internal anatomy. One of the concerns associated with this technique is increased radiation dose to the patient due to the oversampling required to generate the 4DCT. For patients undergoing radiation therapy, this concern is minimal compared to the dose associated with the treatment. For alternative applications, the benefits of the imaging technique must be weighed against the cost of the extra radiation to the patient.

## **B.3 IMRT**

MLCs have been widely adopted in clinical use for conformal radiation therapy. In an effort to increase dose conformality to the target, many treatment centers have implemented Intensity Modulated Radiation Therapy (IMRT). It has been shown that IMRT delivery improves dose conformality over conformal radiation therapy [111]. In IMRT planning, critical structures are defined via manual contouring, and constraints are set to ensure proper dose to the target and dose limits to surrounding healthy structures. After a dosimetrist defines all the constraints, an iterative algorithm calculates the best intensity profile to deliver from each beam angle in order to satisfy the initial conditions. There are two major types of IMRT delivery, S-IMRT and D-IMRT.

### **B.3.1 S-IMRT**

In S-IMRT delivery, during the planning stage a dosimetrist divides each beam angle into a series of segments. These segments are composed of different leaf sequences for a given beam angle, delivering a series of small static conformal beams for each angle. During delivery for a given beam angle, the leaves are aligned to the first segment and the beam is turned on. The dose prescribed for a given segment is delivered and at completion the beam is turned off. The leaves then move to their respective positions for the next segment and the beam is turned on again. In S-IMRT the leaves are never moving when the beam is on, and as a result this technique is often referred to as ‘Step and Shoot’ IMRT. During the planning phase, the segments are adjusted to ensure coverage of the target while minimizing hotspots in the dose profile. At completion, the plan contains a series of beam angles, and a series of segments for each angle.

### **B.3.2 D-IMRT**

In D-IMRT the plans are developed computationally. For each beam angle the fluence for each pixel in the beam’s eye view (BEV) is defined independently. Throughout

delivery the beam is enabled while the leaves are moving. The leaf pairs move such that for a given pixel in the BEV plane, the time between the leading leaf exposing a given pixel and the following leaf shielding a given pixel is sufficient to deliver the appropriate fluence (dose). This relationship can be described as follows:

$$v_r(m, x) = \frac{v_l(m + I(x), x)}{1 - \frac{dI(x)}{dx}v_l(m + I(x), x)} \quad (\text{B.1})$$

where

$m$  = moment in time (conventionally measured in monitor units)

$x$  = position along the direction of leaf motion

$I(x)$  = intensity

$v_r$  = velocity of the right (leading) leaf

$v_l$  = velocity of the left (trailing) leaf

## B.4 Dosimetric Analysis

In order to determine the effectiveness of various motion management techniques, dosimetric analysis is performed to quantitatively analyze the level at which the dose in the presence of motion (target image) matches the dose in the absence of motion (reference image). Dose is conventionally measured by dosimetric film, or arrays of ion chambers or diodes. There are a number of metrics for quantitatively comparing dosimetric accuracy. A brief overview of the most common dosimetric analysis techniques is included below.

### B.4.1 Difference Maps

In difference maps, the dose from the reference image is subtracted from that of the target image on a pixel-by-pixel basis. As a result, positive values indicate overdosing and negative values indicate under dosing. In areas of very steep dose gradients, a very small spatial offset can lead to drastic dosimetric differences.

## B.4.2 Distance to Agreement (DTA)

In the distance to agreement, the dose value for each pixel in the target image is compared to values in the surrounding area on the reference image. The minimum distance needed to find a corresponding dose value is recorded, using interpolation for discretized dose distributions. The DTA function is complementary to difference mapping in that it returns large values for relatively small dose differences in regions of shallow dose gradient.

## B.4.3 Gamma ( $\gamma$ ) Tool

The  $\gamma$  tool effectively combines both dose difference and distance to agreement metrics which each break down in steep and shallow dose gradient regions respectively. The  $\Gamma$  function is defined as the minimum generalized gamma function for all points:

$$\Gamma(\vec{r}_e, \vec{r}_r) = \sqrt{\frac{r^2(\vec{r}_e, \vec{r}_r)}{\Delta d^2} + \frac{\delta^2(\vec{r}_e, \vec{r}_r)}{\Delta D^2}} \quad (\text{B.2})$$

where

$(\vec{r}_e, \vec{r}_r)$  = the positions on the evaluated

and reference images respectively

$r(\vec{r}_e, \vec{r}_r)$  = the spatial distance between the two points  $(\vec{r}_e, \vec{r}_r)$

$\delta(\vec{r}_e, \vec{r}_r)$  = the difference between the

evaluated dose and the reference dose

$\Delta d$  = the distance to agreement criterion (typically 3mm)

$\Delta D$  = the dose agreement criterion (typically 3% of the max dose)

We leave out the details for the sake of brevity; however further information on the  $\gamma$  tool can be found in the literature [45].

## B.5 Intra/Inter -fraction motion

Due to the complicated nature and computational load associated with planning treatments, it is not currently clinically feasible to replan the patient at each fraction using daily volumetric imaging. With this in mind, at each fraction the patient is typically aligned via bony anatomy on orthogonal fluoroscopy images obtained at time of treatment. It is possible that although the bony anatomy is in the same location, the internal soft tissue may not be in the same location. Inter-fraction motion, or motion associated with repositioning the patient on the table between fractions, causes significant error in terms of target localization. In addition, intra-fraction motion can come in many forms. Many target sites are associated with intra-fraction motion (*e.g.* respiratory correlated motion in the lung and prostate shifts due to rectal filling). With this in mind, margins are added to the Clinical Target Volume (CTV) in order to ensure proper coverage when accounting for uncertainty in target position. The resulting Planning Target Volume (PTV) is then used for treatment planning [57]. Reducing the uncertainty in target location can lead to a reduction in PTV margins and allow for dose escalation to the target site.



Figure B.1: The Washington University 4D Phantom.

## B.6 Washington University 4D Phantom

In order to evaluate the accuracy of methods for mitigating respiratory motion, it is necessary to recreate patient motion with precision and accuracy. With this in mind, a 4D phantom was developed capable of reproducing motion to sub millimeter accuracy [52]. The phantom, shown in Figure B.1, contains a platform capable of holding a load sufficient for carrying dosimetric phantoms. It is composed of a four axis motion controller that can be loaded with a custom trajectory at 100hz. Once programmed with a trajectory, the phantom can recreate motion in three dimensions using orthogonally placed stepper motors as well as offer a fourth surrogate axis for independant motion analogous to a respiratory surrogate signal. For many characterization studies described herein, the 4D phantom was used to accurately recreate patient breathing trajectories.

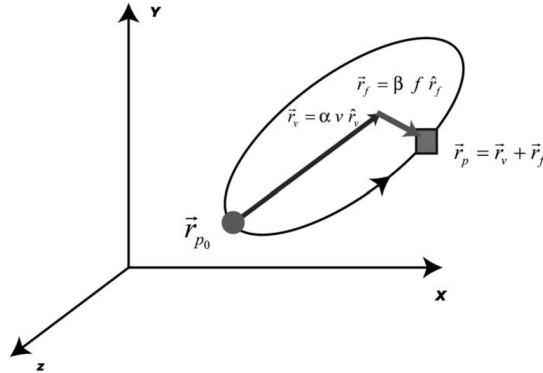


Figure B.2: Lung motion model. The motion of the object at baseline (circle) is shown at a given phase point (square). Component vectors related to the tidal volume ( $\vec{r}_v$ ) and airflow ( $\vec{r}_f$ ) predict the position of the object ( $\vec{r}_p$ ) with respect to baseline ( $\vec{r}_{p0}$ ) at any phase of the breathing cycle.



## B.7 Respiratory Motion Model

The ability to accurately predict tissue motion within the lung as it moves due to respiration is useful for a variety of interventional applications. A respiratory correlated lung motion model has been developed which relies on the signal from an external respiratory surrogate (spirometry) to correlate internal tissue motion with tidal volume and airflow in the lung. [45]. As described visually in Figure B.2 the position of an object within the lung can be predicted based on two independent vectors ( $\hat{r}_v, \hat{r}_f$ ) related to the tidal volume and airflow respectively. Typically the main portion of motion is derived from tidal volume changes in the lung. Hysteresis occurs due to air-flow derived local pressure differences, and this motion is accounted for by the second vector  $\hat{r}_f$ . Conventionally the model is calibrated using the position of the target on a 4DCT image set obtained either via manual segmentation or automatic template matching for high contrast easily identifiable landmarks. Once the 3D target position along with the mean tidal volume and flow is delineated for each phase of the 4DCT, these parameters can be used to calibrate the 5D model. The model yields the target position based on the external surrogate for any tidal volume/airflow as described in equation B.3. Research is ongoing confirming the accuracy of this model for clinical applications.

$$\vec{r}_p = \alpha v \hat{r}_v + \beta f \hat{r}_f \quad (\text{B.3})$$

where

$r_{p0}^{\vec{}}$  = the baseline position at exhalation.

$\vec{r}_p$  = the vector offset from baseline position  $r_{p0}^{\vec{}}$

$\alpha, \beta$  = Model constants (tidal volume, airflow respectively)

$\hat{r}_v, \hat{r}_f$  = Unit tidal volume and airflow component vectors

$v$  = tidal volume

$f$  = airflow

## B.8 Target Localization Techniques

Respiratory correlation has been used extensively in CT and MR imaging in an effort to reduce breathing related image artifacts [75, 69]. More recently, similar techniques have been employed to localize the tumor and gate (turn on/off) the linear accelerator [91, 49, 35]. Conventional gating setups use a variety of techniques to measure breathing motion including: optically tracked external marker blocks, thermocouples, thermistors, strain gauges, and pneumotachographs [38]. Current techniques rely on the use of external markers or sensors to determine the internal position of the target. If a relationship between the external surrogate and the internal target position can be established, the beam can be turned off or ‘gated’ when the target is outside of the delivery volume. Although a correlation exists between external markers and internal tumor position, for some patients’ external marker trajectories do not serve as an adequate surrogate for internal tumor position [16].

Respiration induces considerable deformation within the thoracic cavity. As the diaphragm contracts, internal anatomy compresses and distends. Often the external anatomy exhibits good correlation with the motion of the internal structures such as the diaphragm and/or lung tumors [49, 16]. The external anatomy moves due to respiration; however studies have shown considerable differences between external anatomy and internal motion. These differences can come in the form of correlated motion with a phase lag between the external and internal motion, or less frequently the motion might not exhibit correlation. Margeras and Yorke have reported up to a 0.5 second lag between Varian RPM marker block position and diaphragm position measured fluoroscopically [50]. Koch et al found that correlation was poor and unstable unless the external surrogate measuring skin surface position was near the tumor [36]. In a study from Berbeco et al, lung tumor motion was measured via continuous fluoroscopy concurrently with measurement of external abdominal surface positions [7]. The amount of residual tumor motion, defined as the amount of tumor motion during a respiratory gate based upon the movement of the external surrogate, showed large fluctuations (>300%) for both intra- and inter-fraction motion. The residual motion was found to be up to 8 mm in magnitude, which strongly suggests that external position monitoring cannot accurately reflect the internal position of a tumor for all cases. The periods in which external and internal motion exhibit poor correlation

are often transient; however these transient periods have dosimetric implications [68].

The lack of correlation between internal/external positions has led investigators to examine alternative techniques for accurately tracking the position of targets inside the thoracic cavity. Shirato et al developed a real-time target tracking system that uses four integrated kilovoltage imaging systems [89]. The fluoroscopic imaging system used in this technique provides accurate information on the location of discrete points inside the abdomen. However, accurate tracking of the target comes at the expense of an increased imaging dose. For a single fluoroscope, the estimated skin surface dose rate can be up to 118 cGy/h [93]. In addition, for 3D target tracking, stereoscopic fluoroscopes are necessary which means further accumulated dose due to imaging. The Synchrony<sup>TM</sup>Respiratory Tracking System (RTS) treatment option of the CyberKnife robotic radiotherapy system provides another image based system for tracking internal fiducial markers [85]. With this technique, gold fiducials are placed inside the thoracic cavity near the tumor while the patient wears a vest with LEDs that indicate the position of the chest and abdomen. Before the treatment begins, a series of orthogonal x-ray images are acquired that are used to correlate the position of the external markers to the internal fiducials. A correspondence model is developed and periodic images are obtained during the course of delivery to ensure the continued validity of the correspondence model. While the Synchrony<sup>TM</sup>RTS delivers a lower radiation dose to the patient as compared to continuous fluoroscopic imaging, this is achieved at the expense of intermittent absolute knowledge of internal positions. Previous studies state that the entrance dose per image can be as high as 0.2 cGy [64]. For a 2-hour session with imaging performed every 30 seconds, the patient receives 48 cGy over the course of the treatment due to imaging.

Alternative image based solutions have been investigated which utilize the on board imaging (OBI) functionality of many modern linear accelerators [6]. Similarly to the fluoroscopy based solutions previously mentioned, OBI solutions deliver dose to the patient in order to image and track internal markers/tumors. Another factor limiting this technique is the fact that high energy MV scatter from the treatment beam can degrade the image quality of the kV images typically used for tracking [48]. OBI based methods do have the advantage of providing information about the surrounding tissue, which a pure electromagnetic position monitoring solution cannot provide.

## B.9 Calypso Electromagnetic Position Monitoring

Continuous electromagnetic position monitoring is now available without additional dose to the patient (Calypso Medical, Seattle WA). The system uses one or more wireless transponders which are subject to performance testing as part of the manufacturing operation to ensure they can stand up to high levels of radiation throughout the treatment process. The transponders are implanted into the patient via a 14-gauge needle in a procedure similar to existing gold fiducial implants currently in use clinically. During treatment planning, the location of the transponders is recorded with respect to isocenter, and a plan is developed.

During delivery, an array is placed above the patient. Four source coils in the array excite the transponders via magnetic induction. After excitation, 32 receiver coils in the array detect the resulting response signal. Each transponder contains an RLC circuit tuned to a unique resonant frequency (300kHz, 400kHz, or 500kHz), and they are sequentially excited in order to independently query position information. When the array excites at a particular frequency, only the transponder tuned to that frequency can store the energy to later emit back to the array for detection. For a simple series RLC circuit, the resonant frequency is defined as:  $\omega_o = \frac{1}{\sqrt{LC}}$ . The array is registered to the room via stereoscopic infrared cameras, and hence the transponder position is known with respect to the room isocenter.

Balter et al have reported submillimeter accuracy when tracking the transponders moving at 3 cm/s in a volume that is 14x14 cm in width, and up to 27 cm away from the array [2]. In a study from Santanam et al the system was again found to be sub-mm accurate as confirmed by onboard kilovoltage imaging [78]. In a clinical prostate cancer treatment study, Willoughby et al have shown the system to be functional in a linac environment, even when the linac is treating directly through the array [108]. To date there have been no published failures of the transponders due to radiation dose. The system is currently FDA cleared for use in the prostate, and potential applications in the lung and abdomen (where motion is substantial) are promising.

## B.10 Medtronic StealthStation

The Medtronic StealthStation (pictured Figure 5.1) is an IGS system for minimally invasive surgical procedures. The StealthStation AxiEM technology provides electromagnetic tracking of wired instruments within the body. In this EM tracking implementation, a position variant magnetic field is generated within the patient using three orthogonal coils contained inside of the field generator. Tools for the AxiEM system have one or more coils near the tip, and upon entering the magnetic field a position dependent current is induced. The tools are connected via a wire back to the StealthStation and the amplitude of the induced current allows for continuous 3D localization.

AxiEM tools offer some advantages over optically tracked IGS systems. First, line of sight is not required to track the tools. Additionally, using single-coil tools allows for the potential of flexible tools that could be implanted via a bronchoscope. Optical tools require the tool to be rigid with respect to the optical base which is tracked outside of the body. If the tip of the optical tool bends during implantation with respect to the base, the localization error of the tip will be large.

# References

- [1] James M. Balter, Kwok L. Lam, Cornealeus J. McGinn, Theodore S. Lawrence, and Randall K. Ten Haken. Improvement of CT-based treatment-planning models of abdominal targets using static exhale imaging. *International Journal of Radiation Oncology\*Biology\*Physics*, 41(4):939–943, July 1998.
- [2] James M. Balter, J. Nelson Wright, Laurence J. Newell, Barry Friemel, Steven Dimmer, Yuki Cheng, John Wong, Edward Vertatschitsch, and Timothy P. Mate. Accuracy of a wireless localization system for radiotherapy. *International Journal of Radiation Oncology\*Biology\*Physics*, 61(3):933–937, March 2005.
- [3] Filip Banovac, Patrick Cheng, Enrique Campos-Nanez, Bhaskar Kallakury, Teo Popa, Emmanuel Wilson, Hernan Abeledo, and Kevin Cleary. Radiofrequency ablation of lung tumors in swine assisted by a navigation device with preprocedural volumetric planning. *Journal of Vascular and Interventional Radiology*, 21(1):122–129, 2010.
- [4] Elizabeth A. Barnes, Brad R. Murray, Donald M. Robinson, Lori J. Underwood, John Hanson, and Wilson H. Y. Roa. Dosimetric evaluation of lung tumor immobilization using breath hold at deep inspiration. *International Journal of Radiation Oncology\*Biology\*Physics*, 50(4):1091–1098, July 2001.
- [5] R. I. Berbeco, C. J. Pope, and S. B. Jiang. Measurement of the interplay effect in lung IMRT treatment using EDR2 films. *J Appl Clin Med Phys*, 7(4):33–42, 2006.
- [6] Ross I. Berbeco, Steve B. Jiang, Gregory C. Sharp, George T. Y. Chen, Hassan Mostafavi, and Hiroki Shirato. Integrated radiotherapy imaging system (IRIS): design considerations of tumour tracking with linac gantry-mounted diagnostic x-ray systems with flat-panel detectors. *Physics in Medicine and Biology*, 49(2):243–255, 2004.
- [7] Ross I Berbeco, Seiko Nishioka, Hiroki Shirato, George T Y Chen, and Steve B Jiang. Residual motion of lung tumours in gated radiotherapy with external respiratory surrogates. *Physics in medicine and biology*, 50(16):3655–67, August 2005. PMID: 16077219.

- [8] Anthony M. Berson, Richard Emery, Lara Rodriguez, Gregory M. Richards, Tracy Ng, Seema Sanghavi, and Jean Barsa. Clinical experience using respiratory gated radiation therapy: Comparison of free-breathing and breath-hold techniques. *International Journal of Radiation Oncology\*Biology\*Physics*, 60(2):419–426, October 2004.
- [9] T. Bortfeld, K. Jokivarsi, M. Goitein, J. Kung, and S. B. Jiang. Effects of intra-fraction motion on IMRT dose delivery: statistical analysis and simulation. *Physics in Medicine and Biology*, 47(13):2203–2220, 2002.
- [10] Jeffrey D. Bradley, Sasha Wahab, Mary Ann Lockett, Carlos A. Perez, and James A. Purdy. Elective nodal failures are uncommon in medically inoperable patients with stage i non-small-cell lung carcinoma treated with limited radiotherapy fields. *International Journal of Radiation Oncology\*Biology\*Physics*, 56(2):342–347, June 2003.
- [11] Keith R. Britton, George Starkschall, Susan L. Tucker, Tinsu Pan, Christopher Nelson, Joe Y. Chang, James D. Cox, Radhe Mohan, and Ritsuko Komaki. Assessment of gross tumor volume regression and motion changes during radiotherapy for Non-Small-Cell lung cancer as measured by Four-Dimensional computed tomography. *International Journal of Radiation Oncology\*Biology\*Physics*, 68(4):1036–1046, July 2007.
- [12] K. S. C. Chao, D. A. Low, C. A. Perez, and J. A. Purdy. Intensity-Modulated radiation therapy in head and neck cancers: The mallinckrodt experience. *Radiat. Oncol. Invest*, 90:92–103, 2000.
- [13] Pai-Chun Melinda Chi, Peter Balter, Dershan Luo, Radhe Mohan, and Tinsu Pan. Relation of external surface to internal tumor motion studied with cine CT. *Medical Physics*, 33(9):3116–3123, 2006.
- [14] R. George, P. J. Keall, V. R. Kini, S. S. Vedam, J. V. Siebers, Q. Wu, M. H. Lauterbach, D. W. Arthur, and R. Mohan. Quantifying the effect of intrafraction motion during breast IMRT planning and dose delivery. *Medical Physics*, 30:552, 2003.
- [15] D. P. Gierga, G. T. Y. Chen, J. H. Kung, M. Betke, J. Lombardi, and C. G. Willett. Quantification of respiration-induced abdominal tumor motion and its impact on IMRT dose distributions. *International Journal of Radiation Oncology\*Biology\*Physics*, 58(5):1584–1595, 2004.
- [16] David P Gierga, Johanna Brewer, Gregory C Sharp, Margrit Betke, Christopher G Willett, and George T Y Chen. The correlation between internal and external markers for abdominal tumors: implications for respiratory gating. *International journal of radiation oncology, biology, physics*, 61(5):1551–8, April 2005. PMID: 15817361.

- [17] I. S. Grills, D. Yan, A. A. Martinez, F. A. Vicini, J. W. Wong, and L. L. Kestin. Potential for reduced toxicity and dose escalation in the treatment of inoperable nonsmall-cell lung cancer: A comparison of intensity-modulated radiation therapy (IMRT), 3D conformal radiation, and elective nodal irradiation. *International Journal of Radiation Oncology\*Biography\*Physics*, 57(3):875–890, 2003.
- [18] W. E. L. Grimson, R. Kikinis, F. A. Jolesz, and P. M. Black. Image-guided surgery. *Scientific American*, 280(6):5461, 1999.
- [19] Christopher R. Grindle, Joseph M. Curry, Melissa D. Kang, James J. Evans, and Marc R. Rosen. Preoperative magnetic resonance imaging protocol for endoscopic cranial base image-guided surgery. *American Journal of Otolaryngology*, In Press, Corrected Proof, 2010.
- [20] J. Hanley, M. M. Debois, D. Mah, G. S. Mageras, A. Raben, K. Rosenzweig, B. Mychalczak, L. H. Schwartz, P. J. Gloeggler, and W. Lutz. Deep inspiration breath-hold technique for lung tumors: the potential value of target immobilization and reduced lung density in dose escalation. *Int J Radiat Oncol Biol Phys*, 45(3):603–11, 1999.
- [21] Joseph Hanley, Marc M. Debois, Dennis Mah, Gikas S. Mageras, Adam Raben, Kenneth Rosenzweig, Borys Mychalczak, Lawrence H. Schwartz, Paul J. Gloeggler, Wendell Lutz, C. Clifton Ling, Steven A. Leibel, Zvi Fuks, and Gerald J. Kutcher. Deep inspiration breath-hold technique for lung tumors: the potential value of target immobilization and reduced lung density in dose escalation. *International Journal of Radiation Oncology\*Biography\*Physics*, 45(3):603–611, October 1999.
- [22] G Hanna, Z Wang, and F Yin. SU-FF-T-432: Time-Delay measurement of a varian Real-Time position management system. *Medical Physics*, 33(6):2145, June 2006.
- [23] Claudia I. Henschke, Dorothy I. McCauley, David F. Yankelevitz, David P. Naidich, Georgeann McGuinness, Olli S. Miettinen, Daniel Libby, Mark Pasmantier, June Koizumi, Nasser Altorki, and James P. Smith. Early lung cancer action project: A summary of the findings on baseline screening. *Oncologist*, 6(2):147–152, April 2001.
- [24] B. K.P Horn and B. G Schunck. Determining optical flow. *Artificial Intelligence*, 17:185203, 1981.
- [25] Sui Huang and Donald E. Ingber. Cell tension, matrix mechanics, and cancer development. *Cancer Cell*, 8(3):175–176, September 2005.



- [26] Mikado Imura, Koichi Yamazaki, Hiroki Shirato, Rikiya Onimaru, Masaharu Fujino, Shinichi Shimizu, Toshiyuki Harada, Shigeaki Ogura, Hirotoshi Dosaka-Akita, Kazuo Miyasaka, and Masaharu Nishimura. Insertion and fixation of fiducial markers for setup and tracking of lung tumors in radiotherapy. *International Journal of Radiation Oncology\*Biophysics*, 63(5):1442–1447, December 2005.
- [27] S. B. Jiang, C. Pope, J. H. Kung, T. Bortfeld, and G. T. Y. Chen. An experimental investigation on intra-fractional organ motion effects in lung IMRT treatments. *Physics in Medicine and Biology*, 48(12):1773–1784, 2003.
- [28] Jian-Yue Jin and Fang-Fang Yin. Time delay measurement for linac based treatment delivery in synchronized respiratory gating radiotherapy. *Medical Physics*, 32(5):1293–1296, May 2005.
- [29] J. R. Adler Jr, S. D. Chang, M. J. Murphy, J. Doty, P. Geis, S. L. Hancock, and J. R. Adler. The cyberknife: A frameless robotic system for radiosurgery. *Stereotact Funct Neurosurg*, 69(1-4):124–128, 1997.
- [30] David M Kahler. Image guidance: Fluoroscopic navigation. *Clinical Orthopaedics and Related Research*, 421:70–76 10.1097/01.blo.0000126869.67208.2d, 2004.
- [31] P. J. Keall, V. R. Kini, S. S. Vedam, and R. Mohan. Motion adaptive x-ray therapy: a feasibility study. *Physics in Medicine and Biology*, 46:1–10, 2001.
- [32] P J Keall, V R Kini, S S Vedam, and R Mohan. Potential radiotherapy improvements with respiratory gating. *Australasian physical & engineering sciences in medicine / supported by the Australasian College of Physical Scientists in Medicine and the Australasian Association of Physical Sciences in Medicine*, 25(1):1–6, March 2002. PMID: 12049470.
- [33] Paul Keall. 4-dimensional computed tomography imaging and treatment planning. *Seminars in Radiation Oncology*, 14(1):81–90, 2004.
- [34] Paul J. Keall, Sarang Joshi, S. Sastry Vedam, Jeffrey V. Siebers, Vijaykumar R. Kini, and Radhe Mohan. Four-dimensional radiotherapy planning for DMLC-based respiratory motion tracking. *Medical Physics*, 32(4):942–951, April 2005.
- [35] Vijay R. Kini, Subrahmanya S. Vedam, Paul J. Keall, Sumukh Patil, Clayton Chen, and Radhe Mohan. Patient training in respiratory-gated radiotherapy. *Medical Dosimetry*, 28(1):7–11, 2003.
- [36] Nicholas Koch, H. Helen Liu, George Starkschall, Marc Jacobson, Kenneth Forster, Zhongxing Liao, Ritsuko Komaki, and Craig W. Stevens. Evaluation

- of internal lung motion for respiratory-gated radiotherapy using MRI: part i—correlating internal lung motion with skin fiducial motion. *International Journal of Radiation Oncology\*Biography\*Physics*, 60(5):1459–1472, December 2004.
- [37] H. Dale Kubo, Patrick M. Len, Shin ichi Minohara, and Hassan Mostafavi. Breathing-synchronized radiotherapy program at the university of california davis cancer center. *Medical Physics*, 27(2):346–353, February 2000.
- [38] Hideo D Kubo and Bruce C Hill. Respiration gated radiotherapy treatment: a technical study. *Physics in Medicine and Biology*, 41(1):8391, 1996.
- [39] Patrick Kupelian, Twyla Willoughby, Arul Mahadevan, Toufik Djemil, Geoffrey Weinstein, Shirish Jani, Charles Enke, Timothy Solberg, Nicholas Flores, David Liu, David Beyer, and Lisa Levine. Multi-institutional clinical experience with the calypso system in localization and continuous, real-time monitoring of the prostate gland during external radiotherapy. *International Journal of Radiation Oncology\*Biography\*Physics*, 67(4):1088–1098, March 2007.
- [40] Patrick A. Kupelian, Alan Forbes, Twyla R. Willoughby, Karen Wallace, Rafael R. Maon, Sanford L. Meeks, Luis Herrera, Alan Johnston, and Juan J. Herran. Implantation and stability of metallic fiducials within pulmonary lesions. *International Journal of Radiation Oncology\*Biography\*Physics*, 69(3):777–785, November 2007.
- [41] K M Langen and D T Jones. Organ motion and its management. *International Journal of Radiation Oncology\*Biography\*Physics*, 50(1):265–78, May 2001. PMID: 11316572.
- [42] H Li, PM Boiselle, JO Shepard, B Trotman-Dickenson, and TC McLoud. Diagnostic accuracy and safety of CT-guided percutaneous needle aspiration biopsy of the lung: comparison of small and large pulmonary nodules. *Am. J. Roentgenol.*, 167(1):105–109, July 1996.
- [43] Daniel A. Low and James F. Dempsey. Evaluation of the gamma dose distribution comparison method. *Medical Physics*, 30(9):2455–2464, 2003.
- [44] Daniel A. Low, Michelle Nystrom, Eugene Kalinin, Parag Parikh, James F. Dempsey, Jeffrey D. Bradley, Sasa Mutic, Sasha H. Wahab, Tareque Islam, Gary Christensen, David G. Politte, and Bruce R. Whiting. A method for the reconstruction of four-dimensional synchronized CT scans acquired during free breathing. *Medical Physics*, 30(6):1254–1263, June 2003.
- [45] Daniel A. Low, Parag J. Parikh, Wei Lu, James F. Dempsey, Sasha H. Wahab, James P. Hubenschmidt, Michelle M. Nystrom, Maureen Handoko, and

- Jeffrey D. Bradley. Novel breathing motion model for radiotherapy. *International Journal of Radiation Oncology\*Biography\*Physics*, 63(3):921–929, November 2005.
- [46] Wei Lu, Parag J Parikh, Issam M El Naqa, Michelle M Nystrom, James P Hubenschmidt, Sasha H Wahab, Sasa Mutic, Anurag K Singh, Gary E Christensen, Jeffrey D Bradley, and Daniel A Low. Quantitation of the reconstruction quality of a four-dimensional computed tomography process for lung cancer patients. *Medical physics*, 32(4):890–901, April 2005. PMID: 15895571.
- [47] W. Luo, S. Yoo, J. Wu, Z. Wang, H. Song, and F. Yin. Effect of MV scatter on kV image quality during simultaneous kV-MV imaging. *International Journal of Radiation Oncology\* Biology\* Physics*, 69(3):S671, 2007.
- [48] W. Luo, S. Yoo, Q. J. Wu, Z. Wang, and F.-F. Yin. Analysis of image quality for real-time target tracking using simultaneous kV-MV imaging. *Medical Physics*, 35(12):5501–5509, December 2008.
- [49] G. Mageras, E. Yorke, K. Rosenzweig, F. Fontenla, E. Keatley, and C. Ling. Initial clinical evaluation of a respiratory gating radiotherapy system. In *Engineering in Medicine and Biology Society, 2000. Proceedings of the 22nd Annual International Conference of the IEEE*, volume 3, pages 2124–2127 vol.3, 2000.
- [50] Gig S. Mageras, Alex Pevsner, Ellen D. Yorke, Kenneth E. Rosenzweig, Eric C. Ford, Agung Hertanto, Steven M. Larson, D. Michael Lovelock, Yusuf E. Erdi, Sadek A. Nehmeh, John L. Humm, and C. Clifton Ling. Measurement of lung tumor motion using respiration-correlated CT. *International Journal of Radiation Oncology\*Biography\*Physics*, 60(3):933–941, November 2004.
- [51] Gikas S. Mageras and Ellen Yorke. Deep inspiration breath hold and respiratory gating strategies for reducing organ motion in radiation treatment. *Seminars in Radiation Oncology*, 14(1):65–75, 2004.
- [52] K Malinowski. Use of the 4D phantom to test Real-Time targeted radiation. *Med. Phys.*, 34(6):2611, 2007.
- [53] S. Marnitz, M. Stuschke, J. Bohsung, A. Moys, I. Reng, R. Wurm, and V. Budach. Intraindividual comparison of conventional Three-Dimensional radiotherapy and intensity modulated radiotherapy in the therapy of locally advanced Non-Small cell lung cancer. *Strahlentherapie und Onkologie*, 178(11):651–658, 2002.
- [54] Simone Marnitz, Martin Stuschke, Jrg Bohsung, Anne Moys, Ines Reng, Reinhard Wurm, and Volker Budach. Intraindividual comparison of conventional Three-Dimensional radiotherapy and intensity modulated radiotherapy in the

- therapy of locally advanced Non-Small cell lung cancer. *Strahlentherapie und Onkologie*, 178(11):651–658, November 2002.
- [55] Martin L. Mayse, Parag J. Parikh, Amir Chaudhari, Kristen M. Lechleiter, Steve Dimmer, Roger Hildwein, Mia Park, Daniel Low, and Jefferey Bradley. BRONCHOSCOPIC IMPLANTATION OF ELECTROMAGNETIC TRANSPONDERS IN THE CANINE LUNG. *Chest*, 130(4):166S–c, October 2006.
- [56] M.L. Mayse, R.L. Smith, M. Park, G.H. Monteon, E.H. Silver, P.J. Parikh, D.L. Misselhorn, M.R. Talcott, S. Dimmer, and J.D. Bradley. Development of a non-migrating electromagnetic transponder system for lung tumor tracking. *International Journal of Radiation Oncology\*Biophysics*, 72(1, Supplement 1):S430, September 2008.
- [57] A L McKenzie, M van Herk, and B Mijnheer. The width of margins in radiotherapy treatment plans. *Physics in Medicine and Biology*, 45(11):3331–3342, November 2000. PMID: 11098907.
- [58] James Mechalakos, Ellen Yorke, Gikas S. Mageras, Agung Hertanto, Andrew Jackson, Ceferino Obcemea, Kenneth Rosenzweig, and C. Clifton Ling. Dose-metric effect of respiratory motion in external beam radiotherapy of the lung. *Radiotherapy and Oncology*, 71(2):191–200, May 2004.
- [59] M Mehta, R Scrimger, R Mackie, B Paliwal, R Chappell, and J Fowler. A new approach to dose escalation in non-small-cell lung cancer. *International journal of radiation oncology, biology, physics*, 49(1):23–33, 2001. PMID: 11163494.
- [60] P. Merloz, J. Tonetti, L. Pittet, M. Coulomb, S. Lavallo, and P. Sautot, 1998.
- [61] R Metson, R.E. Gliklich, and M. Cosenza. A comparison of image guidance systems for sinus surgery. *The Laryngoscope*, 108(8):1164–1170, 1998.
- [62] M. W. Mnter, C. Thilmann, H. Hof, B. Didinger, B. Rhein, S. Nill, W. Schlegel, M. Wannemacher, and J. Debus. Stereotactic intensity modulated radiation therapy and inverse treatment planning for tumors of the head and neck region: clinical implementation of the step and shoot approach and first clinical results. *Radiotherapy and Oncology*, 66(3):313–321, 2003.
- [63] Martin J. Murphy. An automatic six-degree-of-freedom image registration algorithm for image-guided frameless stereotaxic radiosurgery. *Medical Physics*, 24(6):857–866, June 1997.

- [64] Martin J. Murphy, James Balter, Stephen Balter, Jr. BenComo, Indra J. Das, Steve B. Jiang, C.-M. Ma, Gustavo H. Olivera, Raymond F. Rodebaugh, Kenneth J. Ruchala, Hiroki Shirato, and Fang-Fang Yin. The management of imaging dose during image-guided radiotherapy: Report of the AAPM task group 75. *Medical Physics*, 34(10):4041–4063, October 2007.
- [65] C Noel and P Parikh. Effect of Mid-Scan breathing changes on quality of 4DCT using a commercial Phase-Based sorting algorithm. *Medical Physics*, In Review, 2010.
- [66] K. Ohara, T. Okumura, M. Akisada, T. Inada, T. Mori, H. Yokota, and M. J. Calaguas. Irradiation synchronized with respiration gate. *Int J Radiat Oncol Biol Phys*, 17(4):853–7, 1989.
- [67] Jeffrey R Olsen, Wei Lu, James P Hubenschmidt, Michelle M Nystrom, Paul Klahr, Jeffrey D Bradley, Daniel A Low, and Parag J Parikh. Effect of novel amplitude/phase binning algorithm on commercial four-dimensional computed tomography quality. *International journal of radiation oncology, biology, physics*, 70(1):243–52, 2008. PMID: 18037590.
- [68] Cihat Ozhasoglu and Martin J. Murphy. Issues in respiratory motion compensation during external-beam radiotherapy. *International Journal of Radiation Oncology\*Biological\*Physics*, 52(5):1389–1399, April 2002.
- [69] Tinsu Pan, Ting-Yim Lee, Eike Rietzel, and George T. Y. Chen. 4D-CT imaging of a volume influenced by respiratory motion on multi-slice CT. *Medical Physics*, 31(2):333–340, February 2004.
- [70] Tinsu Pan, Ting-Yim Lee, Eike Rietzel, and George T. Y. Chen. 4D-CT imaging of a volume influenced by respiratory motion on multi-slice CT. *Medical Physics*, 31(2):333–340, February 2004.
- [71] Lech Papiez and Dharanipathy Rangaraj. DMLC leaf-pair optimal control for mobile, deforming target. *Medical Physics*, 32(1):275–285, 2005.
- [72] Lech Papiez, Dharanipathy Rangaraj, and Paul Keall. Real-time DMLC IMRT delivery for mobile and deforming targets. *Medical Physics*, 32(9):3037–3048, 2005.
- [73] P Parikh, K Lechleiter, K Malinowski, B Sargent, J Peterson, J Newell, J Bradley, and J Low. Dosimetric effects of a 4D magnetic localization system for LINAC beam gating on prostate and lung radiation therapy. *Medical Physics*, 34(6):2625, 2007.
- [74] C R Ramsey, I L Cordrey, and A L Oliver. A comparison of beam characteristics for gated and nongated clinical x-ray beams. *Medical physics*, 26(10):2086–91, October 1999. PMID: 10535624.

- [75] Chester R. Ramsey, Daniel Scaperoth, Don Arwood, and Adrian L. Oliver. Clinical efficacy of respiratory gated conformal radiation therapy. *Medical Dosimetry*, 24(2):115–119, 1999.
- [76] Eike Rietzel, George T.Y. Chen, Noah C. Choi, and Christopher G. Willet. Four-dimensional image-based treatment planning: Target volume segmentation and dose calculation in the presence of respiratory motion. *International Journal of Radiation Oncology\*Biography\*Physics*, 61(5):1535–1550, April 2005.
- [77] K E Rosenzweig, J Hanley, D Mah, G Mageras, M Hunt, S Toner, C Burman, C C Ling, B Mychalczak, Z Fuks, and S A Leibel. The deep inspiration breath-hold technique in the treatment of inoperable non-small-cell lung cancer. *International Journal of Radiation Oncology\*Biography\*Physics*, 48(1):81–7, August 2000. PMID: 10924975.
- [78] Lakshmi Santanam, Kathleen Malinowski, James Hubenshmidt, Steve Dimmer, Martin L. Mayse, Jeffrey Bradley, Amir Chaudhari, Kirsten Lechleiter, Sree Krishna Murty Goddu, Jacqueline Esthappan, Sasa Mutic, Daniel A. Low, and Parag Parikh. Fiducial-Based translational localization accuracy of electromagnetic tracking system and On-Board kilovoltage imaging system. *International Journal of Radiation Oncology\*Biography\*Physics*, 70(3):892–899, March 2008.
- [79] Lakshmi Santanam, Kathleen Malinowski, James Hubenshmidt, Steve Dimmer, Martin L. Mayse, Jeffrey Bradley, Amir Chaudhari, Kirsten Lechleiter, Sree Krishna Murty Goddu, Jacqueline Esthappan, Sasa Mutic, Daniel A. Low, and Parag Parikh. Fiducial-Based translational localization accuracy of electromagnetic tracking system and On-Board kilovoltage imaging system. *International Journal of Radiation Oncology\*Biography\*Physics*, 70(3):892–899, March 2008.
- [80] A Sawant. Geometric accuracy and latency of an integrated 4D IMRT delivery system using Real-Time internal position monitoring and dynamic MLC tracking. *International Journal of Radiation Oncology\*Biography\*Physics*, 72(1):S27–S28, 2008.
- [81] Amit Sawant, Ryan L. Smith, Raghu B. Venkat, Lakshmi Santanam, Byungchul Cho, Per Poulsen, Herbert Cattell, Laurence J. Newell, Parag Parikh, and Paul J. Keall. Toward submillimeter accuracy in the management of intrafraction motion: The integration of Real-Time internal position monitoring and multileaf collimator target tracking. *International Journal of Radiation Oncology\*Biography\*Physics*, 74(2):575–582, June 2009.
- [82] Amit Sawant, Raghu Venkat, Vikram Srivastava, David Carlson, Sergey Povzner, Herb Cattell, and Paul Keall. Management of three-dimensional intrafraction motion through real-time DMLC tracking. *Medical Physics*, 35(5):2050–2061, May 2008.

- [83] A. Schweikard, G. Glosser, M. Bodduluri, M. Murphy, and J. R. Adler. Robotic motion compensation for respiratory movement during radiosurgery. *Computer Aided Surgery*, 5(4):263–277, 2000.
- [84] Artyom Sedrakyan, Jan van der Meulen, James Lewsey, and Tom Treasure. Video assisted thoracic surgery for treatment of pneumothorax and lung resections: systematic review of randomised clinical trials. *BMJ*, 329(7473):1008, 2004.
- [85] Yvette Seppenwoolde, Ross I. Berbeco, Seiko Nishioka, Hiroki Shirato, and Ben Heijmen. Accuracy of tumor motion compensation algorithm from a robotic respiratory tracking system: A simulation study. *Medical Physics*, 34(7):2774–2784, July 2007.
- [86] Gregory C. Sharp, Steve B. Jiang, Shinichi Shimizu, and Hiroki Shirato. Prediction of respiratory tumour motion for real-time image-guided radiotherapy. *Physics in Medicine and Biology*, 49(3):425–440, 2004.
- [87] D. M. Shepard, D. J. Housley, M. K. N. Afghan, B. Sargent, J. Peterson, and J. Newell. WE-E-M100F-06: latency measurements and demonstration of a 4D electromagnetic localization system for LINAC beam gating. *Medical Physics*, 34:2608, 2007.
- [88] S. Shimizu, H. Shirato, H. Aoyama, S. Hashimoto, T. Nishioka, A. Yamazaki, K. Kagei, and K. Miyasaka. High-speed magnetic resonance imaging for four-dimensional treatment planning of conformal radiotherapy of moving body tumors. *Int J Radiat Oncol Biol Phys*, 48(2):471–4, 2000.
- [89] S. Shimizu, H. Shirato, S. Ogura, H. Akita-Dosaka, K. Kitamura, T. Nishioka, K. Kagei, M. Nishimura, and K. Miyasaka. Detection of lung tumor movement in real-time tumor-tracking radiotherapy. *International Journal of Radiation Oncology\* Biology\* Physics*, 51(2):304–310, 2001.
- [90] H. Shirato, S. Shimizu, K. Kitamura, T. Nishioka, K. Kagei, S. Hashimoto, H. Aoyama, T. Kunieda, N. Shinohara, and H. Dosaka-Akita. Four-dimensional treatment planning and fluoroscopic real-time tumor tracking radiotherapy for moving tumor. *International Journal of Radiation Oncology\* Biology\* Physics*, 48(2):435–42, 2000.
- [91] H Shirato, S Shimizu, T Kunieda, K Kitamura, M van Herk, K Kagei, T Nishioka, S Hashimoto, K Fujita, H Aoyama, K Tsuchiya, K Kudo, and K Miyasaka. Physical aspects of a real-time tumor-tracking system for gated radiotherapy. *International journal of radiation oncology, biology, physics*, 48(4):1187–95, November 2000. PMID: 11072178.

- [92] Hiroki Shirato, Toshiyuki Harada, Tooru Harabayashi, Kazutoshi Hida, Hideho Endo, Kei Kitamura, Rikiya Onimaru, Koichi Yamazaki, Nobuaki Kurauchi, Tadashi Shimizu, Nobuo Shinohara, Michiaki Matsushita, Hirotohi Dosaka-Akita, and Kazuo Miyasaka. Feasibility of insertion/implantation of 2.0-mm-diameter gold internal fiducial markers for precise setup and real-time tumor tracking in radiotherapy. *International Journal of Radiation Oncology\*Biological\*Physics*, 56(1):240–247, May 2003.
- [93] Hiroki Shirato, Masataka Oita, Katsuhisa Fujita, Yoshiharu Watanabe, and Kazuo Miyasaka. Feasibility of synchronization of real-time tumor-tracking radiotherapy and intensity-modulated radiotherapy from viewpoint of excessive dose from fluoroscopy. *International Journal of Radiation Oncology\*Biological\*Physics*, 60(1):335–341, September 2004.
- [94] R.L. Smith, A. Sawant, L. Santanam, R. Venkat, J. Newell, B. Cho, P. Poulsen, H. Catell, P. Keall, and P.J. Parikh. IMRT dosimetric measurements from a real-time internal position monitoring system coupled with a dynamic multileaf collimator tracking system. *International Journal of Radiation Oncology\*Biological\*Physics*, 72(1, Supplement 1):S612–S613, September 2008.
- [95] Ryan L. Smith, Kristen Lechleiter, Kathleen Malinowski, D.M. Shepard, D.J. Housley, M. Afghan, Jeff Newell, Jay Petersen, Brian Sargent, and Parag Parikh. Evaluation of linear accelerator gating with Real-Time electromagnetic tracking. *International Journal of Radiation Oncology\*Biological\*Physics*, 74(3):920–927, July 2009.
- [96] Ryan L. Smith, Amit Sawant, Lakshmi Santanam, Raghu B. Venkat, Lawrence J. Newell, Byung chul Cho, Per Poulsen, Herbert Catell, Paul J. Keall, and Parag J. Parikh. Integration of Real-Time internal electromagnetic position monitoring coupled with dynamic multileaf collimator tracking: An Intensity-Modulated radiation therapy feasibility study. *International Journal of Radiation Oncology\*Biological\*Physics*, 74(3):868–875, July 2009.
- [97] Stephen P. Sorensen, Phillip E. Chow, Sergey Kriminski, Paul M. Medin, and Timothy D. Solberg. Image-guided radiotherapy using a mobile kilovoltage x-ray device. *Medical Dosimetry*, 31(1):40–50, 2006.
- [98] V Srivastava, P Keall, A Sawant, and Y Suh. Accurate prediction of Intra-Fraction motion using a modified linear adaptive filter. *Medical Physics*, 34(6):2546, June 2007.
- [99] Craig W. Stevens, Reginald F. Munden, Kenneth M. Forster, Jason F. Kelly, Zhongxing Liao, George Starkschall, Susan Tucker, and Ritsuko Komaki. Respiratory-driven lung tumor motion is independent of tumor size, tumor



- location, and pulmonary function. *International Journal of Radiation Oncology\*Biography\*Physics*, 51(1):62–68, September 2001.
- [100] Y. Suh, S. Dieterich, B. Cho, and P. J. Keall. An analysis of thoracic and abdominal tumour motion for stereotactic body radiotherapy patients. *Physics in Medicine and Biology*, 53(13):3623–3640, 2008.
- [101] Hiroshi Tsukada, Toshiteru Satou, Akira Iwashima, and Takahiro Souma. Diagnostic accuracy of CT-Guided automated needle biopsy of lung nodules. *Am. J. Roentgenol.*, 175(1):239–243, July 2000.
- [102] D. Verellen, K. Tournel, J. Van de Steene, N. Linthout, T. Wauters, V. Vinh-Hung, and G. Storme. Breathing-synchronized irradiation using stereoscopic kV-imaging to limit influence of interplay between leaf motion and organ motion in 3D-CRT and IMRT: dosimetric verification and first clinical experience. *International Journal of Radiation Oncology\*Biography\*Physics*, 66(4S):108–119, 2006.
- [103] Dirk Verellen, Koen Tournel, Nadine Linthout, Guy Soete, Tom Wauters, and Guy Storme. Importing measured field fluences into the treatment planning system to validate a breathing synchronized DMLC-IMRT irradiation technique. *Radiotherapy and Oncology*, 78(3):332–338, March 2006.
- [104] Martin von Siebenthal, Gbor Szkely, Antony J Lomax, and Philippe C Cattin. Systematic errors in respiratory gating due to intrafraction deformations of the liver. *Medical Physics*, 34(9):3620–9, September 2007. PMID: 17926966.
- [105] Richard I. Whyte, Richard Crownover, Martin J. Murphy, David P. Martin, Thomas W. Rice, Malcolm M. DeCamp, Raymond Rodebaugh, Martin S. Weinhaus, and Quynh-Thu Le. Stereotactic radiosurgery for lung tumors: preliminary report of a phase i trial. *Ann Thorac Surg*, 75(4):1097–1101, April 2003.
- [106] Richard I Whyte, Richard Crownover, Martin J Murphy, David P Martin, Thomas W Rice, Malcolm M DeCamp, Raymond Rodebaugh, Martin S Weinhaus, and Quynh-Thu Le. Stereotactic radiosurgery for lung tumors: preliminary report of a phase i trial. *The Annals of thoracic surgery*, 75(4):1097–101, April 2003. PMID: 12683544.
- [107] Twyla R. Willoughby, Alan R. Forbes, Daniel Buchholz, Katja M. Langen, Thomas H. Wagner, Omar A. Zeidan, Patrick A. Kupelian, and Sanford L. Meeks. Evaluation of an infrared camera and x-ray system using implanted fiducials in patients with lung tumors for gated radiation therapy. *International Journal of Radiation Oncology\*Biography\*Physics*, 66(2):568–575, October 2006.
- [108] Twyla R. Willoughby, Patrick A. Kupelian, Jean Pouliot, Katsuto Shinohara, Michelle Aubin, Mack Roach III, Lisa L. Skrumeda, James M. Balter, Dale W.

- Litzenberg, Scott W. Hadley, John T. Wei, and Howard M. Sandler. Target localization and real-time tracking using the calypso 4D localization system in patients with localized prostate cancer. *International Journal of Radiation Oncology\*Biolog\*Physics*, 65(2):528–534, June 2006.
- [109] J. W. Wong, M. B. Sharpe, D. A. Jaffray, V. R. Kini, J. M. Robertson, J. S. Stromberg, and A. A. Martinez. The use of active breathing control (ABC) to reduce margin for breathing motion. *International Journal of Radiation Oncology\*Biolog\*Physics*, 44(4):911–919, 1999.
- [110] Deshan Yang, Issam Naqa, Apte Aditya, Yu Wu, Murty Goddu, Sasa Mutic, Joseph O. Deasy, and Daniel A. Low. DIRART a software suite for deformable image registration and adaptive radiotherapy research. In *World Congress on Medical Physics and Biomedical Engineering, September 7 - 12, 2009, Munich, Germany*, pages 844–847. 2009.
- [111] Michael J. Zelefsky, Zvi Fuks, Laura Happersett, Henry J. Lee, C. Clifton Ling, Chandra M. Burman, Margie Hunt, Theresa Wolfe, E. S. Venkatraman, Andrew Jackson, Mark Skwarchuk, and Steven A. Leibel. Clinical experience with intensity modulated radiation therapy (IMRT) in prostate cancer. *Radiotherapy and Oncology*, 55(3):241–249, June 2000.
- [112] M.J. Zelefsky, S.A. Leibel, P.B. Gaudin, G.J. Kutcher, N.E. Fleshner, E.S. Venkatraman, V.E. Reuter, W.R. Fair, C.C. Ling, Z. Fuks, and Patrick C. Walsh. Dose escalation with Three-Dimensional conformal radiation therapy affects the outcome in prostate cancer. *The Journal of Urology*, 162(4):1550, October 1999.
- [113] Tianyu Zhao, Wei Lu, Deshan Yang, Sasa Mutic, Camille Noel, Parag Parikh, Jeffrey Bradley, and Daniel A. Low. Characterization of free breathing patterns with 5D lung motion model. *Medical Physics*, 36(11):5183–5189, 2009.

# Curriculum Vitae

Ryan L. Smith

- Degrees**                    B.S. Physics / Computer Science, May 2006  
*Illinois Wesleyan University, Bloomington, IL USA*  
Ph.D. Biomedical Engineering, anticipated January 2011  
*Washington University, Saint Louis, MO USA*
- Select Honors  
and Awards**                Medtronic Computer Assisted Surgery Research Award  
Phi Beta Kappa
- Peer-reviewed  
publications**                Ryan L Smith, Jie Wen, Camille Noel, Martin L. Mayse, Parag  
J Parikh. “A system for image guided surgery on targets  
subject to respiratory motion” In preparation
- Martin L. Mayse, Parag J. Parikh, Ryan L Smith, John R.  
Peauroi, David Misselhorn, Michael Talcott, Jeffrey D. Bradley.  
“Long Term Stability of a Wireless Electromagnetic Anchored  
Transponder Bronchoscopically Implanted in the Canine Lung”.  
Submitted 2010
- Ryan L. Smith, Deshan Yang, Andrew Lee, Martin L Mayse,  
Dan Low, Parag J. Parikh. “Accuracy of using internal fidu-  
cials to predict lung target motion” Submitted 2010
- R. L. Smith, A. Sawant, L. Santanam, R. Venkat, J. Newell, B.  
Cho, P. Poulsen, H. Catell, P. Keall, P.J. Parikh. “Integration  
of Real-Time Internal Electromagnetic Position Monitoring  
Coupled with Dynamic Multileaf Collimator Tracking: An  
IMRT Feasibility Study”, *IJROBP* (2009) 74(3) 868-875.
- Amit Sawant, Ryan Smith, Raghu Venkat, Lakshmi Santanam,  
Byung-chul Cho, Per Poulsen, Herbert Cattell, Laurence J

Newell, Parag Parikh, Paul J. Keall. "Towards sub-mm accuracy in the management of intrafraction motion: The integration of real-time internal position monitoring and MLC target tracking", *IJROBP* (2009) 74(2) 575-582.

Ryan L Smith, Kristen Lechleiter, Kathleen Malinowski. M. Shepard, D.J. Housley, M. Afghan, Jeff Newell, Jay Peterson, Brian Sargent, Parag Parikh. "Evaluation of Linac Gating With Real-Time Electromagnetic Tracking", *IJROBP* (2009) 74(3) 920-927.

Ryan L. Smith; G. C. Spalding; K. Dholakia; M. P. MacDonald; "Colloidal Sorting in Dynamic Optical Lattices" 2007 *J. Opt. A: Pure Appl. Opt.* 9 S134-S138

Metzger, N. K.; Marchington, R. F.; Mazilu, M.; Smith, R. L.; Dholakia, K.; Wright, E. M. "Measurement of the restoring forces acting on two optically bound particles from normal mode correlations." 2007 *Physical Review Letters*, vol. 98, Issue 6, id. 068102

P Fischer, H Little, R L Smith, C Lopez-Mariscal, C T A Brown, W Sibbett and K Dholakia "Wavelength dependent propagation and reconstruction of white light Bessel beams 2006 *J. Opt. A: Pure Appl. Opt.* 8 477-482

## **Proceedings**

Parag J Parikh, Kristen M Lechnleiter, Kathleen L Malinowski, Ryan L Smith, Jie Wen, Steve Dimmer. "Tumor correlated CT: A new paradigm for motion compensated CT for image guided-therapy.. *Proceedings of SPIE, Medical Imaging.* April 2009.

R. L. Smith, A. Sawant, L. Santanam, R. Venkat, J. Newell, B. Cho, P. Poulsen, H. Catell, P. Keall, P. J. Parikh. "IMRT Dosimetric Measurements from a Real-Time Internal Position Monitoring System Coupled with a Dynamic Multileaf Collimator Tracking System" *Astro* 2008.

A Sawant, R. L. Smith, R. B. Venkat, L. Santanam, B. Cho, P. Poulsen, H. Cattell, J. Newell, P. Parikh, P. Keall. “Geometric Accuracy and Latency of an Integrated 4D IMRT Delivery System using Real-Time Internal Position Monitoring and Dynamic MLC Tracking” ASTRO 2008.

M.L. Mayse, R.L. Smith, M. Park, G.H. Monteon, E.H. Silver, P.J. Parikh, D.L. Misselhorn, M.R. Talcott, S. Dimmer and J.D. Bradley. “Development of a Non-migrating Electromagnetic Transponder System for Lung Tumor Tracking ” ASTRO 2008.

E. Silver, P. Parikh, D. Yang, R. L. Smith, D. Low. “Fiducial Placement Guidelines for Thoracic Radiation Therapy Determined by 4DCT” AAPM 2008.

Ryan L. Smith; Kristen Lechleiter; Kathleen Malinowski; Parag Parikh M.D. “Incorporating electromagnetic tracking into respiratory correlated imaging for high precision radiation therapy.” Proceedings of SPIE, Medical Imaging. April 2008.

M.P. MacDonald, I. Andreev, G. Milne, R. Rhodes, L. Paterson, A. Riches, K. Dholakia, R.L. Smith and G.C. Spalding, “Sorting in Optically Produced Potential Energy Landscapes”, proceedings of Topical Problems in Biophotonics, Nizhny Novgorod-Moscow-Nizhny Novgorod, August 2007.

R. L. Smith, G. C. Spalding and M. P. MacDonald, “Microfluidic routing in dynamic optical lattices” Proceedings of SPIE, Photonics West. August 2006.

M. P. MacDonald, S. L. Neale, R. Smith, G. C. Spalding and K. Dholakia, “Sorting in an Optical Lattice”, Proceedings of SPIE vol. 5907, August 2005.

May 2011



**EM Lung Guidance, Smith, Ph.D. 2011**